การตรวจสอบผลของอุณหภูมิที่มีต่อสมบัติการขนส่งทางไฟฟ้าของสารกึ่งตัวนำโดยการวัดปรากฏการณ์ฮอลล์

นางสาวเนตรนพิศ ชูค้นหอม

วิทยานิพนธ์นี้เป็นส่วนหนึ่งของการศึกษาตามหลักสูตรปริญญาวิทยาศาสตรมหาบัณฑิต
สาขาวิชาฟิสิกส์ ภาควิชาฟิสิกส์
คณะวิทยาศาสตร์ จุฬาลงกรณ์มหาวิทยาลัย
ปีการศึกษา 2551

INVESTIGATING EFFECTS OF TEMPERATURE ON ELECTRICAL TRANSPORT PROPERTIES OF SEMICONDUCTORS BY HALL EFFECT MEASUREMENT

Miss Natenapit Chookunhom

A Thesis Submitted in Partial Fulfillment of the Requirements
for the Degree of Master of Science Program in Physics
Department of Physics
Faculty of Science
Chulalongkorn University
Academic Year 2008

Thesis Title	Investigating Effects of Temperature on Electrical Transport Properties of Semiconductors by Hall Effect Measurement
By	Miss Natenapit Chookunhom
Field of Study	Physics
Thesis Principal Advisor	Assistant Professor Sojiphong Chatraphorn, Ph.D.
Thesis Co-advisor	Assistant Professor Kajornyod Yoodee, Ph. D.

Accepted by the Faculty of Science, Chulalongkorn University in Partial Fulfillment of the Requirements for the Master's Degree

Deputy Dean for Administrative Affairs,
……Vimolvan Pimpan…… Acting Dean, The Faculty of Science
(Associate Professor Vimolvan Pimpan, Ph. D.)

THESIS COMMITTEE

…………………………………………… Chairman
(Associate Professor Prapaipan Chantikul, Ph. D.)

……S. Chatraph…………………………… Thesis Principal Advisor
(Assistant Professor Sojiphong Chatraphorn, Ph.D.)

……Kajornyod Yoodee…………………… Thesis Co-advisor
(Assistant Professor Kajornyod Yoodee, Ph. D.)

…………………………………………… Member
(Assistant Professor Tonphong Kaewkongka, Ph. D.)

…………………………………………… Member
(Chatchai Srinitiwarawong, Ph.D.)

เนตรนพิศ ชูคันหอม: การตรวจสอบคุณสมบัติการขนส่งทางไฟฟ้าที่ขึ้นอยู่กับอุณหภูมิของสารกึ่งตัวนำโดยการวัดปรากฏการณ์ฮอลล์ (INVESTIGATING EFFECTS OF TEMPERATURE ON ELECTRICAL TRANSPORT PROPERTIES OF SEMICONDUCTORS BY HALL EFFECT MEASUREMENT) อ.ที่ปรึกษาวิทยานิพนธ์หลัก: ผศ. ดร.โศจิพงศ์ ฉัตราภรณ์, อ.ที่ปรึกษาวิทยานิพนธ์ร่วม: ผศ. ดร. ขจรยศ อยู่ดี, 95 หน้า

การเคลื่อนที่ของประจุพาหะในสารกึ่งตัวนำส่งผลโดยตรงต่อการขนส่งทางไฟฟ้าเช่นสภาพต้านทานไฟฟ้า ความสามารถในการเคลื่อนที่ได้ของพาหะและความเข้มข้นของพาหะอิสระ วิธีการที่ใช้อย่างแพร่หลายในการหาค่าเหล่านี้ คือ วิธีการของวานเดอพาวและการวัดปรากฏการณ์ฮอลล์โดยทั้งสองวิธีอยู่บนพื้นฐานของการวัดแบบสี่ขั้ว ในงานวิจัยนี้ได้ออกแบบระบบวัดวานเดอพาวและฮอลล์ควบคุมโดยคอมพิวเตอร์เพื่อใช้ทำการศึกษาการสมบัติการขนส่งทางไฟฟ้าของสารกึ่งตัวนำ เช่น อินเดียมแอนติโมไนด์ (InSb) อินเดียมทินออกไซด์ (ITO) และซิงค์ออกไซด์โด๊ปด้วยอะลูมินัม (AZO) สารตัวอย่างอินเดียมแอนติโมไนด์ถูกใช้เป็นตัวสอบเทียบระบบ โดยผลการวัดที่ 77 เคลวินสอดคล้องกับผลที่แสดงไว้ในใบรายงานผลจากผู้ผลิต สำหรับผลการวัดสารตัวอย่างอินเดียมทินออกไซด์พบว่าจากค่าสภาพต้านทานไฟฟ้าที่เพิ่มขึ้นเมื่ออุณหภูมิสูงขึ้นเป็นผลเนื่องมาจากการสั่นของโครงผลึกซึ่งเป็นพฤติกรรมของตัวนำ สำหรับผลการวัดฟิล์มบางซิงค์ออกไซด์โด๊ปด้วยอะลูมินัมพบว่าความสามารถในการนำของพาหะขึ้นอยู่กับกลไกสองชนิด คือ การนำไฟฟ้าที่เกิดจากการกระตุ้นด้วยความร้อน (thermal activated conduction) ซึ่งมีผลในช่วงอุณหหภูมิสูงกว่า 100 เคลวิน ด้วยพลังงานในการกระตุ้นมีค่าประมาณ 19 มิลลิอิเลกตรอนโวลต์ และในช่วงอุณหภูมิต่ำกว่า 80 เคลวิน การกระโดดด้วยช่วงที่ไม่คงที่ (variable range hopping) จะมีบทบาทสำคัญ ดังนั้นช่วงเปลี่ยนอุณหภูมิ (cross over) สำหรับทั้งสองกลไกอยู่ประมาณอุณหภูมิระหว่าง 80 ถึง 100 เคลวิน

ภาควิชา ฟิสิกส์ ลายมือชื่อนิสิต เนตรนพิศ ชูคันหอม
สาขาวิชา ฟิสิกส์ ลายมือชื่ออ.ที่ปรึกษาวิทยานิพนธ์หลัก
ปีการศึกษา 2551 ลายมือชื่ออ.ที่ปรึกษาวิทยานิพนธ์ร่วม ขจรยศ อยู่ดี

4872341723: MAJOR PHYSICS

KEY WORDS: ELECTRICAL PROPERTIES / HALL EFFECT / TEMPERATURE DEPENDENT

NATENAPIT CHOOKUNHOM: INVESTIGATING EFFECTS OF TEMPERATURE ON ELECTRICAL TRANSPORT PROPERTIES OF SEMICONDUCTORS BY HALL EFFECT MEASUREMENT THESIS PRINCIPAL ADVISOR: ASST. PROF. SOJIPHONG CHATRAPHORN, PH.D., THESIS COADVISOR: ASST. PROF. KAJORNYOD YOODEE, PH.D., 95 pp.

Motion of charged carriers in semiconductor is directly related to its electrical transport properties, i.e. resistivity, mobility and carrier concentration. The widely used technique to obtain such properties is the van der Pauw (vdP) method and the Hall effect measurement, both employ the four-point probe technique. In this thesis, the computer-controlled vdP and Hall effect measurement system have been designed and used for studying electrical transport properties of semiconductors such as InSb, Indium-Tin-Oxide (ITO) and Aluminum-doped Zinc Oxide (AZO). The InSb was used as a sample to calibrate the system. The measurement results at 77 K were in good agreement with those issued from the manufacturer. For the ITO thin films, it was observed that the resistivity was rising with increasing temperature due to the lattice vibration, indicating the behavior of metallic conduction. For the measurement results of AZO thin films, it was found that there were two mechanisms involving in the conduction of the carriers. The thermally activated band conduction was dominant in the high temperature range ($T > 100$ K). From this result, the activation energy was approximately 19 meV. For the low temperature range ($T < 80$ K), the variable range hopping became dominant. Thus, the cross-over region for the two competing mechanisms was between 80-100 K.

Department : Physics Student's Signature : Natenapit Chookunhom
Field of Study : Physics Principal Advisor's Signature : S.
Academic Year : 2008 Co-advisor's Signature : Kajornyod Yoodee

Acknowledgements

I would like to express my sincere gratitude and appreciation to my thesis advisors, Assistant Professor Dr. Sojiphong Chatraphorn and Assistant Professor Dr. Kajornyod Yoodee for their supervision, suggestion, kindness suggestion and discussion throughout the course of this thesis.

I wish to express my special thanks to Dr. Chanwit Chityuttakan for technical assistance and discussions during the period of my course of thesis.

I especially would like to thank the thesis committee, Associate Professor Dr. Prapaipan Chantikul, Dr. Tonphong Kaewkongka and Dr. Chatchai Srinitiwarawong for their reading and comments on this thesis.

I would like to acknowledge the National Institute of Metrology (Thailand) to about the opportunity to let me spend time in this course.

Many thanks to my friends , Rachsak Sakdanuphab, Bancha Arthibenyakul, Kriangkri Wantong, and all colleagues in Semiconductor Physics Research Laboratory, Department of Physics, Chulalongkorn University, for their friendship and encouragement. I also wish to thank Dr. Sivinee Sawadiaree for many guidance and helpful discussions.

I especially would like to thank Eak Khumthukthit for understanding and everything he have done for me.

Finally, I wish to express my gratitude to my parents and my sister for their encouragement everything they support me.

Contents

List of Tables

Table **Page**

List of Figures

Figure **Page**

CHAPTER I

INTRODUCTION

The properties of material such as structural properties, optical properties or the electrical properties can be characterized using several techniques. In this thesis, the works are focused on the measurements of electrical properties of semiconducting materials. The charged particles transportation is directly related to the electrical conductivity of the matter. The density of the charged particles is one of the important intrinsic and extrinsic properties toward an understanding of the electrical properties of semiconductor or other materials. In order to obtain electrical properties of the materials, several techniques are being applied. The direct method used to obtain the electrical properties is by the measurement of resistance R [1]. A known dimensions of sample are used and then the resistivity ρ is calculated from $R = \rho L/A$, where L and A is the length and the cross sectional area of the sample, respectively. The problem of this technique is the measured resistivity may contain the contact resistance and the resistance of the cables of the measuring tools. The effect of excess resistance can be eliminated by using the four-points probe technique. The sample in this measurement should have a uniform cross-sectional area and the applied current must be low enough to prevent the heating of the sample. However, the most applicable method to characterize electrical conductivity is the van der Pauw measurement technique. In 1958, L. J. van der Pauw applied the method to characterize the resistivity of material based on the four-points probe technique. The Hall effect measurement is based on similar configurations of the van der Pauw technique with the addition of applied magnetic fields. The thin flat samples are usually placed perpendicular to the magnetic field with electric current flowing in the plane of the sample. The transverse force is exerted on charged particles by the magnetic field. This force pushes the moving charged carriers to one side of the conductor until the Lorentz force is zero in equilibrium. The voltage between the two sides of the conductor, known as the Hall voltage, are then produced. E. H. Hall discovers this phenomenon in 1879 known as the Hall effect. In the present, the van der Pauw and the Hall effect measurements are one of the well known methods to measure the electrical conductivity or resistivity, mobility and carrier concentration with high precision and high accuracy. These measurements are normally nondestructive.

To measure the electrical properties of materials by using the van der Pauw and the Hall effect measurement, several configurations should be applied to the sample. Thus, it is inconvenience to change the configurations manually. In order to solve this problem, data acquisition tools are used to switch the configurations. The accurate results of the measurements are obtained by the computer-controlled system. In this case, the measurement conditions can be defined by users. Not only the convenience from the computer-controlled measurement system can be obtained, but also the accurate and reliable results can be readily available.

The semi-automated system will be designed and used to investigate the thermally activated electrical transport properties in a wide temperature range of semiconducting materials, such as Indium Tin Oxide (ITO) and Aluminum-doped Zinc Oxide (AZO), etc. In this case, the cryogenic system is utilized. By cooling down the samples to the temperature of about 20 K and heating up to room temperature, the temperature dependences of their electrical properties are investigated and discussed.

Objectives of the research:

1) To design a computer-controlled system for the van der Pauw and the Hall effect measurement.
2) To develop measurement method for electrical properties of semiconductors with high accuracy.
3) To describe the electrical transport mechanisms of Indium Antimonide, Indium Tin Oxide and Aluminum-doped Zinc Oxide as a function of temperature.

The procedures of the thesis are:

1) to study the electrical properties of semiconductor,
2) to design a semi-automated system for investigating the electrical properties,
3) to calibrate the system by using a known semiconductor, e. g. InSb,
4) to investigate the temperature dependence of ITO and AZO using the designed system.

This thesis is divided into three major parts. In the first part, the basic principles of the van der Pauw and the Hall effect measurements are described. The second part provides a flow chart, a schematic diagram of the semi-automated measurement system and the calibrations of the measurement system. In the last parts, the measurement results and conclusions of some semiconductors such as ITO and AZO are described. The outline of the thesis is as followings.

In chapter 2, the theoretical background and the fundamental principles such as van der Pauw measurement, the Hall effect measurement and the temperature dependent of the semiconductor are reviewed.

In chapter 3, the designed concept, the schematic diagram and the capability of the program are provided. Also the list of equipments used in the semi-automated van der Pauw and Hall measurement system are included. The interfacing and wiring and the details of the automatic control are explained. Finally, the sample preparation such as procedures for the preparation sample holder, sample itself Ohmic contacts are described.

In chapter 4, the used of known sample, Indium Antimonide (InSb), for the calibration of the computer-controlled van der Pauw and the Hall measurements are provided. Also the comparisons between measurement results and the manufacturer certificate are shown.

The next two chapters, 5 and 6, the results of the Indium Tin Oxide (ITO) and Aluminum doped Zinc Oxide (AZO) thin films measured by the system will be discussed. Their electrical conductivity measurements at different temperatures will be concluded.

In chapter 7, according to the investigated measurement results in the previous chapters, the most significant results such as thermally activated temperature are summarized and concluded.

CHAPTER II

THEORETICAL BACKGROUND

In this chapter, the theory involving characterizations of electrical properties such as resistivity, mobility and carrier concentration base on the van der Pauw and the Hall effect measurement method are described. In addition, the temperature dependent of electrical properties and the thermal activated of these quantities of semiconductors are also briefly discussed.

2.1 Resistivity [2]

The meaning of electrical resistivity may be simply described as how strongly a material opposes the flow of electric current. The material with low resistivity indicates that the material readily allows movement of electrical charge. The definition of the electrical resistivity can be considered by applied an electric field $\vec{E}$ to the sample which has a cross sectional area A and length L. This sample has a carrier concentration n as shown below.

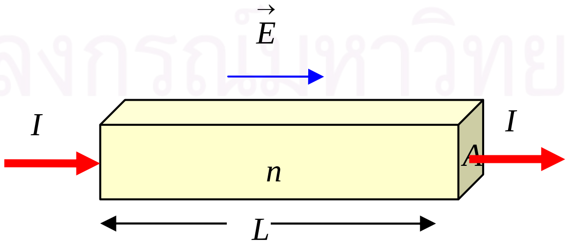

Figure 2.1: Current conduction in a bar of a conductor.

The electrical resistivity is usually written as:

$$\rho = \frac{RA}{L}\,, \tag{2.1}$$

where ρ is the resistivity ($\Omega \cdot cm$),

R is the electrical resistance (Ω),

L is the length of the specimen (m) and

A is the cross section of the specimen (m^2).

The current density $\vec{J}$ is related to the applied electric field and can be written as:

$$\vec{J} = \hat{\sigma} \cdot \vec{E}\,, \tag{2.2}$$

where $\vec{E}$ is electric field (V/m),

$\hat{\sigma}$ is the conductivity tensor.

From Fig. 2.1, the current density $\vec{J}$ is given by

$$I = \int \vec{J} \cdot d\vec{A}\,, \tag{2.3}$$

where I is the electrical current. Also $\vec{J}$ is related to the drift velocity of the charge carrier given by

$$\vec{J} = -qn\vec{v}_n\,, \tag{2.4}$$

where q is the electronic charge = 1.602×10^{-19} C,

$\vec{v}$ is the drift velocity of the electron.

For the linear relation ship of $\vec{v}$ and $\vec{E}$, i.e. $\vec{v} = -\mu_n \vec{E}$ then $\vec{J}$ in Eq. (2.4) can be written as

$$\vec{J} = qn\mu\vec{E}\,. \tag{2.5}$$

In the materials that have mixed types of carriers such as electrons (n) and holes (p), then we have

$$\vec{J}_n = qn\mu_n \vec{E} \text{ for electron,} \tag{2.6.1}$$

$$\vec{J}_p = qp\mu_p \vec{E} \text{ for hole,} \tag{2.6.2}$$

where p is the hole concentration.

Thus the total current density is

$$\vec{J} = \vec{J}_n + \vec{J}_p , \tag{2.7}$$

$$\vec{J} = q(n\mu_n + p\mu_p)\vec{E} . \tag{2.8}$$

The comparison between the Eq. (2.2) and Eq. (2.8) leads to the resistivity given by

$$\rho = \frac{1}{q(n\mu_n + p\mu_p)} . \tag{2.9}$$

2.2 The van der Pauw Method [2]

One of the most commonly used methods for measuring resistance or resistivity is the van der Pauw method. In 1958 L. H. van der Pauw discovered an elegant method to evaluate the electrical resistivity. Electrical transport properties of materials, such as conductors and semiconductors, can be obtained by this method. Sample of any arbitrary shapes can be investigated by this method based on a four point probe technique.

An infinite plane of thickness d of conducting material is considered as in Fig 2.2. The resistivity is given by ρ and the current $2i$ is applied to point M.The current flows from point M in the radial direction (r) symmetrically to infinity.

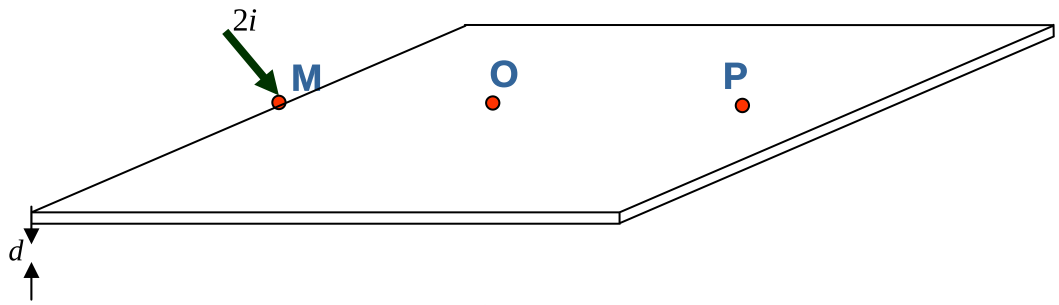

Figure 2.2: The sample with applied current $2i$ *at point M.*

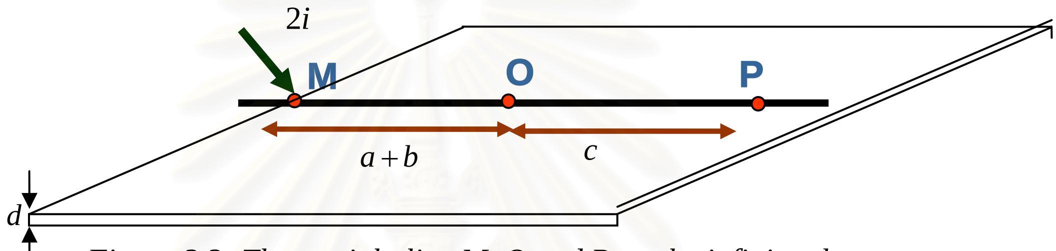

Figure 2.3: The straight line M, O and P on the infinite plane.

Using Ohm's law, the relationship of the electric field $\vec{E}$ and the current density $\vec{J}$ can be written as

$$\vec{E} = \frac{1}{\hat{\sigma}}\vec{J} = \frac{\rho 2i}{2\pi rd} = \frac{\rho i}{\pi rd}, \tag{2.10}$$

where $\hat{\sigma}$ is the conductivity.

Consider any two points O and P which are lying on a straight line with point M, as in Fig. 2.3, the potential difference between the points O and P can be derived as follow:

$$V_p - V_O = -\int_o^P E dr = -\int_{a+b}^{a+b+c} \frac{\rho i}{\pi rd} dr \tag{2.11}$$

$$V_P - V_O = -\frac{\rho i}{\pi d}\ln\left(\frac{a+b+c}{a+b}\right) \tag{2.12}$$

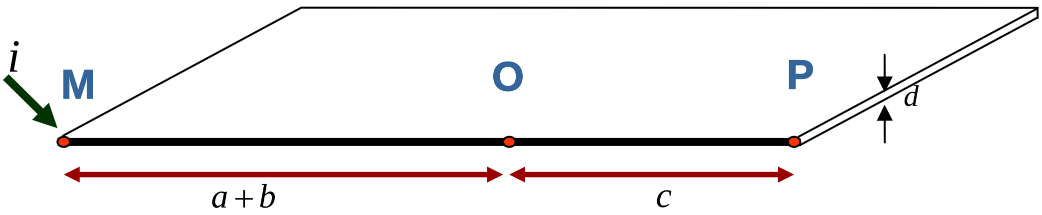

Figure 2.4: The straight line M, O and P on the infinite half plane. The current is reduced from $2i$ *to* i.

Since there is no current flow perpendicular to the line through point M, O and P in Fig. 2.4, the results in Eq. (2.12) is still hold if half-plane of the sample is removed. Then the current is reduced to a half.

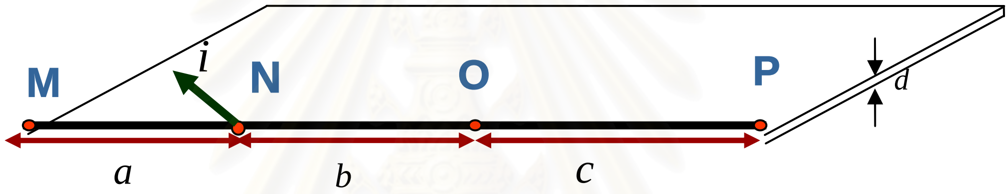

Figure 2.5: The straight line M, N, O and P on the infinite half plane with the current take from point N.

If the current i is taken out from the point N, as shown in Fig. 2.5. According to Eq. (2.11), we get

$$V_p - V_O = -\int_o^P E dr = -\int_b^{b+c} \frac{\rho(-i)}{\pi r d} dr \, , \tag{2.13}$$

$$V_P - V_O = \frac{\rho i}{\pi d} \ln\left(\frac{b+c}{b}\right). \tag{2.14}$$

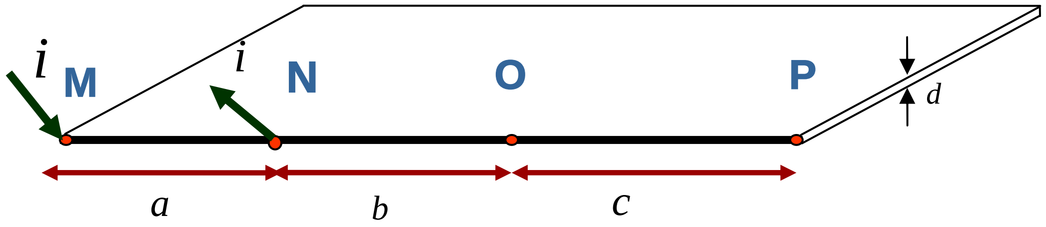

Figure 2.6: The superposition of figure 2.4 and figure 2.5.

Thus, $V_p - V_O$ when there are both an applied current and a taken out current at point M and point N, respectively (Fig. 2.6) is as a superposition of Fig. 2.4 and Fig. 2.5 or Eq. (2.12) and Eq. (2.14) as follows

$$V_p - V_O = \frac{-\rho i}{\pi d}\ln\left[\frac{(a+b+c)}{(a+b)}\right] + \frac{\rho i}{\pi d}\ln\left[\frac{(b+c)}{(b)}\right],$$

$$= \frac{\rho i}{\pi d}\ln\left[\frac{(a+b)(b+c)}{(a+b+c)b}\right]. \qquad (2.15)$$

The resistance of the infinite half plane can be written in the following equation

$$R_{MN,OP} = \frac{\rho}{\pi d}\ln\left[\frac{(a+b)(b+c)}{(a+b+c)b}\right], \qquad (2.16)$$

The Eq. (2.16) can be rewritten in an exponential form as

$$\left[\frac{(a+b+c)b}{(a+b)(b+c)}\right] = e^{-\frac{\pi d}{\rho}R_{MN,OP}}. \qquad (2.17)$$

If we shift the point where the current is applied from point M to point N then taken out at point O, Eq. (2.17) then becomes

$$\left[\frac{ac}{(a+b)(b+c)}\right] = e^{-\frac{\pi d}{\rho}R_{NO,PM}}. \qquad (2.18)$$

Adding Eq. (2.17) and Eq. (2.18) together, we obtain

$$e^{-\frac{\pi d}{\rho}R_{MN,OP}} + e^{-\frac{\pi d}{\rho}R_{NO,PM}} = 1. \qquad (2.19)$$

Let $\pi d R_{MN,OP} = x_1$ and $\pi d R_{NO,PM} = x_2$, Eq. (2.19) can be rewritten as

$$e^{-\frac{x_1}{\rho}} + e^{-\frac{x_2}{\rho}} = 1. \qquad (2.20)$$

We can also write $x_1 = \frac{1}{2}\left[(x_1 + x_2) + (x_1 - x_2)\right]$ and $x_2 = \frac{1}{2}\left[(x_1 + x_2) - (x_1 - x_2)\right]$, Eq. (2.20) become

$$e^{-\frac{1}{2\rho}[(x_1+x_2)+(x_1-x_2)]}+e^{-\frac{1}{2\rho}[(x_1+x_2)-(x_1-x_2)]}=1,$$

$$e^{\frac{-[x_1+x_2]}{2\rho}}(e^{-\frac{1}{2\rho}[x_1-x_2]}+e^{+\frac{1}{2\rho}[x_1-x_2]})=1,$$

where $(e^{-\frac{1}{2\rho}[x_1-x_2]}+e^{+\frac{1}{2\rho}[x_1-x_2]}) = 2\cosh\left[\frac{x_1-x_2}{2\rho}\right]$,

then, $$e^{\frac{-[x_1+x_2]}{2\rho}}\cosh\left[\frac{x_1-x_2}{2\rho}\right]=\frac{1}{2}. \qquad (2.21)$$

Now, we define $\dfrac{x_1+x_2}{2\rho}=\dfrac{\ln 2}{f\left(\dfrac{R_{MN,OP}}{R_{NO,PM}}\right)}$; $f\left(\dfrac{R_{MN,OP}}{R_{NO,PM}}\right)$ is the correction factor.

(2.22)

Thus, Eq. (2.21) becomes

$$e^{\frac{-\ln 2}{f\left(\frac{R_{MN,OP}}{R_{NO,PM}}\right)}}\cosh\left[\frac{x_1-x_2}{2\rho}\right]=\frac{1}{2},$$

$$e^{\frac{-\ln 2}{f\left(\frac{R_{MN,OP}}{R_{NO,PM}}\right)}}\cosh\left[\frac{\frac{x_1}{x_2}-1}{\frac{x_1}{x_2}+1}\times\frac{(x_1+x_{2)}}{2\rho}\right]=\frac{1}{2},$$

$$\cosh\left[\frac{\frac{R_{MN,OP}}{R_{NO.PM}}-1}{\frac{R_{MN,OP}}{R_{NO,PM}}+1}\times\frac{\ln 2}{f\left(\frac{R_{MN,OP}}{R_{NO,PM}}\right)}\right]=\frac{1}{2}e^{\frac{\ln 2}{f\left(\frac{R_{MN,OP}}{R_{NO,PM}}\right)}}. \qquad (2.23)$$

Equation (2.23) is used to iteratively solve for the correction factor. Since, we have the correction factor on both sides of the Eq. (2.23), when the correction factor is found, we can obtain the resistivity from Eq. (2.22),i.e.

$$\rho=\frac{\pi d}{\ln 2}\left(\frac{R_{MN,OP}+R_{NO,PM}}{2}\right)f\left(\frac{R_{MN,OP}}{R_{NO,PM}}\right), \qquad (2.24)$$

where $f\left(\frac{R_{MN,OP}}{R_{NO,PM}}\right)$ is the correction factor which depends on the ratio of the value of the two resistances.

In general case for a finite arbitrary sample, the resistivity can be written as

$$\rho = \frac{\pi d}{\ln 2}\left(\frac{R_A + R_B}{2}\right) f\left(\frac{R_A}{R_B}\right), \qquad (2.25)$$

where R_A is resistance when the voltage is measured across point 1 and point 2 and the current is applied at point 4 and taken out at point 3 and R_B is resistance when the voltage across point 2 and point 3 when the current is applied at point 4 and taken out at point 1 as shown in Fig. 2.7. The correction factor in general case can also be obtained from Eq. (2.23).

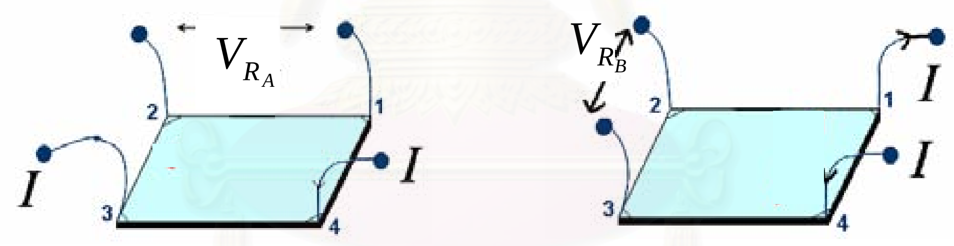

Figure 2.7: The configuration of difference positions where the current is taken of.

2.3 The characterization resistance R_A and R_B

To obtain the resistance R_A and R_B accurately, the data analysis must be used accordingly. The raw data of the measured voltage and applied current are recorded. Assuming the I-V data are linear. All of them are used to analyze the resistance by the uncertainty of a linear plot which is described as the following;

The straight line plot of the experimental data has an uncertainty in each point. The slope of the straight line and the interception also has an uncertainty due to the propagation of the uncertainty. Each pair current (I) and voltage (V) data is given as (I_i, V_i). The resistance is the slope of the plot between the applied current and the measured voltage. Consider the χ^2 from the experiment

$$\chi^2 = \sum_{i=1}^{N} \frac{(V_i^{th} - V_i^{\exp})^2}{\Delta V_i^2}, \tag{2.26}$$

where $V_i^{th} = RI_i + V_0$ is the theoretical value of the voltage at the applied current I_i, $V_i^{\exp}$ is the value obtained from the experiment and it is called V_i from now on , ΔV_i is the uncertainty of the data point i^{th}. Assuming that the uncertainty of V is the same in every point, then $\Delta V_i = \Delta V$ and Eq. (2.26) can be written as

$$\chi^2 = \sum_{i=1}^{N} \frac{(RI_i + V_0 - V_i\ )^2}{\Delta V_i^2}. \tag{2.27}$$

The best fit for R and V_0 can be obtained by minimizing χ^2 with respect to R and with respect to V_0, respectively. One obtains the following set of equations:

$$\frac{\partial \chi^2}{\partial R} = \sum_{i=1}^{N} \frac{2I_i(RI_i + V_0 - V_i)}{(\Delta V)^2} = 0, \tag{2.28}$$

$$\frac{\partial \chi^2}{\partial V_0} = \sum_{i=1}^{N} \frac{2(RI_i + V_0 - V_i)}{(\Delta V)^2} = 0. \tag{2.29}$$

Rewriting Eq. (2.28) and Eq. (2.29), we obtain

$$\sum_{i=1}^{N} I_i V_i = R\sum_{i=1}^{N} I_i^2 + V_0 \sum_{i=1}^{N} I_i, \tag{2.30}$$

and

$$\sum_{i=1}^{N} V_i = R\sum_{i=1}^{N} I_i^2 + NV_0. \tag{2.31}$$

V_0 can be calculated from Eq. (2.27);

$$V_0 = \frac{\sum_{i=1}^{N} V_i - R\sum_{i=1}^{N} I_i}{N} . \qquad (2.32)$$

The R can be found in terms of N, I_i and V_i;

$$R = \frac{N\sum_{i=1}^{N} I_i V_i - \sum_{i=1}^{N} V_i \sum_{i=1}^{N} I_i}{N\sum_{i=1}^{N} I_i^2 - (\sum_{i=1}^{N} I_i)^2} . \qquad (2.33)$$

From the van der Pauw measurement, the raw data of applied current and measured voltage in the both configurations can be used to calculate the resistance R_A and R_B, respectively.

The correction factor is solved by using Eq. (2.23). This factor also depends on the ratio of the two calculated resistances R_A and R_B. The correction factor $f(\frac{R_A}{R_B})$ is shown in Fig. 2.8.

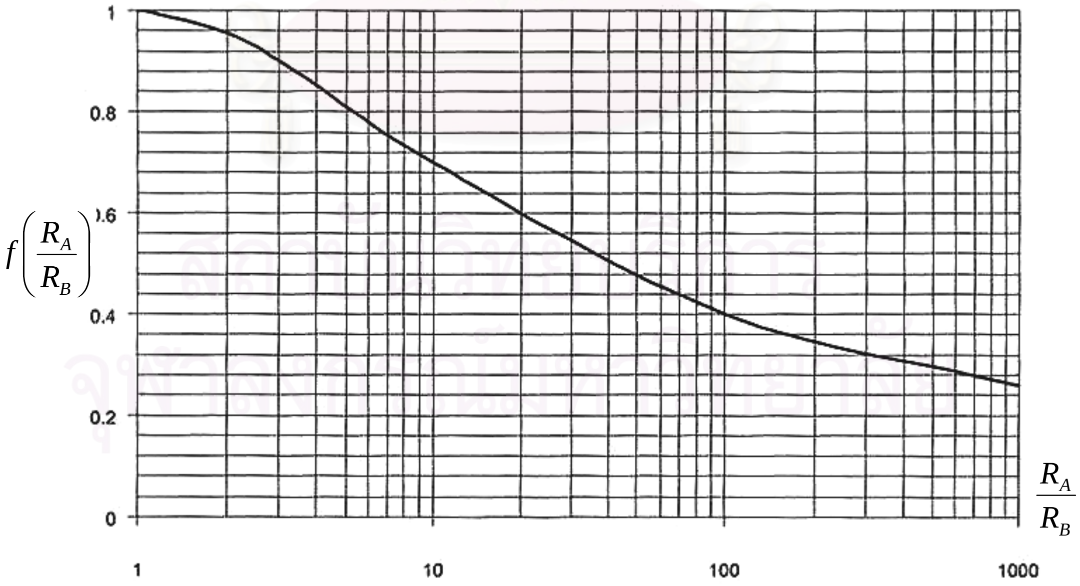

Figure 2.8: The correction factor f as a function of the ratio of calculated resistor.

2.4 The Hall Effect Measurement [3]

The Hall effect measurement which is a method normally used to determine the carrier concentration and the type of carrier. This method is also used to investigate the Hall mobility of materials.

2.4.1 Hall Effect and Lorentz Force

The Lorentz force is the force exerted on a charged particle in an electromagnetic field. The particle will experience a force due to electric field of $q\vec{E}$, and due to the magnetic field $q\vec{v}\times\vec{B}$.

$$\vec{F} = q\vec{E} + q\vec{v}\times\vec{B} \quad , \qquad (2.34)$$

$\vec{F}$ is the force (N),

$\vec{E}$ is the electric field (V/m),

$\vec{B}$ is the magnetic field (T),

q is the electric charge of the particle (coulomb), and

$\vec{v}$ is the instantaneous velocity of the particle (m/s).

Figure 2.9 shows the magnetic field will exert force on the carriers in $\vec{z}$ direction. In the steady state, there is no current flowing along $\vec{z}$ direction, the force due to the electric field along this direction will cancel out the magnetic field. The establishment of voltage in $\vec{z}$ direction is known as Hall voltage. The Hall effect refers to the potential difference (Hall voltage) on the opposite sides of an electrical conductor through which an electric current is flowing, due to a magnetic field applied perpendicular to the plane of current.

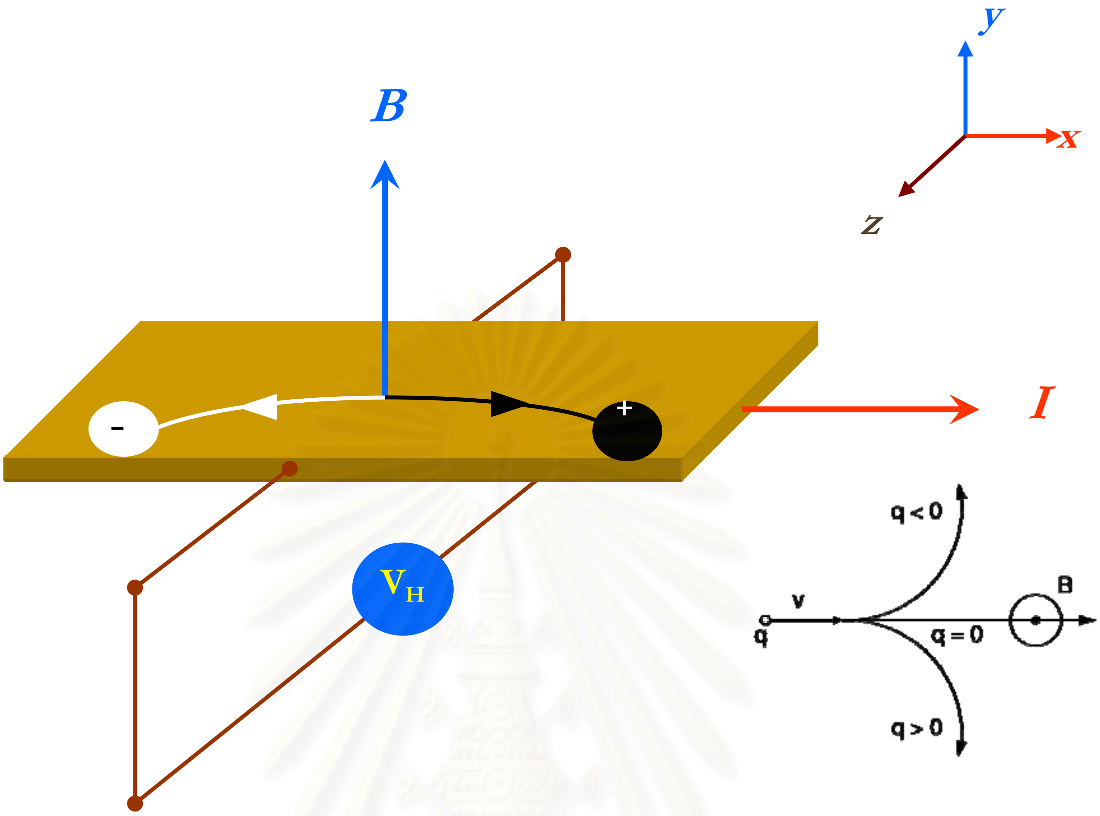

Figure 2.9: The n-type and p-type semiconductor in the applied electric and magnetic field.

2.4.2 Hall Mobility and Carrier Concentration [3]

The Lorentz force (Fig. 2.9) for the Hall effect Phenomenon can be express by

$$qE_z = qv_x B_y \text{ or } E_z = v_x B_y \qquad (2.35)$$

The Hall voltage in Eq. (2.37) is an electric field in $\vec{z}$ direction. Using the electron drift velocity, Eq. 2.37 can be rewritten as

$$E_z = -\left(\frac{J_n}{qn}\right) B_y ,$$

$$E_z = -R_H J_n B_y \qquad (2.36)$$

where R_H is defined by $R_H \equiv \frac{-1}{qm}$;(m is the majority carriers). (2.37)

The Hall resistance R_{H_n} for the n-type semiconductor can be defined as

$$R_{H_n} \equiv \frac{-1}{qn}. \tag{2.38}$$

Similarly for the p-type semiconductor, the Hall resistance R_{H_p} can be obtained as

$$R_{H_p} \equiv \frac{-1}{qp}. \tag{2.39}$$

The Hall mobility is defined by

$$\mu \equiv \frac{|R_H|}{\rho}. \tag{2.40}$$

The relation between the resistivity and their mobility is in Eq. (2.37) and Eq. (2.40). For an extrinsic semiconductor, the difference between the two carrier concentrations is huge. Equation (2.9) can then be reduced to

$$\rho = \frac{1}{qn_m\mu_m}, \tag{2.41}$$

where n_m and μ_m are the type of semiconductor and the mobility of the majority of the carrier. The mobility and carrier concentration relation is given by

For the n-type semiconductor

$$\mu_n = \frac{1}{qn\rho}, \tag{2.42}$$

and for the p-type semiconductor

$$\mu_p = \frac{1}{qp\rho}. \tag{2.43}$$

2.5 Temperature dependent and Relaxation Time [5]

In a perfect crystalline material, the free electron, whose mass is m_e and charge is *e*, can move in all directions without collision in the external electric field $\vec{E}$. The equation of motion is given by

$$m_e \frac{d\vec{v}}{dt} = e\vec{E} . \tag{2.44}$$

On the other hand, for an imperfect crystalline, such as ionized impurities, vibrations of the optical phonons cause the colliding of the electrons. In the steady state, the average velocity can be given by

$$< v >= e\vec{E}\frac{< \tau >}{m_e} , \tag{2.45}$$

where τ is the mean free time or the relaxation time.

Using Ohm's law, the relation between the relaxation time and the electrical conductivity and mobility are given in the set of the following equations;

$$\hat{\rho} = \frac{1}{\hat{\sigma}} = \frac{m_e}{ne^2 < \tau >} , \tag{2.46}$$

and

$$\mu = \frac{e < \tau >}{m_e} , \tag{2.47}$$

where n is the carrier concentration.

From the classical theory of electrical transport of conventional semiconductors, the temperature dependence of the electrical conductivity can be determined from the convolutions of temperature dependence of the relaxation time for various scattering processes for carriers, i.e. τ_n for electrons, and τ_p for holes. In general, the mobility is a function of these relaxation times of the scattering process. There are two major interaction mechanisms affect carrier mobility.

The net relaxation time also due to other scattering mechanisms and can be given by

$$\frac{1}{\tau} = \sum_{i=1}^{N} \frac{1}{\tau_i}. \qquad (2.48)$$

where τ_i is the relaxation time due to the related scattering mechanism.

The net reciprocal mobility can be obtained from

$$\frac{1}{\mu} = \sum_{i=1}^{N} \frac{1}{\mu_i}. \qquad (2.49)$$

where τ_i is the mobility from the related scattering mechanism.

In addition to those mechanisms, scatterings from the other contributions, such as grain boundary, etc., may be taken into account in Eq. (2.41). The following table shows the scattering mechanisms normal in the semiconductor. Temperature dependences of the scattering mechanisms of GaAs [4] are shown in Fig. 2.10.

Table 2.1: The scattering mechanism in the imperfect crystal [4].

Scattering mechanism	**Relaxation Time**	**Conductivity mobility**
Neutral impurity	$\tau = \frac{m}{20 N_n h a_0}$	$\mu = \frac{\lvert e \rvert}{20 N_n h a_0}$
Ionized impurity	$\tau = \frac{16\sqrt{2m}\pi\varepsilon^2}{N_i Z^2 e^4} \frac{E^{\frac{3}{2}}}{[\ln(1+4k^2\lambda^2 - \frac{4k^2\lambda^2}{1+4k^2\lambda^2}]}$	$\mu = \frac{\frac{128\sqrt{2\pi}\varepsilon^2 (k_B T)^{\frac{3}{2}}}{N_i Z^2 e^4}}{\ln[1+(\frac{128\pi\varepsilon k_B T)^2}{2Ze^2 N_c^{1/3}}]}$
Deformation potential	$\tau = \frac{\pi\rho h^4 s^2 E^{-1/2}}{2E_2^1 (m)^{3/2} k_B T}$	$\mu = \frac{2\sqrt{2\pi}\rho h^4 s^2 \lvert e \rvert}{3E_1^2 (m)^{5/2} (k_B T)^{3/2}}$
Piezoelectric	$\tau = \frac{2\sqrt{2}\pi\rho h^2 s^2 \varepsilon^2 E^{-1/2}}{(ehpz)^2 (m)^{1/2} k_B T}$	$\mu = \frac{16\sqrt{2}\rho h^2 s^2 \varepsilon^2 \lvert e \rvert}{3(ehpz)^2 (m)^{3/2} (k_B T)^{1/2}}$
Polar optical phonon	-	$\mu_{po} = 1.04 \times 10^{15} \frac{\sqrt{T}(e^{T_{po}/T} - 1)(T_{po}/T)}{T_{po}}$

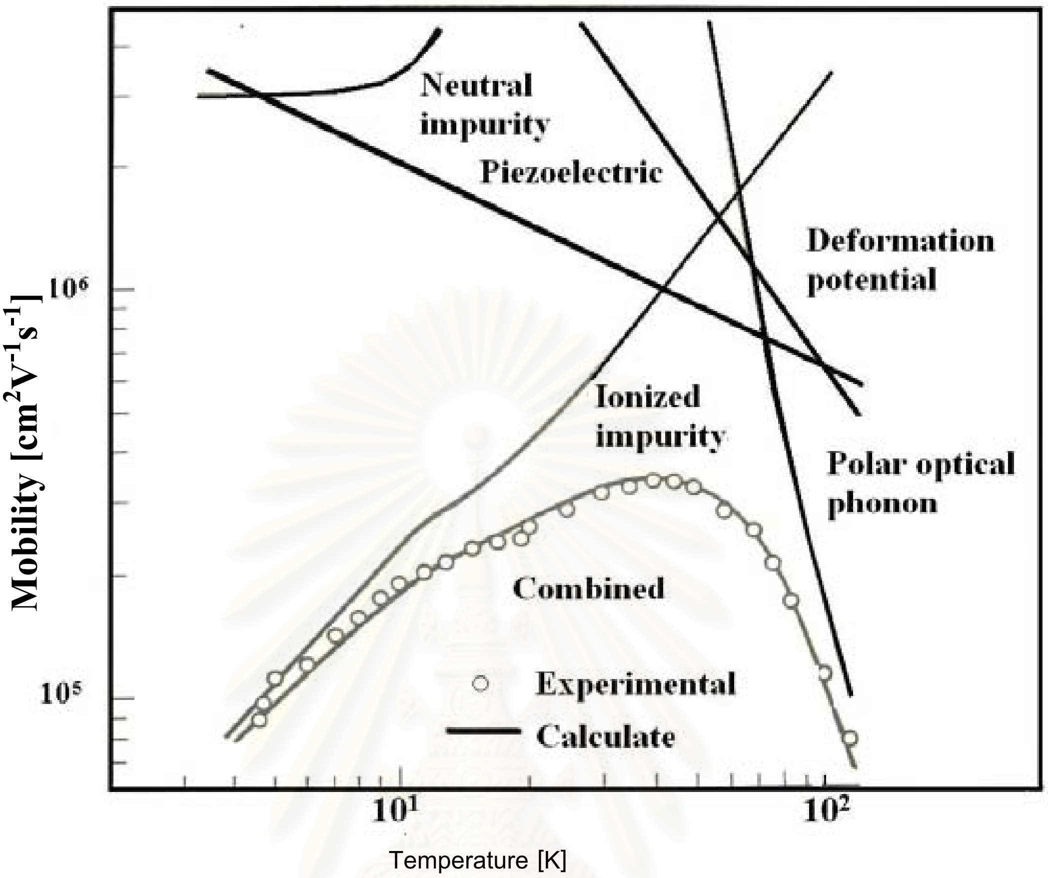

Figure 2.10: The scattering mechanism of GaAs versus temperature[4].

CHAPTER III

VAN DER PAUW AND HALL MEASUREMENT SETUP

In this chapter, the details of semi-automated electrical properties measurement system for thin samples based on the van der Pauw and the Hall effect technique, the schematic diagram of the measurement and the experiment setup will be described.

3.1 Design Concept

The van der Pauw and the Hall effect measurement system consists of a current source, a digital multimeter for voltage measurement and a data acquisition

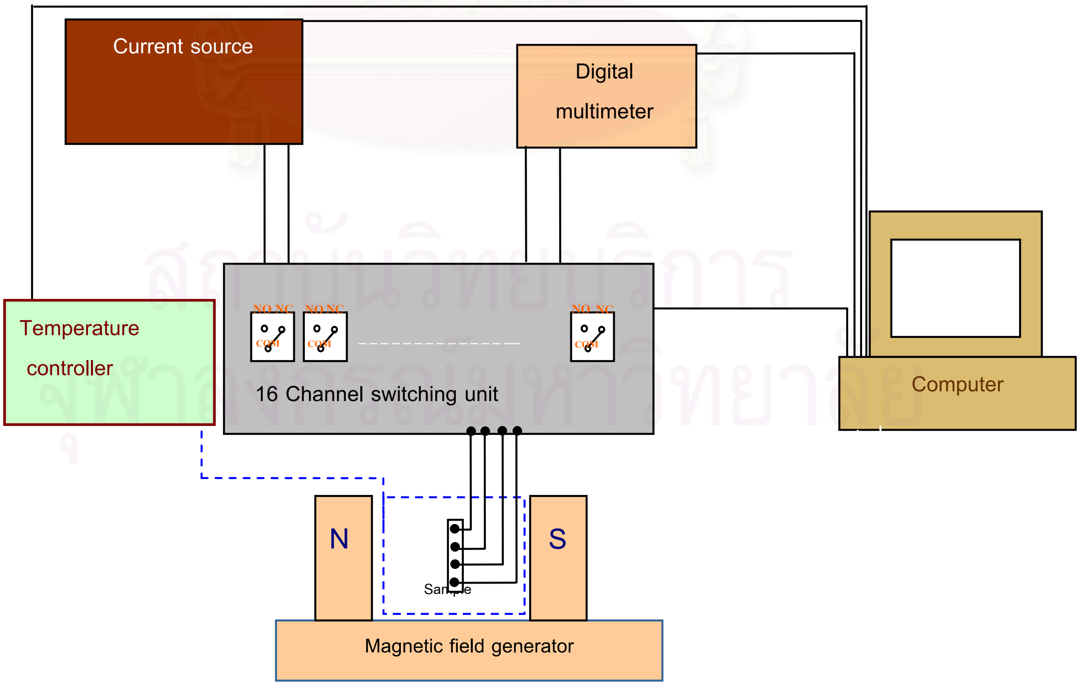

Figure 3.1: The schematic diagram of the van der Pauw and Hall measurement setup.

(relay switching unit) connecting together by a computer interface. The principle of the operation is that the current is applied to the sample between two points, and then the digital voltmeter is used to measure the voltage drop across the other two points. To change the configurations, both the current source and the voltmeter are switched by a set of relay switches controlled by a computer. Figure 3.1 shows the schematic diagram of the equipment setup of the van der Pauw and Hall effect measurement system.

3.1.1 Operation Flow Chart

The van der Pauw and the Hall measurement method is the technique used to characterize the electrical properties of materials. However, our system is designed for the samples with low resistivity. The flow chart of the van der Pauw and the Hall effect measurement system is shown in Fig. 3.2. The actual codes for controlling equipment and data acquisition are written on Agilent VEE version 7.5.

3.1.2 Capability of the System

- The system can be used to investigate the electrical properties of semiconductors or metals at temperature ranging from 10 K to 300 K.
- Range of applied current: 1 nA to 100 mA
- Magnetic field strength: ~ ± 800 mT

3.2 Equipment and their Functions

To achieve the reliable van der Pauw and Hall measurement system, the equipment used need to have high precision.

In this section, the details of equipment for the van der Pauw and Hall measurement system will be briefly described.

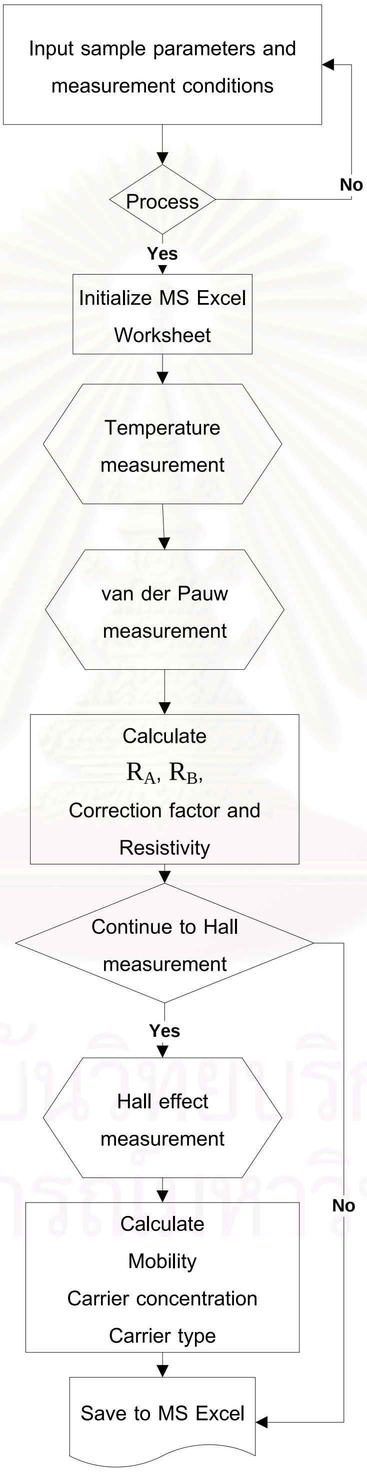

Figure 3.2: Flow chart of van der Pauw and Hall Measurement system.

Figure 3.3: The 6 ½ digital multimeter Keithey model 196.

3.2.1 Keithley 196 Digital Multimeter

The digital multimeter(DMM) is used to measure the voltage across two points on the surface of the sample. The Keithey 196 DMM (shown in Fig 3.3) 6½ multimeter is chosen and can measure the voltage in the range of ± 0.0000001 to ±300.00000 Volts. The rate of sampling time of the digital multimeter can be set between 1 ms to 3 ms. The range of selected voltage and the sampling rate of the digital multimeter can be chosen at the front panel or by the computer-controlled program. For the computer-controlled program, auto range and sampling rate of 3 ms are selected. The interfacing system between the DMM and the computer is General Purpose Interface Bus (GPIB).

3.2.2 Keithley 237 High Voltage Source Measure Unit

To generate the stable current, the Keithley 237 high voltage source measure unit as shown in Fig. 3.4 is used as a current source. The current source can provide a wide range of current from 1 nA to 100 mA, thus it can be used for a certain range of value resistance of samples.

Figure 3.4: The current source Keithley Model 237

3.2.3 Agilent 34970 Data Acquisition and 34903A Switching Unit

Agilent data acquisition model 34970 and the 34903A switching unit as shown in Fig 3.5 are used together to change the configurations of the measurement. The 34903A module consists of twenty relay switches which only sixteen of them are used in the setup. Each corner of the sample is connected to four relay switches and linked to the current source and the voltage measuring device. The properties of relays in this equipment are summarized in Table 3.1.

Figure 3.5: Agilent data acquisition model 34970 and the relay switching unit 34903A.

Table 3.1: The maximum input of the relay switch.

Input function	Maximum value
voltage	300 V
current	1 A
switching power	50 W

3.2.4 Magnetic Core

In order to measure the Hall effect, the constant magnetic fields are required. The magnetic fields are controlled by a current flowing through two sets of coil. The direction of the magnetic field can be switched by changing the polarity of the current source. The magnetic core used in this set up is shown in Fig 3.6. The strength of the magnetic field is calibrated versus the applied current using a magnetic Hall probe. The magnetic field strength at the position of the sample was found to be 794 mT and 814 mT depending on the polarity of the applied current. These numbers are used as the parameter in calculating the mobility and the carrier concentration.

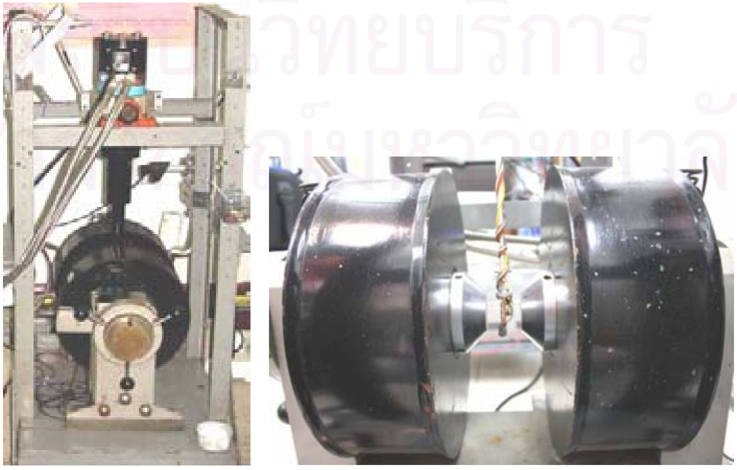

Figure 3.6: The magnetic core used in the Hall effect measurement system.

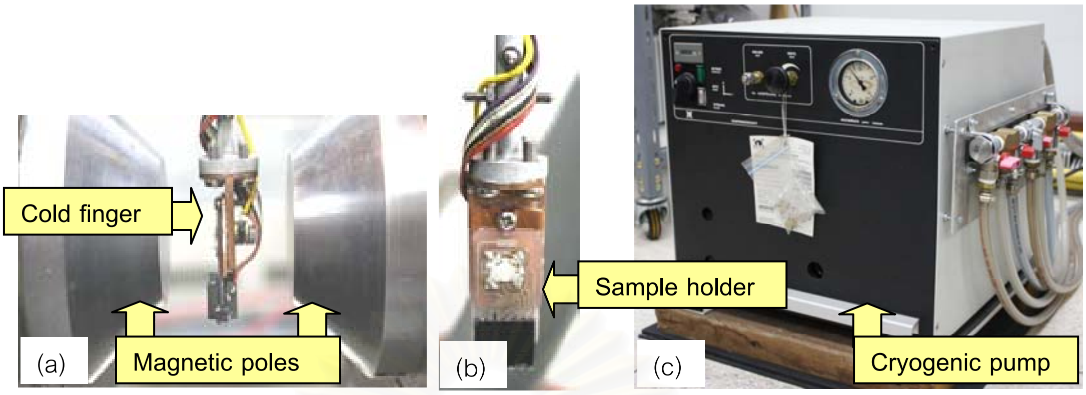

Figure 3.7: The cold finger and He-compressor used for low temperature measurement (a) The cold finger and magnetic poles, (b) The cold finger of sample holder, (c) The Leybold type RW2 cryogenic pump.

3.2.5 Cryogenic System

To obtain the resistivity, mobility and carrier concentration of samples at room temperature, the designed van der Pauw and Hall effect measurement system can be used in a simple manner. But for temperature dependent measurement, a cryogenic system is required. The cryogenic system consists of a cold finger; a closed cycle He-compressor and a vacuum pump. The Leybold type RW2 cryogenic is used in this setup and shown in Fig. 3.7.

3.2.6 Chiller

The water cooling tank is also necessary for cooling the magnetic field coils and the He-compressor to prevent the over heat of the coil and is used as the heat exchange for the He-compressor.

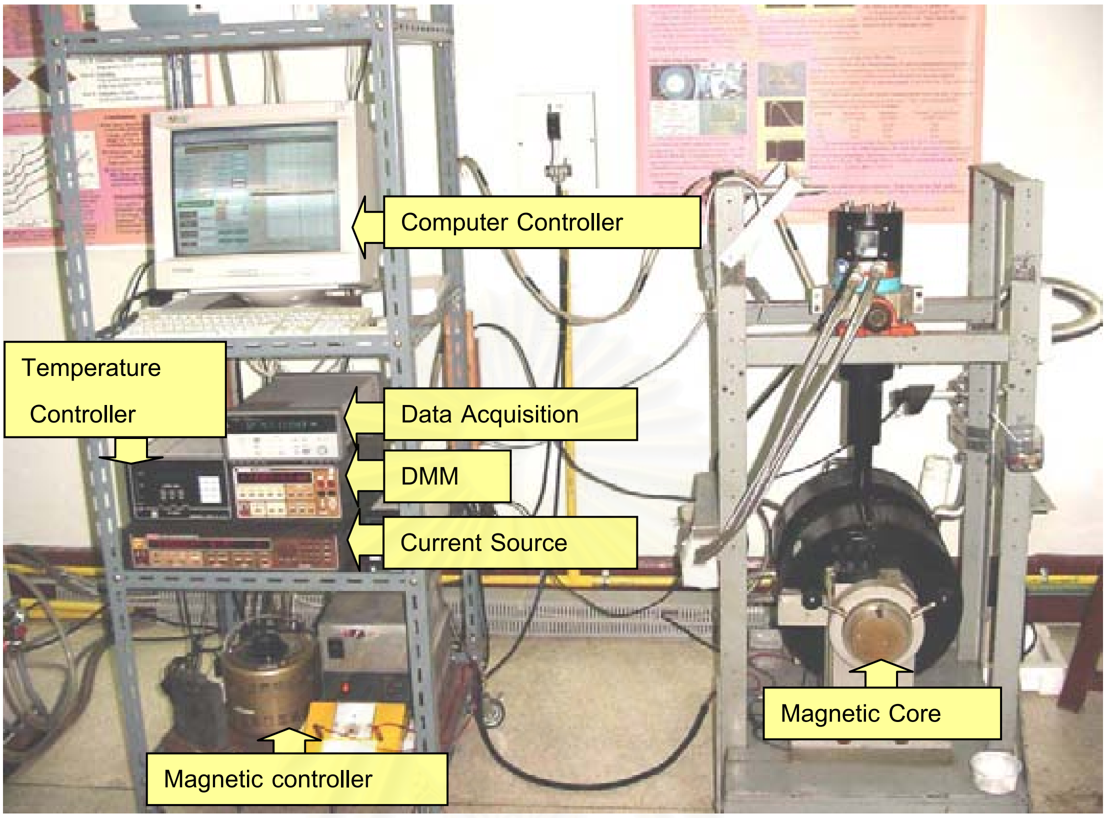

Figure 3.8: The complete setup of van der Pauw and Hall measurement system.

3.2.7 Temperature Controller

To investigate the temperature dependent measurement, two temperature sensors are used to read the temperature of the cold finger. One is the silicon diode sensor used to measure the temperature at the head of the vacuum chamber. Another silicon diode sensor is used to obtain the temperature near the sample holder. The temperature controller is used to keep temperature constant and also for the read-out for the investigation of the temperature dependent measurement. The complete setup of the van der Pauw and the Hall effect measurement system is shown in Fig. 3.8.

3.3 Interfacing and Wiring of the System

3.3.1 Wiring up the 34903A Relay Switches and the Sample Holder

The cable connections between the commercial Agilent 34903A relay switches which consist of the twenty-channel-relay switches and the sample holder are done through the commercially available DB9 connectors. The user can change between the room temperature probe and the low temperature probe by using this connector. Only sixteen relays are used in a group of four which are connected to one corner of the sample. These relays are connected to both the digital multimeter and the current source. Figure 3.9 shows the wiring of the 34903A together with the voltmeter, current source, DB9 connector and the sample holder.

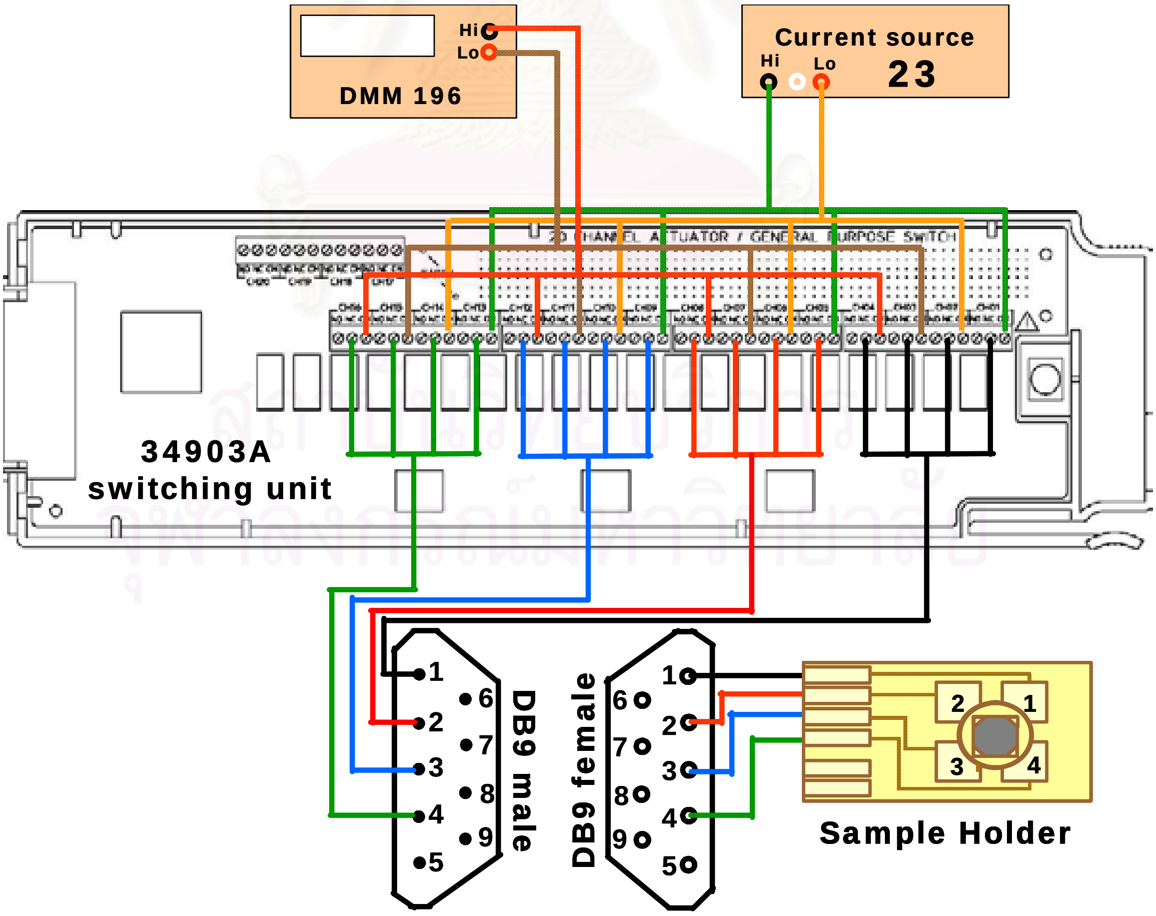

Figure 3.9: The connection of the relay switch 34903A and DB9 connectors.

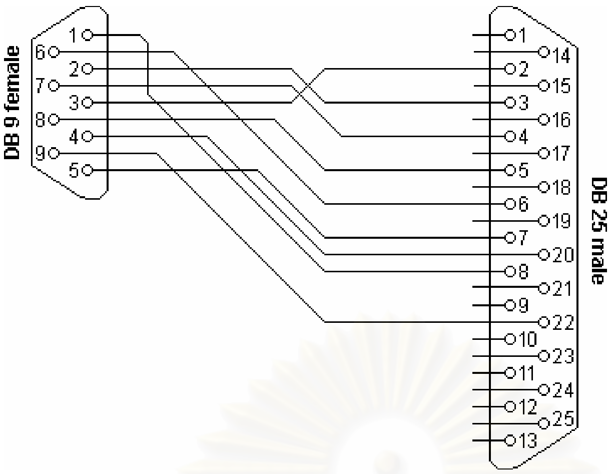

Figure 3.10: The DB9 and DB25 connecting for the temperature controller and PC.

3.3.2 Connection between the Temperature Controller and the PC

In order to control the temperature controller, RS232 serial interface is preferred. To connect the temperature controller to a computer, the correct type of interface cable must be used. The DB9 connector is used to connect to the serial port of the computer and the DB25 is used to connect to the temperature controller. Figure 3.10 describes the connection pins between the DB9 and DB25 connectors.

3.4 Semi-Automatic Control

This section describes the procedure of semi-automated van der Pauw and Hall effect measurement program.

The first part is to input the data into the program as shown on the upper left region in Fig. 3.11. The information input are such as the file name, sample name, sample thickness, the measured resistance of the sample, the magnetic field strength also the name of user. The first output information is from the van der Pauw measurement. The value of applied current and the reading voltage are plotted real time and used for the calculation of R_A and R_B, as described in chapter 2.

The values of R_A and R_B are then used to obtain the correction factor and the resistivity, also previously described in chapter 2. Note that the plot of R_A and R_B also give the information of whether or not the contacts are Ohmic. After the resistivity is obtained, the program continues to determine the mobility and carrier concentration from the Hall effect measurement.

The details of Agilent VEE control code will be described in the following section. For the low temperature measurement, after the user click start button at the upper left, the temperature measurement part will be operated and described by the labeling numbers in Fig 3.12.

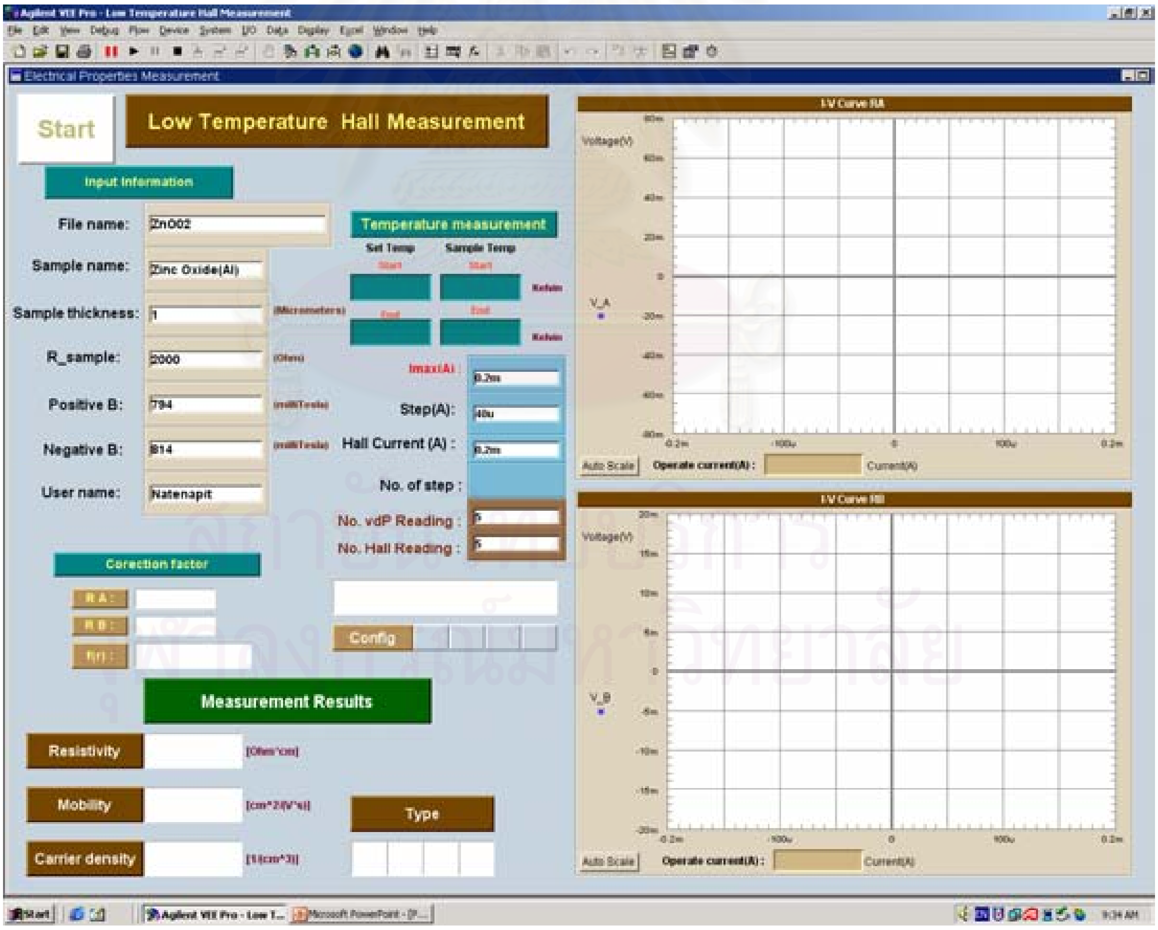

File name: ZnO02

Sample name: Zinc Oxide(Al)

Sample thickness: 1 (Micrometers)

R_sample: 2000 (Ohms)

Positive B: 794 (milliTesla)

Negative B: 814 (milliTesla)

User name: Natenapit

Imax(A) : 0.2m

Step(A): 40u

Hall Current (A) : 0.2m

No. vdP Reading : 5

No. Hall Reading : 5

Figure 3.11: van der Pauw and Hall Measurement Program interface.

In the temperature measurement sections, the codes which can be separated in four parts are described. The upper two parts are the temperature measurement at the started program codes where another two parts in the lower region are the codes for the end of temperature measurement. The label no. 1 in Fig. 3.12 is the control code for the LTC60 temperature controller. The outputs from the temperature controller consist of both string and number. The label in no. 2 and no. 3 are used to remove the string from the output, only the number is selected. Next, label no. 4 is for showing the measurement values and will be saved to the selected cell in label no. 5. The T1 and the t1 in label no. 4 stand for the measured temperature at the top of the cold finger and the measured temperature close to the sample holder, respectively. The measured temperature at the sample holder during the low temperature Hall effect measurement is used to identify the name of the initialized MS Excel spreadsheet. The following labels no. 6 and no.7 are the codes to combine the measured temperature with the informed filename.

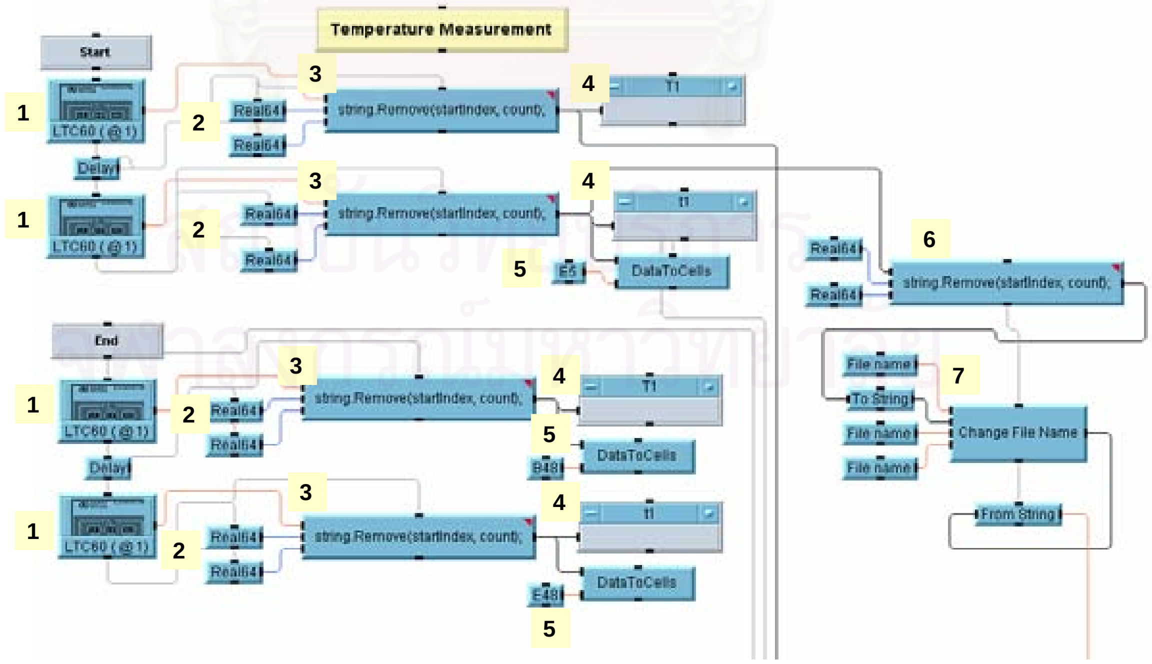

Figure 3.12: The Agilent VEE code on temperature measurement part.

Next, the set of the voltage measurement codes which are used in both van der Pauw and Hall effect measurement are shown. These set of codes are used in several parts in this program such as two configurations of voltage measurement, V_{R_A} and V_{R_B}, in the vdP part as shown in Fig. 3.13 and four configurations of measured voltage in Hall measurement as shown in Table 3.3. The codes in the Fig 3.14 are started at the Agilent 34901A data acquisition which is switched to the selected configuration in label no. 1. Then, the number of counts from the informed input will be collected in the label no. 2 as a number of measurement loops and used in the label no. 3. Following by label no. 4, the default of digital voltmeter is set and waiting for the next command. The informed current is collected in the label no. 5. After that the collected data are used in label no. 6 as a generate current from the Keithley 237 current source to the sample and then display the value in the label no. 7. The label ‘Get DMM’ in no. 8 is collected the number of informed voltage measurement then used in labels no.9 and no. 10. Following by the voltmeter Keithley 196 control label in no. 10 is the measured voltage across the selected configuration then, the raw data are shown in label no. 11 and collected in the sliding collector in the label no. 12. Then, the average of the measurement voltage is calculated in the label no. 13 and then show in label no. 14. The set of average value is shown in the code no. 15 and the number of value in these set are corresponding to the number of informed loop.

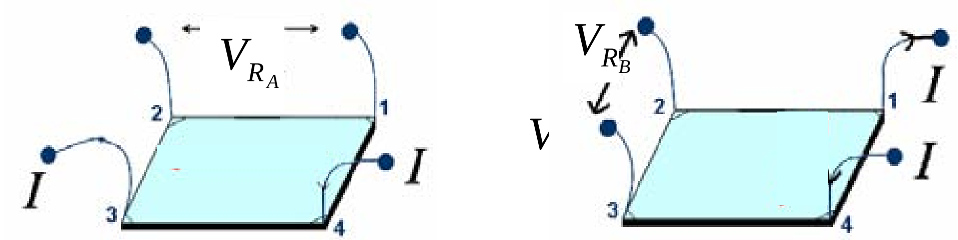

Figure 3.13: The configurations in the van der Pauw measurement V_{R_A} *and* V_{RB}.

Table 3.3: Configurations for the Hall effect measurement.

Configuration	**No Magnetic field**	**Positive Magnetic field**	**Negative Magnetic field**
Hall 1 **1324**	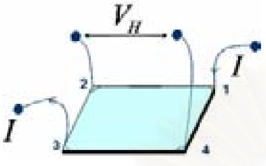	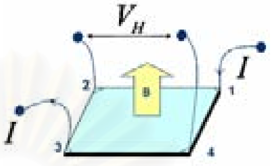	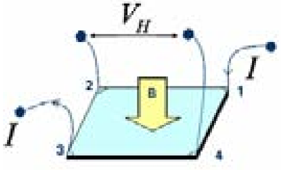
Hall 2 **3124**	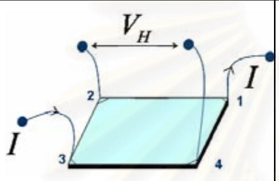	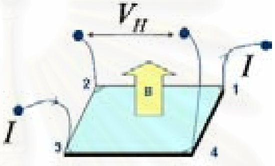	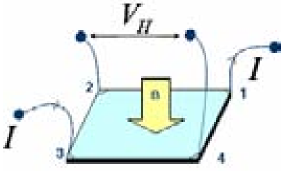
Hall 3 **4213**	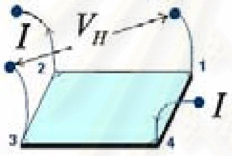	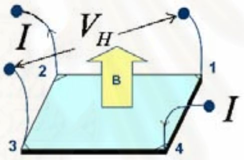	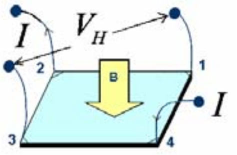
Hall 4 **2413**	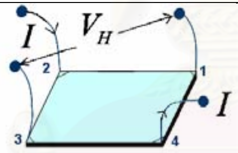	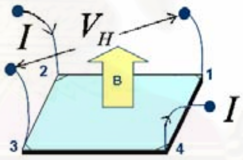	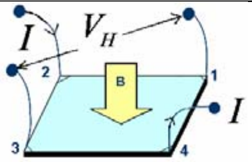

The labels no. 16 and no. 17 are shown the save of the output data to the cell in Ms excel. Then, the applied current and measured voltages are plotted on the right region of the program. The label no. 19 is used to turn the current source to standby following by the switching unit in label no. 20 is turned the relay off before the next configuration is performed.

The results in the previous description i.e. the applied current and the measured voltage are used to obtain the resistance value as described in Eq. (2.33), chapter 2. In Fig. 3.15, the calculation codes for the resistance calculation R_A and R_B are shown.

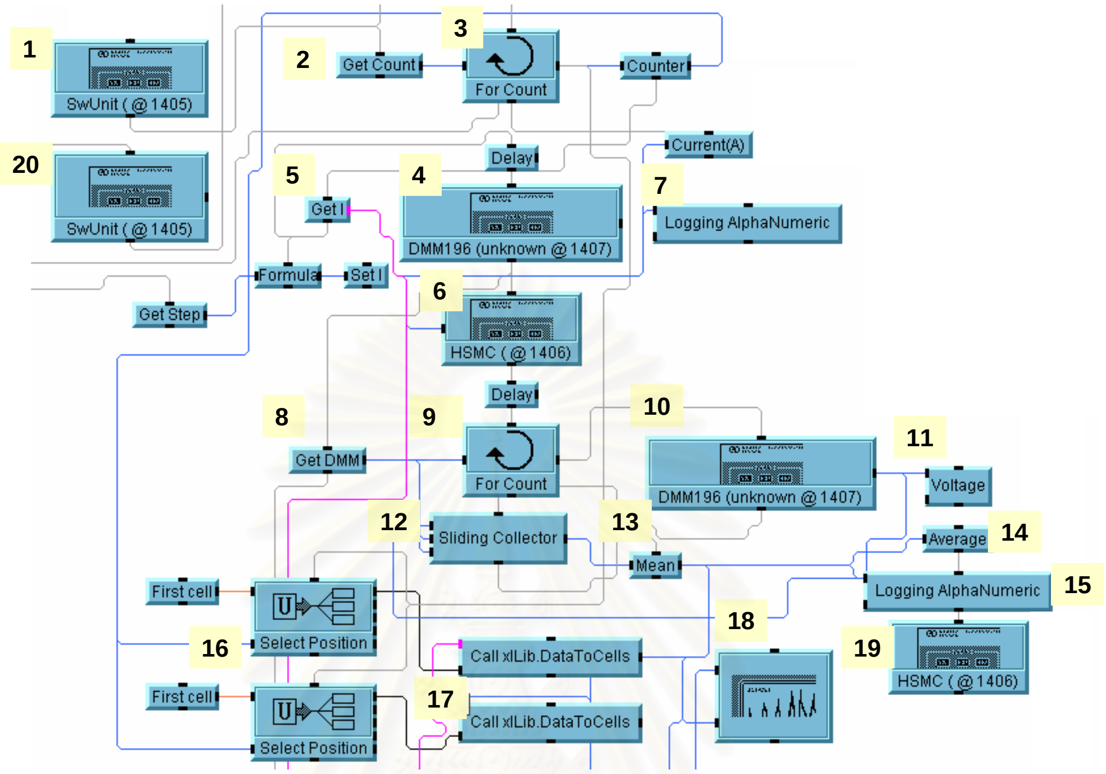

Figure 3.14: The set of voltage measurement codes using in vdP and Hall measurement.

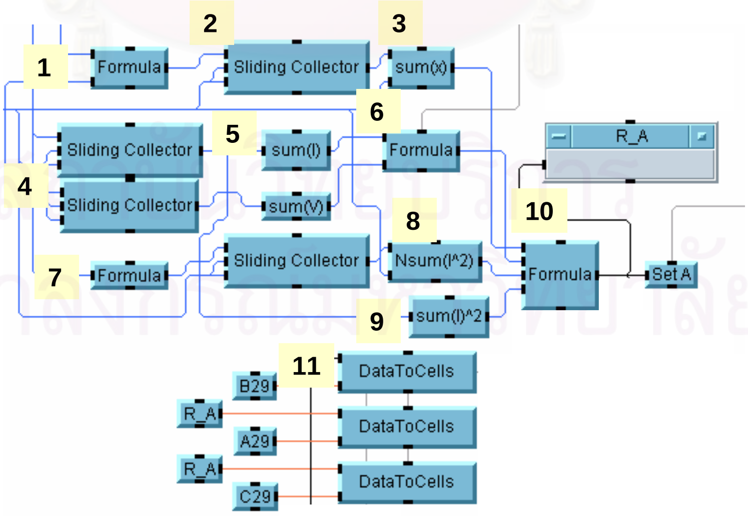

Figure 3.15: The calculation code of R_A and R_B.

The label no. 1 is the multiplication of applied current and measured voltage before collecting them in the label no. 2, then summarized in the label no.3. The next labels no. 4 to no. 6 are collected for the applied current and measured voltage then summarized in label no. 5 and multiplied them in label no. 6. Labels no. 7 shows the square of current and multiply by the number of measurements in label no. 8. The last part is the square of the summation current in the label no. 9. These calculation parameters are used to evaluate the resistance value both R_A and R_B which is written in Eq. (2.33) and will be shown in label no.10. The calculated resistance R_A and R_B will be used to obtain the correction factor and resistivity.

The correction factor calculation code is shown in Fig. 3.16. The investigated resistance value R_A and R_B are used as a parameter for correction factor evaluation as shown in label no. 1 and label no. 2. Then, label no.3 in this section is compared the ratio of the two resistance values. If the result is less than 1.5, the step of correction factor calculation will be 0.0001 in the upper part of the codes. The lower part shows the case of the ratio value more than 1.5, then the number 0.001 is used as a step of this investigation. The calculation of the correction factor is described in details in chapter 2, section 2.2. The set of codes in the upper and lower part of the Fig. 3.16 will be explained as the followings. Start at the label no. 4, the loop of calculation then, label no. 5 shows the calculation of step in the correction factor evaluation and the result which shown in label no. 6 is the used correction factor. The obtained resistances in the previous section are collected in the label no. 7. Then, all parameters are fitted in Eq. (2.23) in the label no. 8 and are shown in the label no. 9. Next, the label no. 10 is compared for the two sides of Eq. (2.23), then, the obtained correction factor is shown in label no .12. This loop will terminate in label no. 13 when the results both sides of this equation are equal.

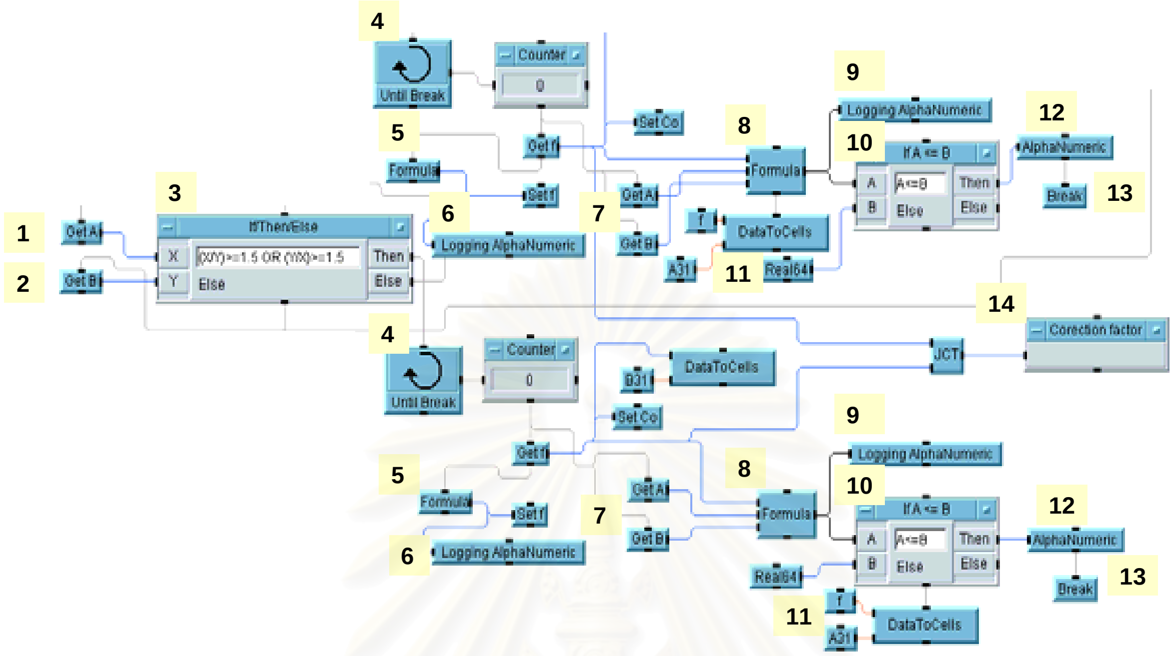

Figure 3.16: Evaluation of the correction factor.

The next expression code is the resistivity calculation shown in Fig. 3.17. The first parameter Pi = 3.14 is used in label no.1. The following, label no. 2 is the expression of the value $\ln(2)$. Next, the label no. 3 is the thickness of the sample. The labels no. 4 to no. 6 are for the calculated resistances R_A, R_B and the correction factor, respectively. All parameters are used to calculate the resistivity in label no. 7, then the labels no. 8 to no .10 are the values of resistivity and its unit. The results of the obtained resistivity is shown in the label no. 11.

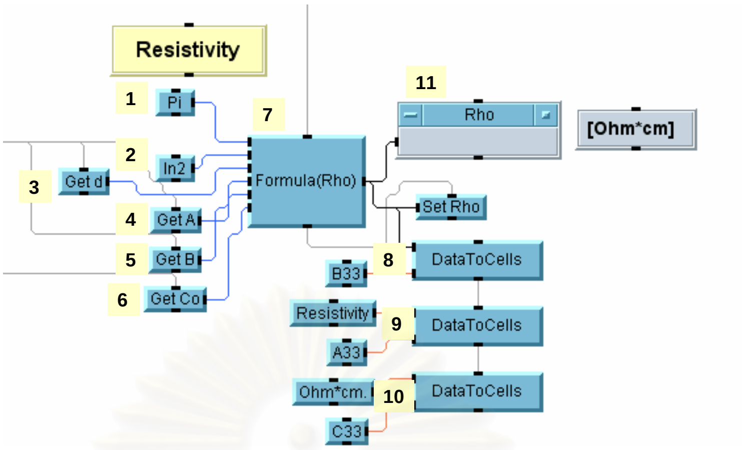

Figure 3.17: The resistivity calculation.

Moving to the Hall effect calculation section, the calculated resistivity is used as a parameter for carrier concentration and the mobility calculation which will be described in Fig. 3.18. These codes show the Hall effect calculation which are two measurement results. In the upper region, the carrier concentration is calculated where as the mobility is investigated in the lower region. The carrier concentration calculation consists of five parameters which are expressed in the labels no. 1 to no. 6 and evaluates in the label no. 7. The label no. 1 collectes both the positive and negative magnetic field strength before calculating the average value in label no. 2. Next, label no. 3, q is electronic charge which is equal to 1.602×10^{-19} C. The following label no. 4 is the applied current in the Hall effect measurement and the label no. 6 is the different of the measured voltage with the magnetic field and without the magnetic filed calculation. The last label in no. 5 is the thickness of the sample. The result of carrier concentration is obtained and shown in the label no. 7 and no.8, then saved in the code no.9.

Finally, the last calculation is the Hall mobility which is shown in the lower set of codes in the Fig 3.18. Three parameters are used in this calculation i.e. the carrier concentration in the label no. 10, the resistivity in the label no. 11 and the electronic charge q in label no. 12.

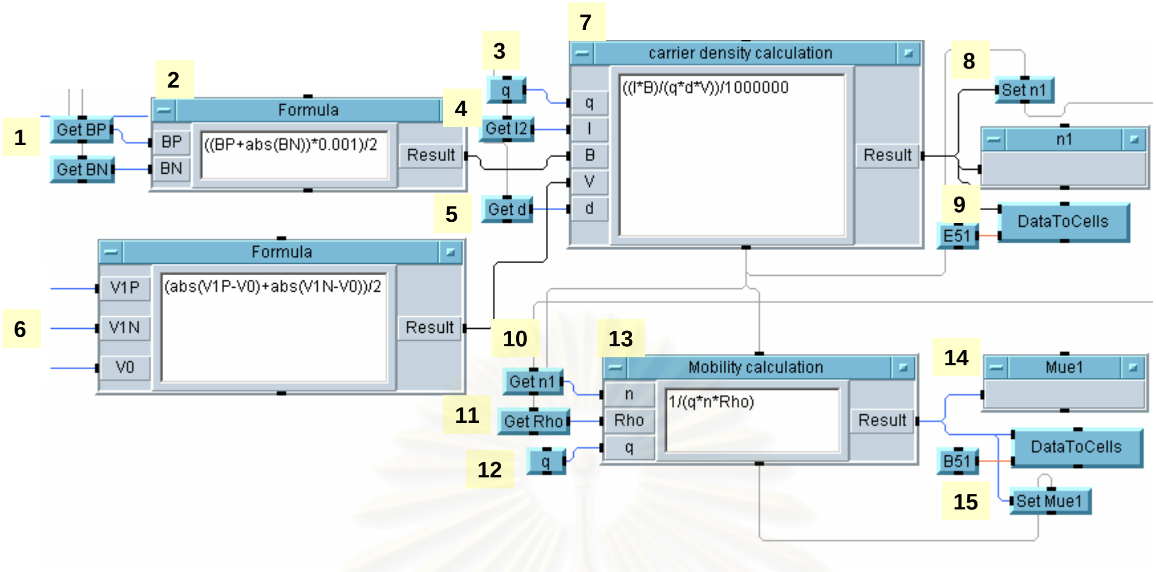

Figure 3.18: Calculate average mobility and carrier concentration.

This set of codes is corresponds to the Eq. (2.38) or Eq. (2.39) in chapter 2 depend on the major carrier. Label no. 13 is for the calculation, then the result is shown in label no. 14 and save in the label no. 15.

The saved results in every set of codes are reported in the MS Excel as shown in Fig. 3.19. The vdP section is report in the row no. 1 to row no. 24. The rows no. 1 to row no. 4 and the row no. 6 are the input data whereas row no. 5 shows the measured temperature at the start of the measurement. The next row no. 8 to row no. 18 shows the raw data of the average applied current and the average measured voltage. In the row no. 20 to row no. 24 are the evaluated results of the resistance R_A, R_B, the correction factor and the resistivity, respectively.

The row no. 25 to row no. 48 are reported as the results of the Hall effect measurement section. Row no. 26 and row no. 27 shows the used magnetic field strength. Row no. 29 to row 40 are the average data of the measured voltage of the Hall configuration with and without the magnetic field.

As shown in Table 3.3, there are four configurations for Hall effect measurement. Row no. 42 to row no. 45 reported the calculated mobility and carrier concentration of these configurations. Then the average of them is shown in row no. 47. The last row in the report shows the measured temperature at end of the measurement.

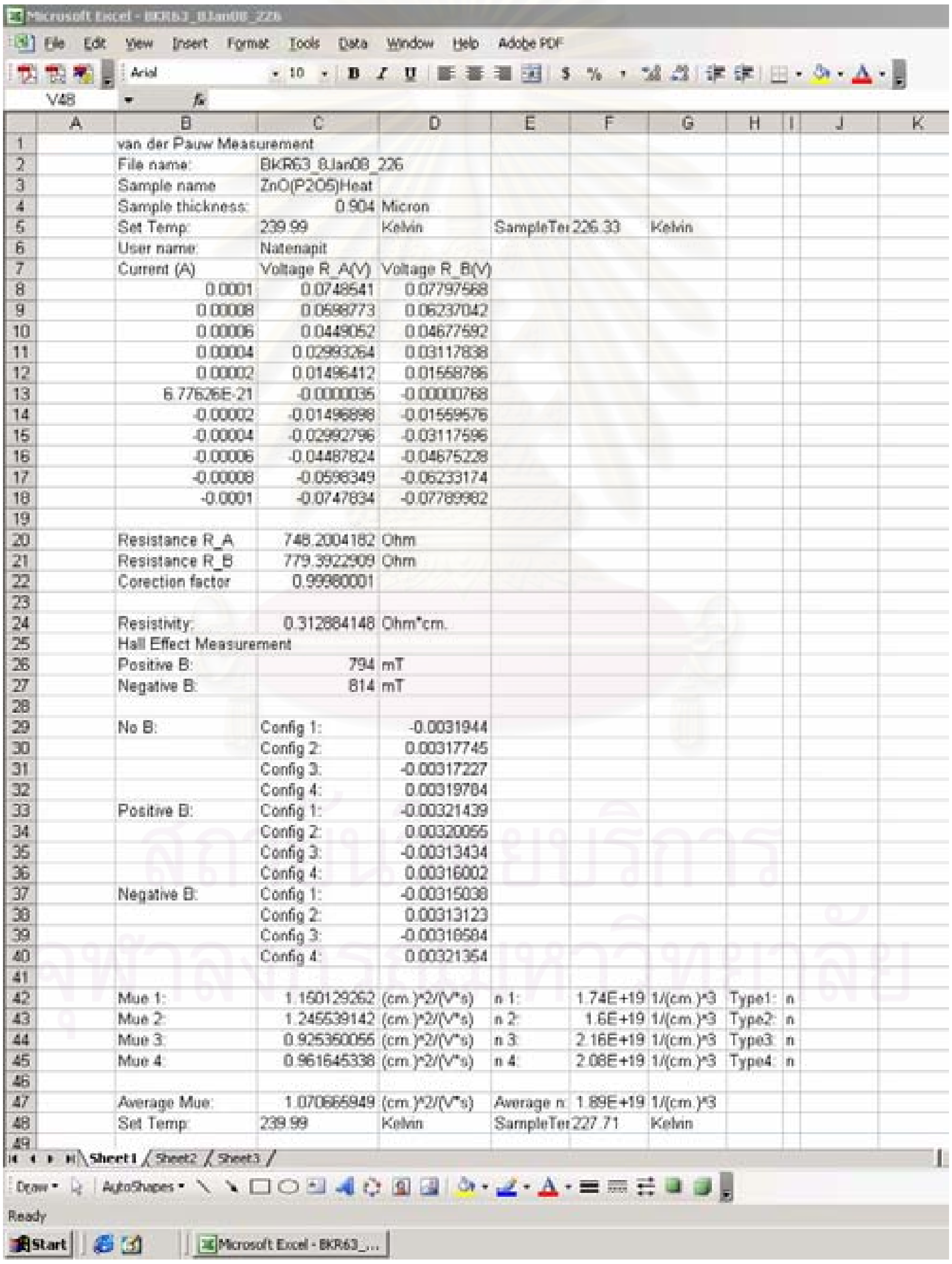

	A	B	C	D	E	F	G	H	I	J	K
1		van der Pauw Measurement									
2		File name:	BKR63_8Jan08_226								
3		Sample name	ZnO(P2O5)Heat								
4		Sample thickness:	0.904	Micron							
5		Set Temp:	239.99	Kelvin	SampleTe	226.33	Kelvin				
6		User name:	Natenapit								
7		Current (A)	Voltage R_A(V)	Voltage R_B(V)							
8		0.0001	0.0748541	0.07797568							
9		0.00008	0.0598773	0.06237042							
10		0.00006	0.0449052	0.04677592							
11		0.00004	0.02993264	0.03117838							
12		0.00002	0.01496412	0.01558786							
13		6.77626E-21	-0.0000035	-0.00000768							
14		-0.00002	-0.01496898	-0.01559576							
15		-0.00004	-0.02992796	-0.03117596							
16		-0.00006	-0.04487824	-0.04675228							
17		-0.00008	-0.0598349	-0.06233174							
18		-0.0001	-0.0747834	-0.07789982							
19											
20		Resistance R_A	748.2004182	Ohm							
21		Resistance R_B	779.3922909	Ohm							
22		Corection factor	0.99980001								
23											
24		Resistivity:	0.312884148	Ohm*cm.							
25		Hall Effect Measurement									
26		Positive B:	794	mT							
27		Negative B:	814	mT							
28											
29		No B:	Config 1:	-0.0031944							
30			Config 2:	0.00317745							
31			Config 3:	-0.00317227							
32			Config 4:	0.00319784							
33		Positive B:	Config 1:	-0.00321439							
34			Config 2:	0.00320055							
35			Config 3:	-0.00313434							
36			Config 4:	0.00316002							
37		Negative B:	Config 1:	-0.00315038							
38			Config 2:	0.00313123							
39			Config 3:	-0.00318584							
40			Config 4:	0.00321354							
41											
42		Mue 1:	1.150129262	(cm.)^2/(V*s)	n 1:	1.74E+19	1/(cm.)^3	Type1:	n		
43		Mue 2:	1.245539142	(cm.)^2/(V*s)	n 2:	1.6E+19	1/(cm.)^3	Type2:	n		
44		Mue 3:	0.925360055	(cm.)^2/(V*s)	n 3:	2.16E+19	1/(cm.)^3	Type3:	n		
45		Mue 4:	0.961645338	(cm.)^2/(V*s)	n 4:	2.08E+19	1/(cm.)^3	Type4:	n		
46											
47		Average Mue:	1.070665949	(cm.)^2/(V*s)	Average n:	1.89E+19	1/(cm.)^3				
48		Set Temp:	239.99	Kelvin	SampleTe	227.71	Kelvin				
49											

Figure 3.19.: The MS Excel report of the van der Pauw and the Hall effect measurement program.

To check the results from the designed program, the manual program was designed. This consists of the same equipment as the semi-automatic one but some of the control parts were controlled in the front panel of the equipment. These will make the results more reliable. Figure 3.20 is the screen of manual program using for configuration check.

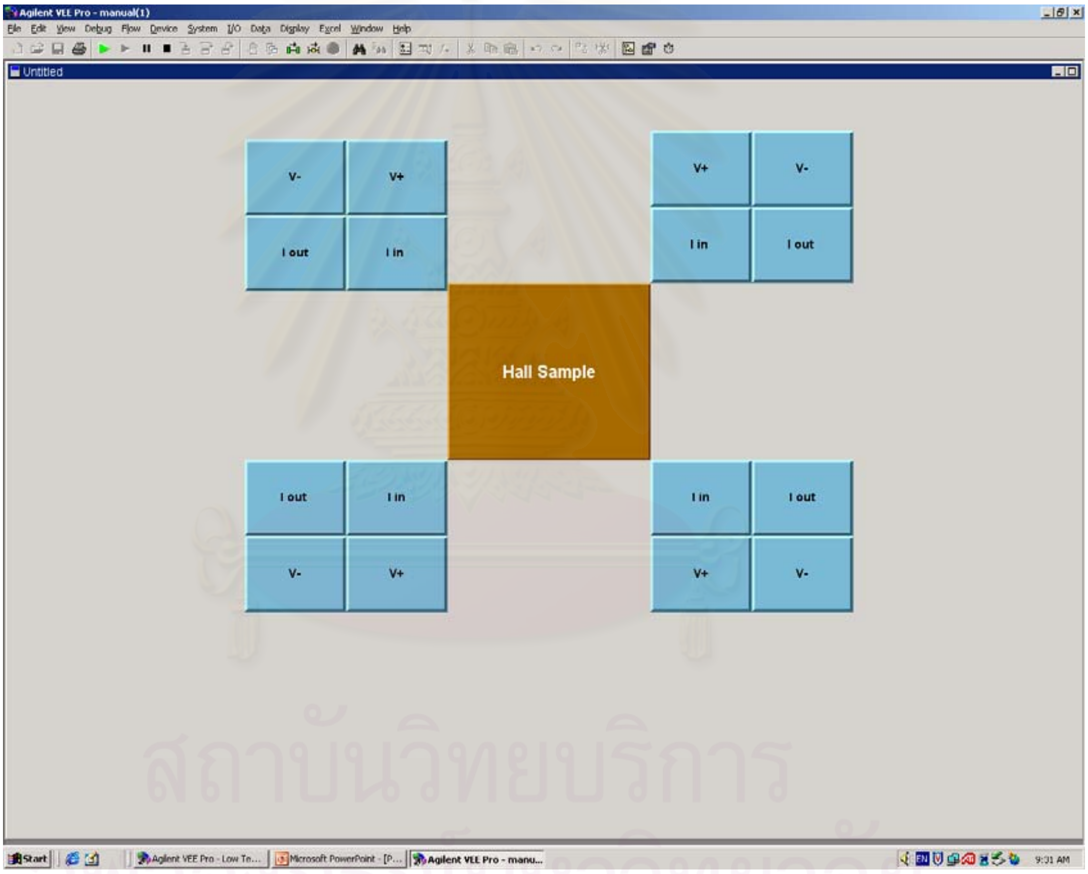

Figure 3.20: The manual program which user can control at the front panel of the equipment.

3.5 Sample Preparation

In order to use the van der Pauw method, the width and the length of the sample must be much larger than the sample thickness. The errors in calculations can be reduced by making the sample symmetrically. The thin film materials with the area of less than 5 mm × 5 mm were prepared in this experiment.

3.5.1 Sample Holder

The sample holder is made from a piece of Copper and a printed circuit board (PCB) glued together by special binder Master Bond EP30FL epoxy that consists of two parts mixed together by the weight ratio of 4 Part A:1 Part B. Here, we use 10 g of Part A and 2.5 g of Part B. The mixed binder should be gentle stirred and the bubbles should be avoided during the stirring process. The dimensions of the sample holder are;

(i) 2 mm thick Copper plate should be cut into 2.5 cm × 1.5 cm.
(ii) printed circuit board (PCB) of 2.5 cm × 1.5 cm.

The final the shape should be in the shape of 3.5 cm × 1.5 cm as shown in Fig. 3.21.

3.5.2 Preparation of Ohmic Contact

In order to use the van der Pauw method, four Ohmic contacts are also required at four corners of the sample. They must be placed on the boundary of the sample as small as possible.

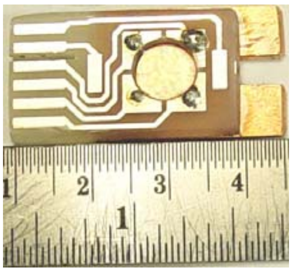

Figure 3.21: The 3.5 cm × 1.5 cm using in the Hall Effect measurement system.

These contacts are metal to semiconductor contacts. The Ohmic contact is a low resistance junction which providing conduction in both directions between the metal and the semiconductor. Ideally, the current through the Ohmic contact is a linear function of the applied voltage. The contact preparation is the most important step in the measurement process.

3.5.2.1 Preparation of Shadow Mask for Evaporation of Metal Contacts

The following procedures describe how to prepare the masks at the four corners. A glass slides are used as a base of the sample and the Aluminum foil is wrapped tightly around the glass slide. Then, the 5 mm×5 mm sample is placed on the wrapped glass slide and covered with Aluminum foil again as shown in Fig 3.22 (a). A small rod rolled over the surface of glass slide to eliminate the air bubble. After that, a small pin is used to make a hole at the corners as shown in Fig 3.22(b). The metal can then be evaporated and deposited at the opening corners on the sample surface.

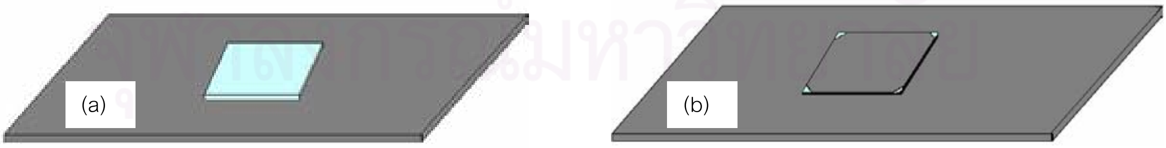

Figure 3.22: The mask preparation before thermal evaporation. (a) The sample place on the raped glass slide. (b) The required contact on the raped sample on glass slide.

3.5.2.2 Thermal Evaporation

The thermal evaporation is used to evaporate materials for Ohmic contact. The prepared glass slide with sample and the suitable Ohmic contact materials are loaded into the thermal evaporation vacuum chamber (Fig. 3.23). After the process of sample evaporation the sample should be annealed in vacuum with the pressure of about 8×10^{-6} mbar immediately.

Figure 3.23: The used equipment to evaporate Ohmic contact.

CHAPTER IV

SYSTEM CALIBRATION

To ensure that the system operates correctly and reliably, the calibration of the system was performed using a known sample. The bulk indium antimonide (InSb) wafer was used as a known semiconducting sample for the calibration. The preparation of the InSb samples and the measurement are described in this chapter.

4.1 The Properties of Indium Antimonide [7]

Indium antimonide(InSb) is a crystalline compound made from pure elements indium and antimony. It has the appearance of dark grey silvery metal pieces or powder with vitreous luster. The InSb is a semiconductor material from the III-V group with an energy gap of about 0.17 eV at 300 K and 0.23 eV at 80 K. The crystal structure is zinc blende with a lattice constant of 6.48 Å.

4.2 Preparation of InSb Samples

The bulk InSb samples were prepared by the following procedures;

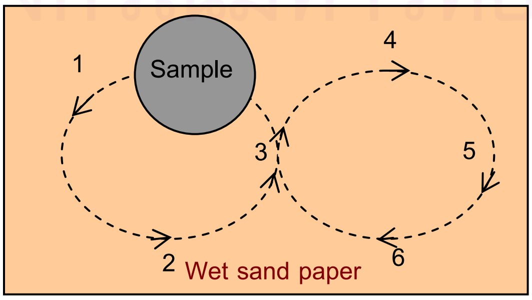

Figure 4.1: The Figure-8 polishing method.

(I) Polish the surface of the InSb wafer with a wet sand paper. The deionized water is preferred for the wetting. The sample was manually polished in a figure-8 manner, as shown in Fig. 4.1, to ensure the uniform thickness.

(II) The InSb wafer was then scribed into a 3 mm×3 mm, shown in Fig. 4.2, using a sharp tungsten needle. Then, a small cylinder was used to roll softly over the back side of the wafer along the scribed line. The sample would be cracked along the direction of the line.

(III) Sample cleaning process: The InSb samples were cleaned with solvents i.e. TCE, acetone, methanol and deionized water, respectively, in an ultrasonic bath.

(IV) Thickness of InSb sample was measured by a micrometer and summarized in Table 4.1.

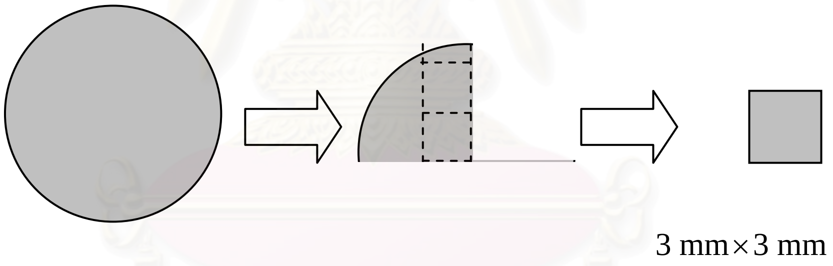

Figure 4.2: The cutting of $3\,mm \times 3\,mm$ InSb wafer.

Table 4.1: The thickness of InSb samples used for the calibration of the system.

Sample No.	**Thickness (μm)**
InSb ISC 145	420
InSb ISC 598	504

(V) Preparation of Ohmic contact: The Ohmic contact of InSb is Ni/Au. The 2,000 Å of Ni was deposited first and then followed by 1,500 Å of Au by thermal evaporation. The size of contacts was minimized and the shape is shown in Fig. 4.3(a).

(VI) Annealing process: After the evaporation of Ohmic contact, the samples were annealed in vacuum at 150 °C for 1 hour to ensure good surface contact.

(VII) Sample mounting: The samples were mounted in the sample holder as shown in Fig. 4.3(b) using a double-sided tape or silicone paste on the back side of the samples. The 0.05 mm gold wires were used to connect from the PCB to the four Ohmic contacts of the sample. We note that a double-sided tape or silicone paste used for conducting samples while silver paste can be used only for a sample with non-conducting substrate.

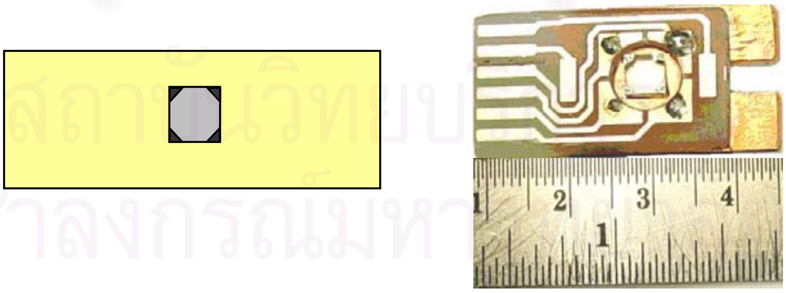

(a) (b)

Figure 4.3: (a) The shape of Ohmic contact Ni/Au on $3\,mm \times 3\,mm$ *InSb sample. (b)The InSb bulk which four corners are wired to the holder.*

4.3 Calibration Results

Tables 4.2 and 4.3 show the measurement results of electrical properties i.e. resistivity, mobility and carrier concentration of the two InSb samples for the temperature ranging from ~ 20 K to 300 K. The resulting plots of the conductivity vs. temperature are shown in Fig. 4.4, the mobility vs. temperature are shown in Fig. 4.5, and the log of carrier concentration vs. 1,000/temperature are shown in Fig. 4.6.

Table 4.2: The measurement results of InSb No. ISC 145.

Temperature[K]	**Resistivity** **[$\Omega \cdot cm$]**	**Mobility** **[$cm^2V^{-1}s^{-1}$]**	**Carrier concentration[cm^{-3}]**
20.56	6.94E-02	472,299	1.91E+14
22.60	6.75E-02	484,814	1.91E+14
32.50	5.55E-02	587,960	1.91E+14
40.54	4.83E-02	676,292	1.92E+14
50.65	4.43E-02	737,561	1.91E+14
60.82	4.55E-02	714,800	1.92E+14
76.86	5.19E-02	582,283	1.93E+14
88.98	6.03E-02	534,711	1.94E+14
101.10	7.11E-02	450,675	1.95E+14
113.73	8.41E-02	376,753	1.97E+14
127.51	9.93E-02	304,864	2.07E+14
142.05	1.16E-01	227,781	2.37E+14
156.11	1.26E-01	168,450	2.95E+14
169.25	1.17E-01	135,556	3.95E+14
180.33	9.56E-02	125,077	5.23E+14
197.01	6.10E-02	122,973	8.33E+14
209.77	4.19E-02	120,117	1.24E+15
220.13	3.08E-02	116,098	1.75E+15
242.10	1.70E-02	105,115	3.49E+15
249.59	1.41E-02	99,531	4.46E+15
259.64	1.11E-02	92,904	6.08E+15
269.68	8.82E-03	88,750	7.98E+15
280.83	7.03E-03	85,321	1.04E+16
287.26	6.24E-03	85,739	1.17E+16
300.00	4.70E-03	79,720	1.67E+16

Table 4.3: The measurement results of InSb No. ISC 598.

Temperature[K]	**Resistivity** **[$\Omega \cdot cm$]**	**Mobility** **[$cm^2V^{-1}s^{-1}$]**	**Carrier concentration[cm^{-3}]**
21.57	9.99E-02	448,463	1.40E+14
29.26	8.78E-02	511,140	1.39E+14
35.95	7.89E-02	563,732	1.40E+14
45.11	7.16E-02	621,415	1.40E+14
55.12	6.99E-02	634,533	1.41E+14
64.62	7.26E-02	611,593	1.41E+14
77.15	8.06E-02	544,016	1.43E+14
85.17	8.95E-02	485,791	1.44E+14
94.56	1.00E-01	421,073	1.48E+14
105.26	1.14E-01	347,682	1.57E+14
114.59	1.29E-01	283,183	1.71E+14
123.02	1.44E-01	226,738	1.91E+14
133.40	1.59E-01	178,976	2.20E+14
144.10	1.75E-01	137,553	2.60E+14
152.66	1.79E-01	113,864	3.06E+14
186.07	8.97E-02	101,625	6.86E+14
203.10	5.71E-02	102,700	1.07E+15
211.91	4.35E-02	102,670	1.40E+15
223.74	3.10E-02	103,627	1.95E+15
231.18	2.51E-02	101,950	2.44E+15
238.77	2.03E-02	99,329	3.10E+15
244.70	1.75E-02	96,391	3.71E+15
256.06	1.35E-02	92,691	5.00E+15
262.68	1.15E-02	89,161	6.08E+15
274.60	8.91E-03	83,107	8.44E+15
287.94	6.87E-03	78,247	1.16E+16
300.00	5.14E-03	67,325	1.81E+16

Figure 4.4 shows that the conductivity of InSb in the temperature range 50 K to 200 K is relatively constant corresponding to the conduction of the ionized impurity carriers which is independent of temperature. The increasing of the

conductivity above 200 K is due to the increasing of intrinsic carriers and it increases exponentially with temperature.

It was found that the mobility of the carriers, shown in Fig. 4.5, was rising to the maximum value 737,561 cm^{2}V^{-1}s^{-1} and 634,533 cm^{2}V^{-1}s^{-1} for the sample no. 145 and no. 598, respectively in the temperature range below 50 K. Then, it starts to decline with the increasing temperature in the range of 50 K to 150 K.

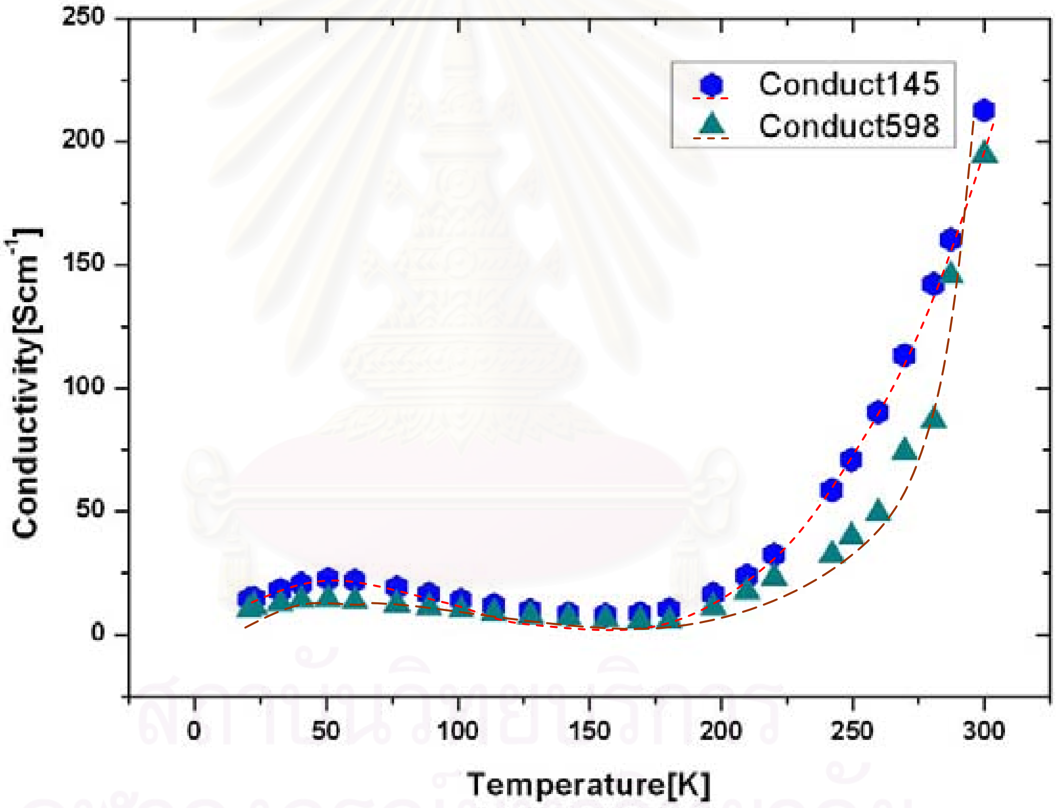

Figure 4.4: The temperature dependent of InSb conductivity.

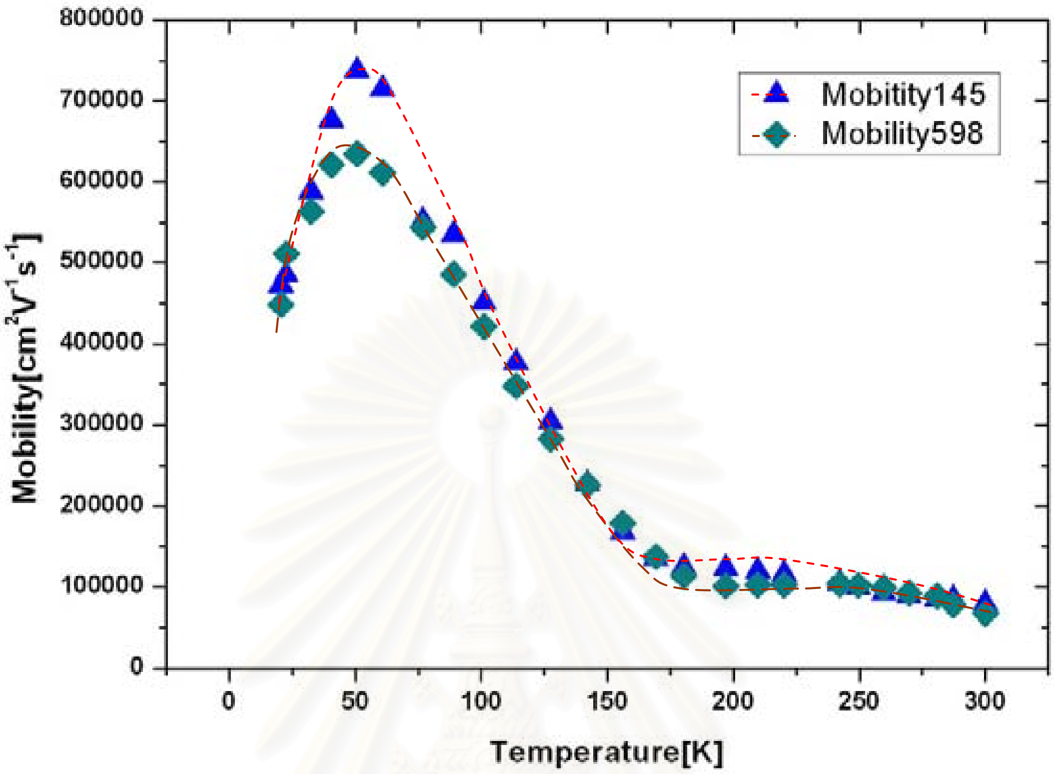

Figure 4.5: The plot of InSb mobility versus temperature.

This result corresponds to the scattering mechanisms as seen in other materials such as GaAs which was a contribution of several scattering mechanisms as shown in chapter 2, Fig. 2.10. The mobility was somewhat independent of temperature throughout the high temperature range (200K to 300 K) of measurement with the average value of about 100,000 cm^{2}V^{-1}s^{-1}.

One can also see that the carrier concentration of both InSb samples can be divided into two regions. The first one is for the temperature above 100 K carrier concentration are rising with increasing temperature, which is due to the nature of intrinsic carriers, where for the temperature below 100 K carrier concentration are constant which is due to the extrinsic carriers, as shown in Fig. 4.6. This agrees with the theory discussed in appendix A.

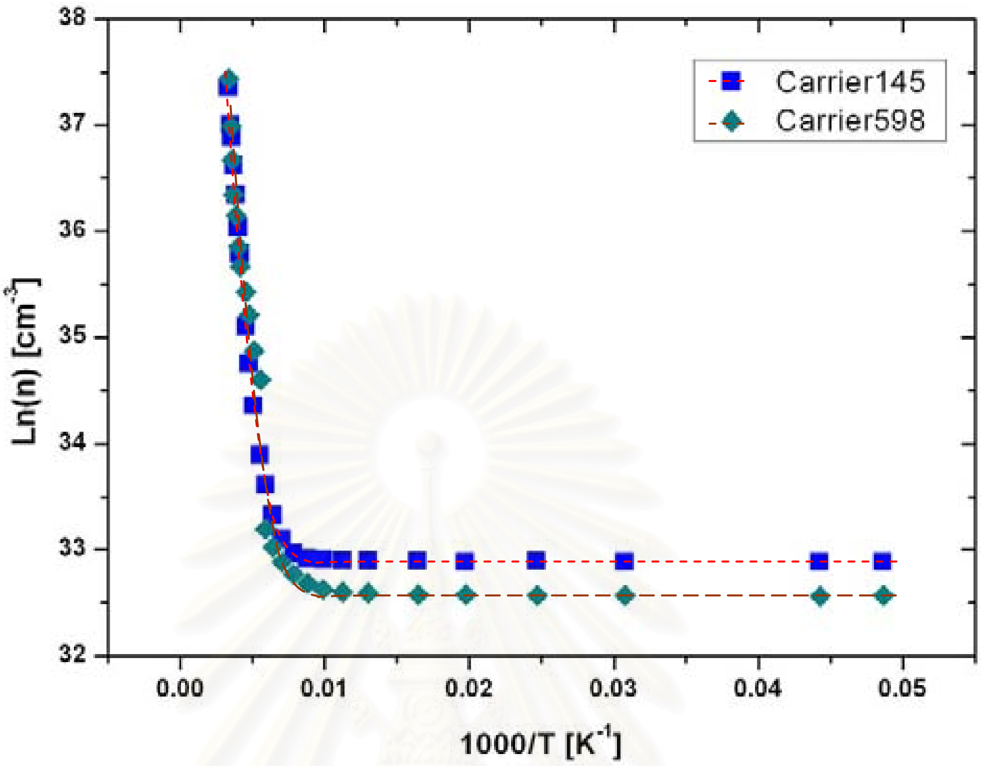

Figure 4.6: The plot of InSb carrier concentration and inverse temperature.

The measurements of the InSb samples at 77 K compared with the certificate obtained from the manufacturer are shown in the Table 4.4. It is obviously seen that the results obtained from our system are in the range issued by the manufacturer. However the electrical properties can be varied over time, the results of the carrier mobility of InSb ISC145 is slightly out of the specified range.

Table 4.4: Comparisons of the measurement results and the certificate of InSb @77K.

Sample @ 77K	**Resistivity** $[\Omega \cdot cm]$	**Mobility** $[cm^2/Vs]$	**Carrier Concentration** $[1/cm^3]$
Certificate of ISC145	0.044 – 0.095	510,200 - 552,600	1.19 - 2.78 $\times 10^{14}$
Measurement of ISC 145	0.052	582,283	1.93×10^{14}
Certificate of ISC 598	0.041 - 0.087	502,800 - 568,900	1.27 - 3.06 $\times 10^{14}$
Measurement of ISC 598	0.081	544,016	1.43×10^{14}

4.4 Conclusion

The calibration of system was performed on the known semiconducting material, i.e. InSb. The manufacturer certificates were used to verify the calibration. The InSb samples were prepared with uniform thickness and the Ohmic contacts were achieved by thermal evaporation of Ni/Au. The resistivity, mobility and carrier density of the InSb were measured by the designed computer-controlled system. The measurement results are consistent with the manufacturer certificates. Thus the computer-controlled van der Pauw and the Hall effect measurement system can be used to investigate the electrical properties.

CHAPTER V

ELECTRICAL PROPERTIES OF INDIUM TIN OXIDE THIN FILM

In this chapter, the van der Pauw and the Hall effect measurement system are used to perform the measurements of the electrical properties of the Indium Tin Oxide (ITO). The ITO thin films used here were fabricated in the laboratory and had never been characterized for their temperature dependent electrical properties.

5.1 Introduction

Indium-Tin-Oxide (ITO) is one of promising materials used in optoelectronics devices, including photovoltaic devices, since it can be fabricated in such a way that it exhibits very high optical transparency as well as being a good conductor. In particular, the n-type ITO films have been used as a transparent conducting window layer in many thin film solar cells [8]. The good transparent conducting oxide (TCO) films should have high optical transparency and low electrical resistivity. Many groups in the community have performed experiments to investigate the scattering mechanisms of ITO films in the recent years [9]. Nevertheless the results are still inconsistent. Here, low temperature van der Pauw and Hall measurements was used to perform the temperature dependence of electrical properties, i.e. resistivity, mobility and carrier density of the ITO films.

From the classical theory of electrical transport of conventional semiconductors, the temperature dependence of the electrical conductivity can be determined from the convolutions of temperature dependence of the relaxation time for various scattering processes for carriers, i.e. τ_n for electrons, and τ_p for holes. In general, the mobility is a function of these relaxation times of the scattering processes. There are two major interaction mechanisms affecting carrier mobility. One is the mobility from the lattice scattering process μ_L, and another the mobility from the ionized impurity scattering process μ_I. These two mechanisms follow the temperature dependence as [10]

$$\mu_L \propto T^{-3/2},$$

$$\mu_I \propto T^{3/2},$$

where T is absolute temperature. The net mobility μ can be obtained from

$$\frac{1}{\mu} = \frac{1}{\mu_L} + \frac{1}{\mu_I}. \qquad (5.1)$$

In addition to those mechanisms, scattering from other contributions, such as grain boundary, etc., may be added to Eq. (5.1).

For the high carrier concentration ($n > 10^{20}$) of ionized impurity or heavily doped semiconductors or sometime called degenerate semiconductors, the external dopants are assumed to be the defects of such semiconductors including the ITO materials. These defects are the main scattering center of the charged carriers. When the charged carriers are scattered by impurity ions the energy dependence of mobility is given by [10]

$$\mu_I = \frac{e}{m^*}\tau_i(E_F)$$
$$= \left(\frac{2}{m^*}\right)^{1/2} \frac{\varepsilon^{1/2} E_F^{3/2}}{\pi e^3 N_i Z^2} \frac{1}{\ln\left(1+\frac{\varepsilon E_F}{N_i^{1/3} Z e^2}\right)^2}, \qquad (5.2)$$

where $\tau_i(E_F)$ is the relaxation time of the scattering process near the Fermi level E_F, ε is the static dielectric constant of the films, m^* is the effective mass of electrons, Ze is the charge of the ion core and N_i is the concentration of impurity scattering centers. From Eq. (5.2), we could see that the ionized impurity scattering mobility of degenerate semiconductors is independent of temperature.

At high temperature range, the contribution of lattice vibration scattering is given by [10]

$$\mu_L = \frac{e\pi^2\hbar^4 c_{11}}{2m^*(2m)^{3/2}\Delta_c^2 N}\frac{E^{-1/2}}{kT}, \qquad (5.3)$$

where c_{11} is elasticity constant modulus, Δ_c is the divergence of strain and N is concentration of matrix atoms. From Eq. (5.3), at $E = E_F$, the mobility is proportional to $1/T$.

The lattice vibration scattering of degenerate semiconductor dominates the mobility at high temperature, however, the carrier concentration is independence of temperature.

Grain boundaries scattering in polycrystalline form the potential barrier between two crystallites. The barriers affect the mobility due to the grain boundary scattering and is given by [11]

$$\mu_g = AT^{-\frac{1}{2}} e^{-(eV_B / kT)}, \qquad (5.4)$$

where V_B is the potential barrier between the grain boundaries and A is a constant. In the degenerate semiconductors, Fermi–Dirac statistic is more appropriate than Maxwell–Boltzmann statistic, thus the mobility in Eq. (5.4) can be expressed as [12]

$$\mu_g = BT^{-1} e^{-(eV_A / kT)}, \qquad (5.5)$$

where $V_A = V_B - (E_F - E_c); E_F - E_c$ is the distance between Fermi level and the bottom of conduction band. For the high carrier concentration, the mobility from grain boundary may be neglected.

5.2 Fabrication and Preparation of ITO Thin Films

The ITO thin films were deposited on soda-lime glass substrates by RF magnetron scattering technique at different substrate temperatures of 60°C, 230°C, 270°C and 300°C using the sputtering power of 80 W and the sputtering gas pressure of 6×10^{-3} mbar. The sputtering target consists of 90% In_2O_3 and 10% SnO_2. The fixed and varying parameters used in this fabrication are shown in the Table 5.1. The average optical transmission of the obtained ITO thin films is above 90% in the visible region [8]. Figure 5.1 shows the transparency of fabricated ITO thin films. Electrical contacts to the ITO films were made by the thermal evaporation of Ni/Al to ensure Ohmic contacts. In order to use the van der Pauw method, four Ohmic contacts are required and connected with gold wires to the sample holder which is mounted on the cold finger of the closed cycle refrigerator. Ideally, the applied current and the voltage measurement must be linear for a good Ohmic contact. The ITO films were cooled down using the closed-cycle He cryogenic system to 25 K and heated up to room temperature for the electrical properties measurements.

5.3 Measurements of Electrical Properties

The electrical properties of the polycrystalline ITO thin films were investigated by the van der Pauw and the Hall effect measurements. The measurement results are concluded in Table 5.2. The Hall effect measurements by the measuring of Hall voltage (V_H) indicated that all the carriers of ITO thin films were n-type. Figures 5.2 to 5.5 show the plot of resistivity and mobility vs. 1/temperature of the ITO thin films fabricated with the substrate temperatures of 60°C, 230°C, 270°C and 300°C, respectively.

In Fig. 5.2, it can be seen that, below 100 K, the resistivity of the ITO films fabricated at 60°C is independent of temperature whose value is about 3.25×10^{-3} $\Omega\cdot$cm and rising to about 3.65×10^{-3} $\Omega\cdot$cm at room temperature. The rising of the resistivity with increasing temperature suggests that the ITO thin film behaves like a conductor, i.e. the contribution from the lattice vibration dominates at high temperature range. The mobility measurement also shows the same behavior at low temperature, i.e. it is constant with the average value about 35.5 cm^2/Vs at temperatures below 100 K and gradually decreases to about 31 cm^2/Vs at room temperature.

Table 5.1: The parameters used in the Indium Tin Oxide fabrication process.

Fixed parameters	
RF sputtering power	80 Watt
Target – Substrate distance	4.5 cm
Sputtering gas pressure	6×10^{-3} mbar
Oxygen patial pressure	0.5 %
Sputtering time	10 minutes
Varying parameters	
Substrate temperature	60, 230, 270, 300 ˚C

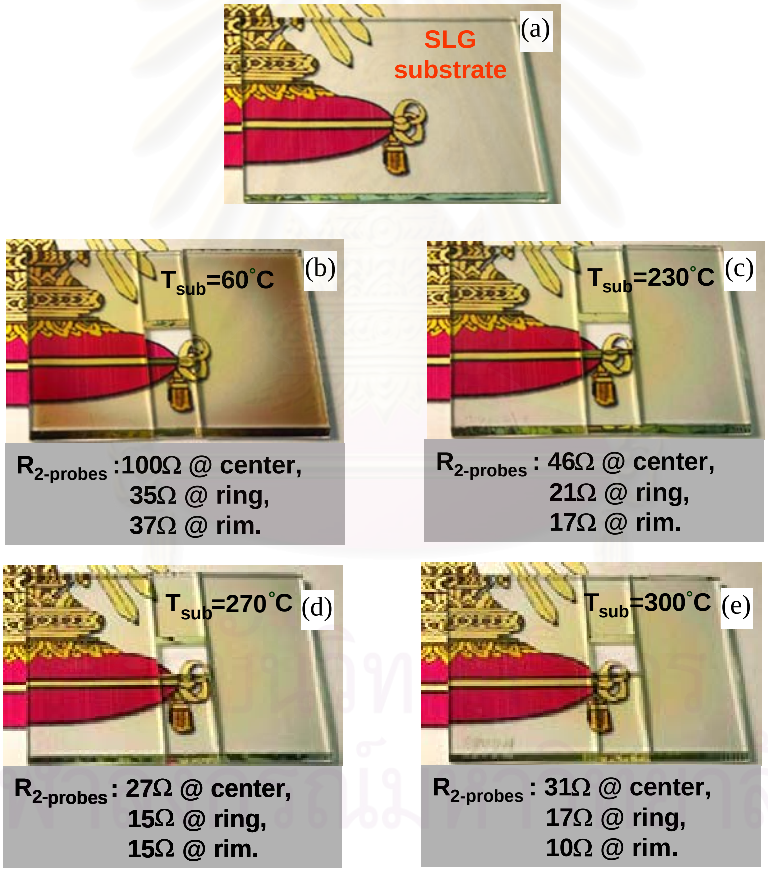

Figure 5.1: The picture of (a) soda lime glass substrate and the Indium Tin Oxide substrate temperatures were varied from (b) 60 ˚C, (c) 230 ˚C, (d) 270 ˚C and (e)300 ˚C.

Table 5.2: The measurement results of electrical properties of ITO.

Substrate Temperature in the Fabrication of ITO Film	**Resistivity [Ω·cm]**		**Mobility [cm^2/Vs]**
	Measurement Temperature < 100 K	**Measurement Temperature > 100 K**	
60 ˚C	3.25×10^{-3}	3.25×10^{-3}-3.65×10^{-3}	31-35.5
230 ˚C	1.76×10^{-3}-1.73×10^{-3}	1.73×10^{-3}-1.77×10^{-3}	24.5-25
270 ˚C	1.08×10^{-3}	1.08×10^{-3}-1.12×10^{-3}	31-32.5
300 ˚C	1.25×10^{-3}-1.24×10^{-3}	1.24×10^{-3}-1.28×10^{-3}	28-30.6

Figure 5.3 shows the results of ITO films fabricated with the substrate temperature of 230 ˚C. The resistivity starts to decline in the low temperature from 25 K to 100 K and increasing for the temperature range above 100 K. It is also shown that many interaction mechanisms affect carrier mobility and the values are varied about 24-25 cm^2/Vs.

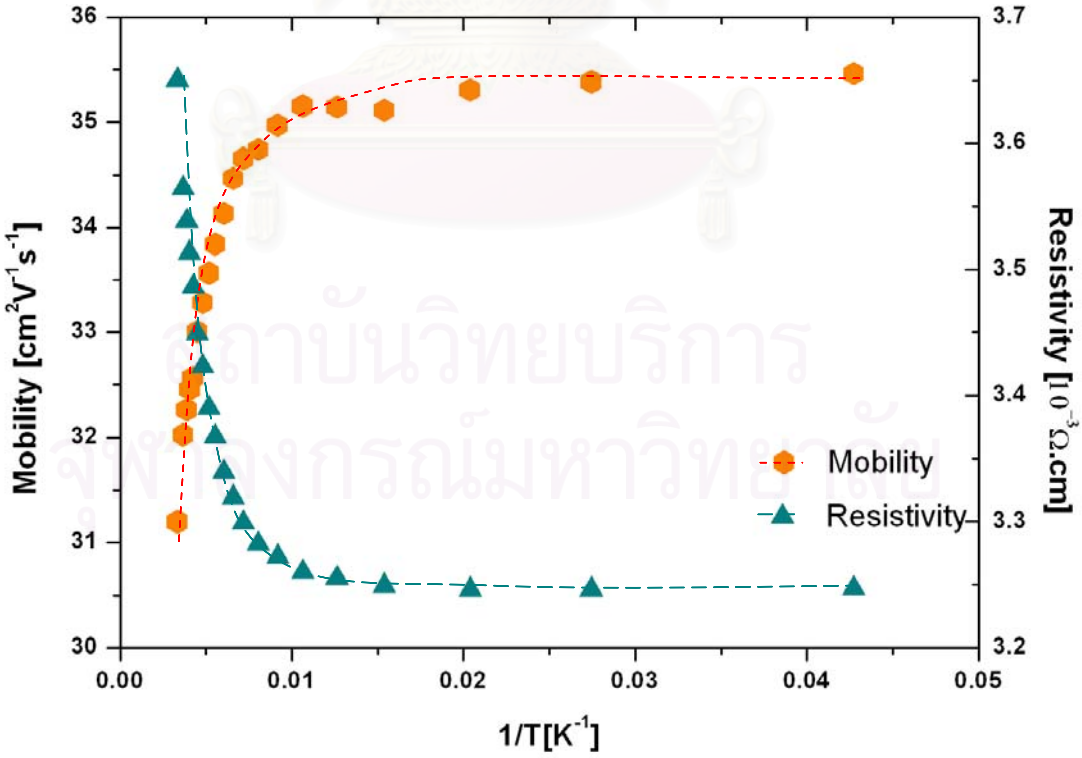

Figure 5.2: The relation between resistivity and mobility of the Indium Tin Oxide film with substrate temperature 60 ˚C.

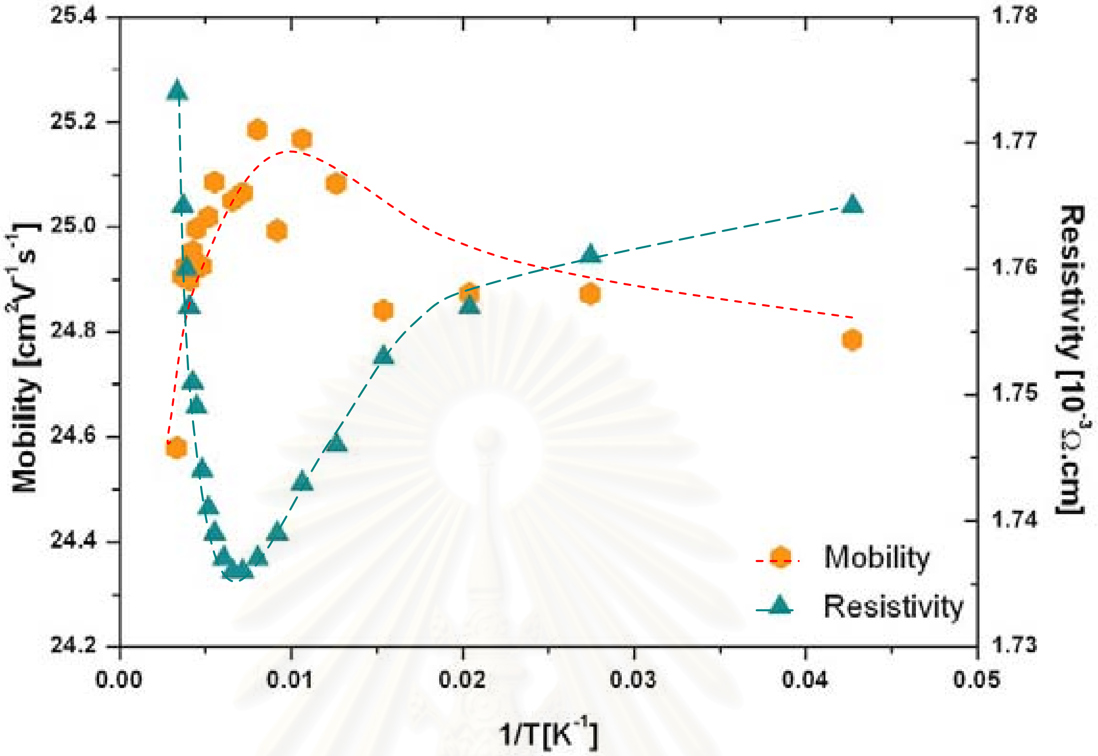

Figure 5.3: The plot between temperature and electrical properties of Indium Tin Oxide with 230 ˚C substrate temperature.

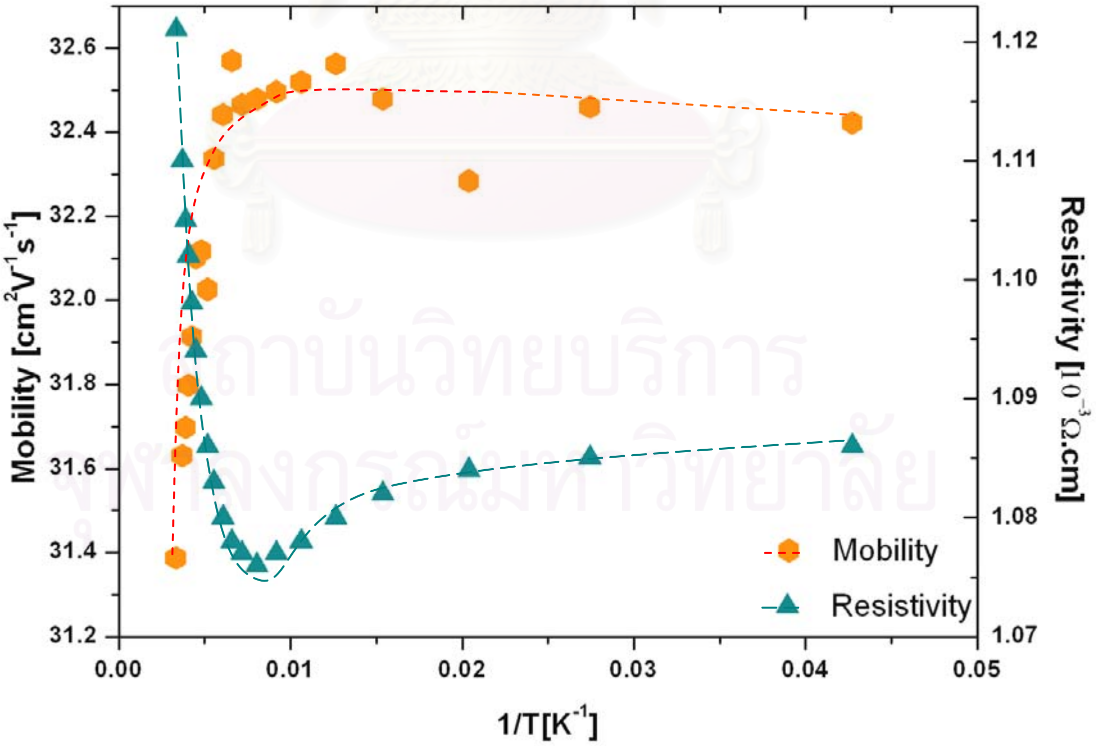

Figure 5.4: The plot of 270 ˚C Indium Tin Oxide electrical properties versus temperature.

Figure 5.4 shows the resistivity of the ITO thin film fabricated at 270 ˚C. It's values varied in the range of 1.07×10^{-3} Ω·cm to 1.08×10^{-3} Ω·cm at temperature below 100 K and rising to 1.12×10^{-3} Ω·cm in the range of temperature between 100 K up to room temperature. On the other hand, the mobility is invariant, about 32.5 cm^2/Vs, at temperature below 100 K and start to decline at temperature between 100 K up to room temperature.

The measurements of the resistivity and the mobility for the ITO thin films fabricated with the substrate temperature of 300˚C is shown in Fig. 5.5. It can be seen that the resistivity varies between 1.24×10^{-3} -1.26×10^{-3} Ω·cm below 100 K before rising to about 1.27×10^{-3} Ω·cm at room temperature.

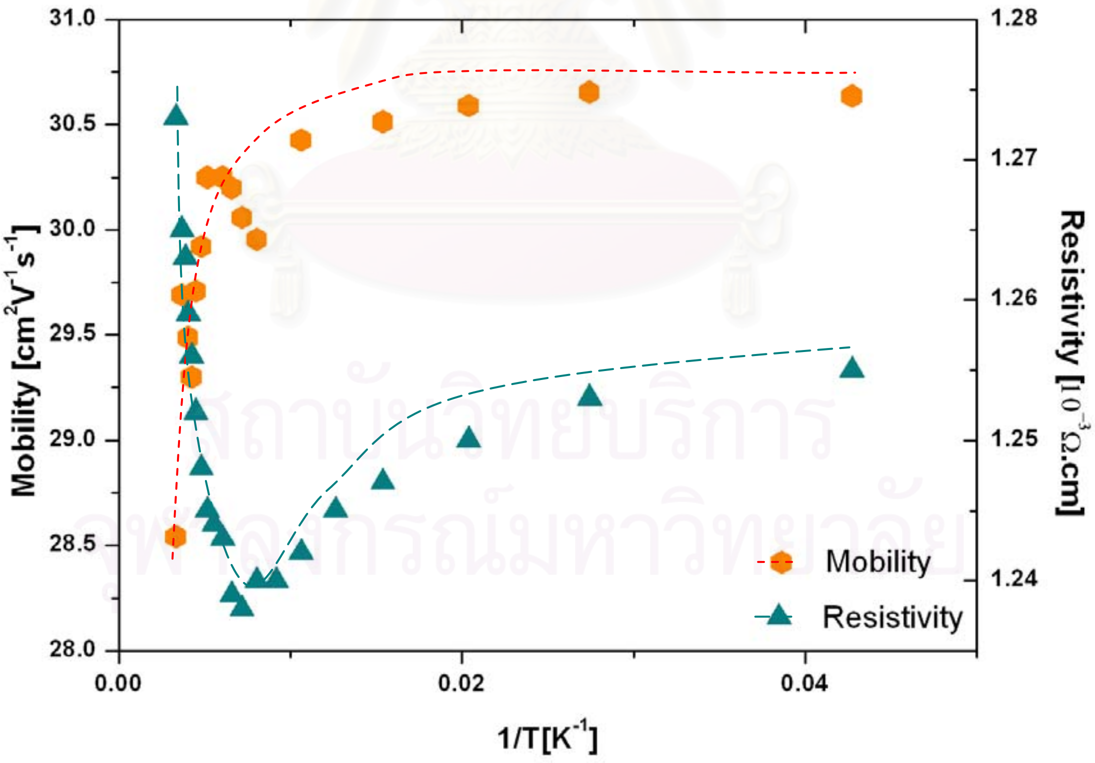

Figure 5.5: The temperature dependent of electrical properties of substrate temperature 300 ˚C Indium Tin Oxide.

This suggests that there are two competing mechanisms at the intermediate range of temperature before the behavior of a conductor wins at high temperature range. The mobility measurement shows the temperature independence at low temperature range with the value about 30.7 cm^2/Vs then dropping to the about 28.5 cm^2/Vs at room temperature.

The carrier concentrations vs. temperatures of four ITO films are shown in Fig. 5.6. It can be seen that the carrier concentrations are independent of temperature throughout the range of measurement from 25 K to 300 K with the average values of 5.0×10^{19} cm^{-3}, 1.4×10^{20} cm^{-3}, 1.8×10^{20} cm^{-3} and 1.7×10^{20} cm^{-3} for the ITO thin films fabricated at 60˚C, 230˚C, 270˚C and 300˚C, respectively.

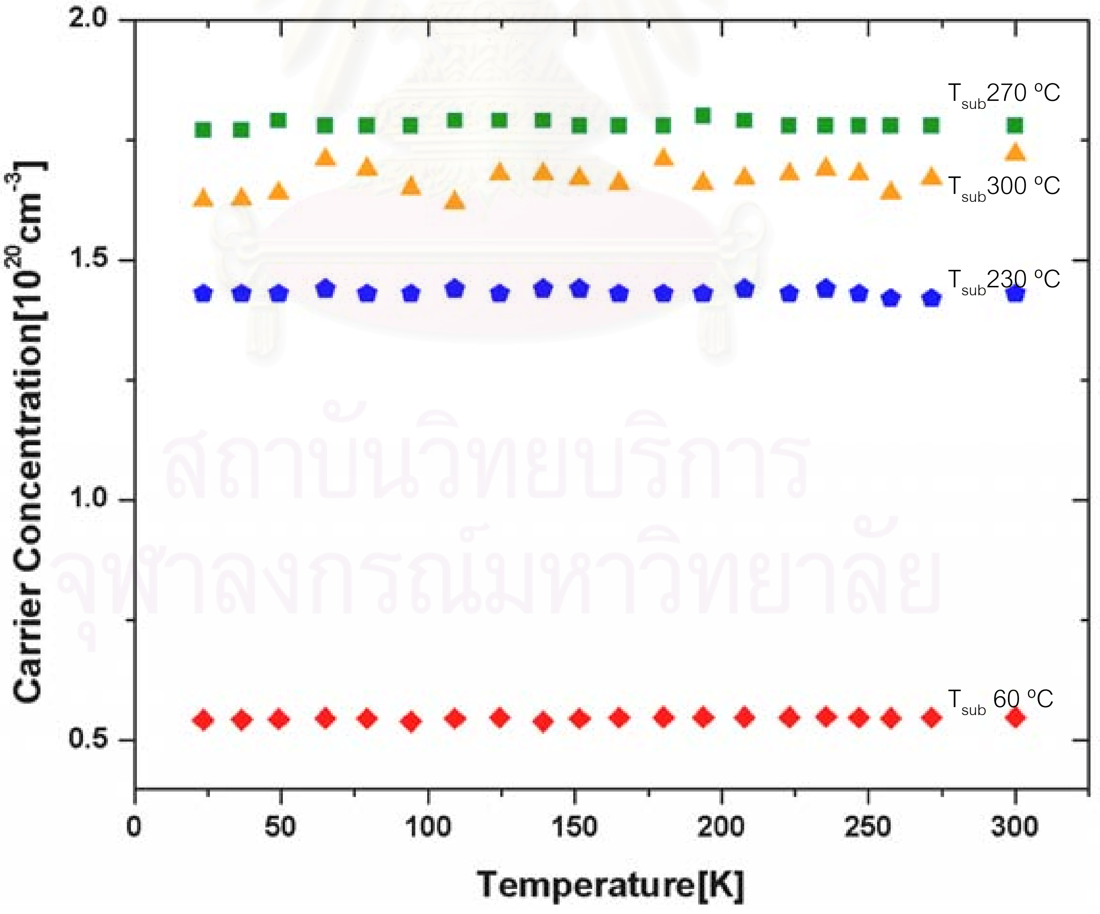

Figure 5.6: The plot of carrier concentration of ITO versus temperature.

The results are also concluded in Table 5.3. The type of carriers were investigated by the measured Hall voltage (V_H). It is noted that the carrier freeze-out was not observed in all data.

Table 5.3: The measurement results of ITO carrier concentration.

Substrate Temperature	**Carrier concentration**	**Carrier Type**
60 °C	0.5×10^{20} cm^{-3}	n
230 °C	1.4×10^{20} cm^{-3}	n
270 °C	1.8×10^{20} cm^{-3}	n
300 °C	1.7×10^{20} cm^{-3}	n

5.4 Conclusions

The ITO thin films deposited on soda-lime glass substrates by RF magnetron sputtering technique were used to study the temperature dependence of electrical properties. The average optical transmittance which was not the main interest and not mentioned here was above 90% in the visible region. The observed energy gap was about 3.64 eV at room temperature. To study the effect due to temperature, the ITO films were cooled to about 25 K and measured for its electrical properties up to room temperature using van der Pauw and Hall effect measurements. It was found experimentally that the resistivity was somewhat constant below 100 K and rising with increasing temperature towards room temperature. The carrier mobility remains constant at low temperature and declines towards the room temperature. Surprisingly, the carrier concentration remains constant throughout the temperature range. The results suggest that the optical properties of ITO thin films are semiconductor-like while its electrical properties are metal-like.

It is worth to mention that the electrical transport properties of the ITO thin films do not quite follow any temperature dependence of existing carrier transport theory for conventional semiconductors. At low temperature range, the carrier transport properties, e.g. resistivity and mobility, are temperature dependent and become a conductor at high temperature towards the room temperature. That is the lattice vibration becomes the main scattering mechanism as seen from the rising of resistivity vs. temperature at high temperature range. The competing behaviors of a conductor and a semiconductor are observed at intermediate temperature ranges (80 K-150 K) for the ITO thin films fabricated at high substrate temperatures. The carrier concentrations remain constant throughout the temperature range in all ITO samples and qualitatively consistent with the mobility when compared among the samples. These measurements show that the suitable transparent conducting oxide is the ITO fabricated with the substrate temperature at 270 °C because it has lowest resistivity, high carrier concentration and high transparency.

CHAPTER VI

ELECTRICAL PROPERTIES OF ALUMINUM-DOPED ZINC OXIDE THIN FILMS

In this chapter, the results of electrical characterization of Al-doped Zinc Oxide (AZO) thin film are discussed. The temperature dependent of their electrical properties such as resistivity, mobility and carrier concentration were be investigated using the system designed and discussed in chapter 3.

6.1 Introduction

Al-doped ZnO or AZO thin film is another transparent conducting oxide (TCO) material used in various optoelectronic devices including thin film solar cells. It can be fabricated in such a way that it exhibits very high optical transparency while still being a good conductor. AZO has some advantages over other TCOs in terms of lower material cost, more abundant material supply and less toxicity. However, the electrical transport mechanisms are still unclear as to those of the conventional semiconductors.

To study the conduction mechanisms in the Al-doped ZnO film, electrical conductivity measurements were performed at varied temperature ranges. The conductivity theoretically follows the equation [13]:

$$\sigma = \sigma_0 e^{\left(-E_a/kT\right)} \tag{6.1}$$

where, σ_0 is a constant, E_a is the activation energy of the electron transport in the conduction band, k is the Boltzmann's constant and T is the absolute temperature.

While the thermal activated band conduction mechanism at higher temperatures was derived from charge transport in the conduction band, the variable range hopping conduction mechanism was derived in the low temperature regions [13]. At low temperature, the electrons in doped semiconductor hop from one level to another in the impurity band. In this conduction process, the conduction behavior was very well described by variable range hopping (VRH). The expression of conductivity for VRH is given by

$$\sigma = \sigma_{h0} \exp\left[-\left(\frac{T_0}{T}\right)^{1/4}\right], \tag{6.2}$$

where σ_{h0} and T_0 is given by

$$\sigma_{h0} = \frac{3e^2 \nu_{ph}}{(8\pi)^{1/2}}\left[\frac{N(E_F)}{\alpha kT}\right]^{1/2} \text{ and } T_0 = \left[\frac{16\alpha^3}{kN(E_F)}\right]. \tag{6.3}$$

In Eq. (6.3), ν_{ph} is the phonon frequency at Debye temperature, $N(E_F)$ is the density of localized electron state at Fermi level E_F and α is the inverse localization length of the localized state. From Eq. (6.2) and Eq. (6.3), we can see that

$$\ln\left(\sigma T^{1/2}\right) \propto T^{-1/4}. \tag{6.4}$$

6.2 Deposition and Preparation of AZO Thin Film

The Al-doped ZnO thin films were deposited on soda-lime glass substrates by RF magnetron sputtering technique at room temperature. The sputtering conditions are: RF power of 80 Watt, Ar Pressure of 6 x 10^{-3} mbar and deposition time of 75 minutes. These yield the film of about 1.4 μm, thick.

The four Ohmic contacts were deposited by the thermal evaporation of (2,000 Å Ni /1,500 Å Au). The sample was placed on the housing by using silver paste and the four contacts were connected with 0.05 mm diameter gold wires.

The measurements of temperature dependence of electrical transport properties was employed on Al-doped ZnO film by using van der Pauw and Hall effect measurement together with closed cycle He-cryogenic system. The film was cooled down to about 25 K and measured for the electrical properties up to room temperature.

6.3 Results and Discussion

The plot of $\ln(\sigma)$ versus reciprocal temperature is shown in Fig. 6.1. It can be seen that the electrical conductivity can be separated into two ranges, high temperature range and low temperature range. For the high temperature range above 100 K, the data can be fitted with Eq. (6.1) while in the low range the results are not complied with this equation. It can be observed that the electrical conductivity caused by thermally activated band conduction given by Eq. (6.1) occurs at the temperature above 100 K, i.e. the linear relationship between $\ln(\sigma)$ and $1{,}000/T$. The slope of this plot which is equal to $-E_a/k$ can be used to estimate the activation energy (E_a). It was found that the activation energy is approximately 19 meV. For the low temperature range, the results do not agree with Eq. (6.1), suggesting the mechanisms involved is not the thermally activated conduction.

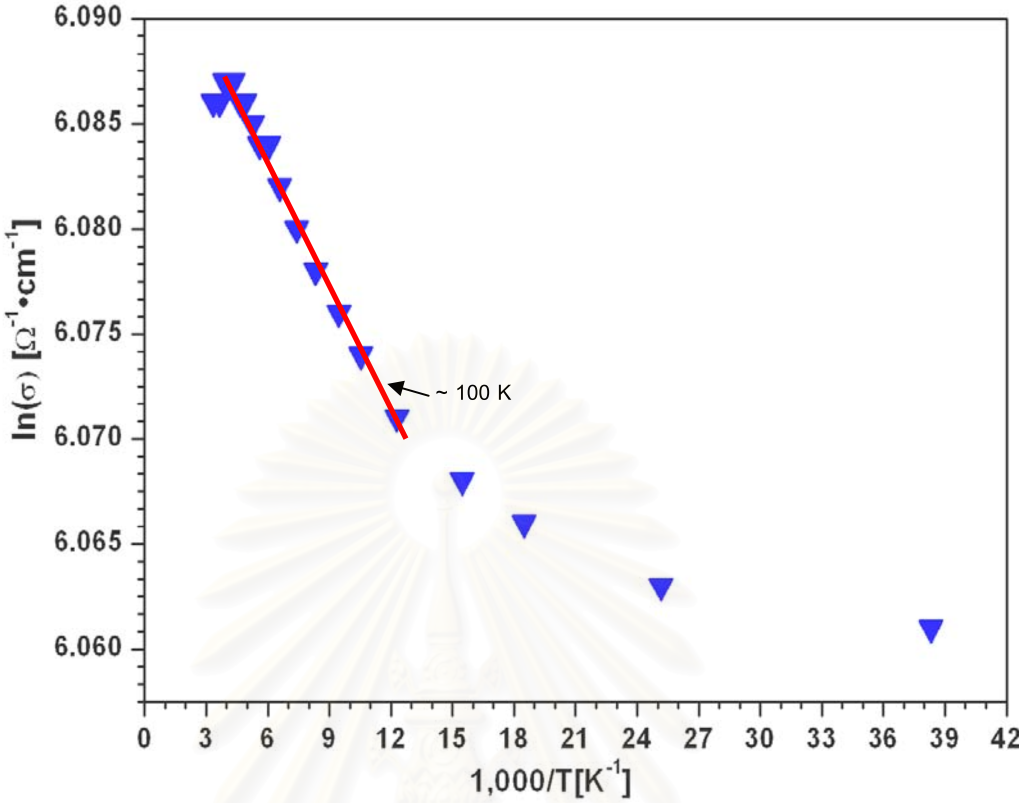

Figure 6.1: The electrical conductivity versus temperature of Al-doped ZnO thin film.

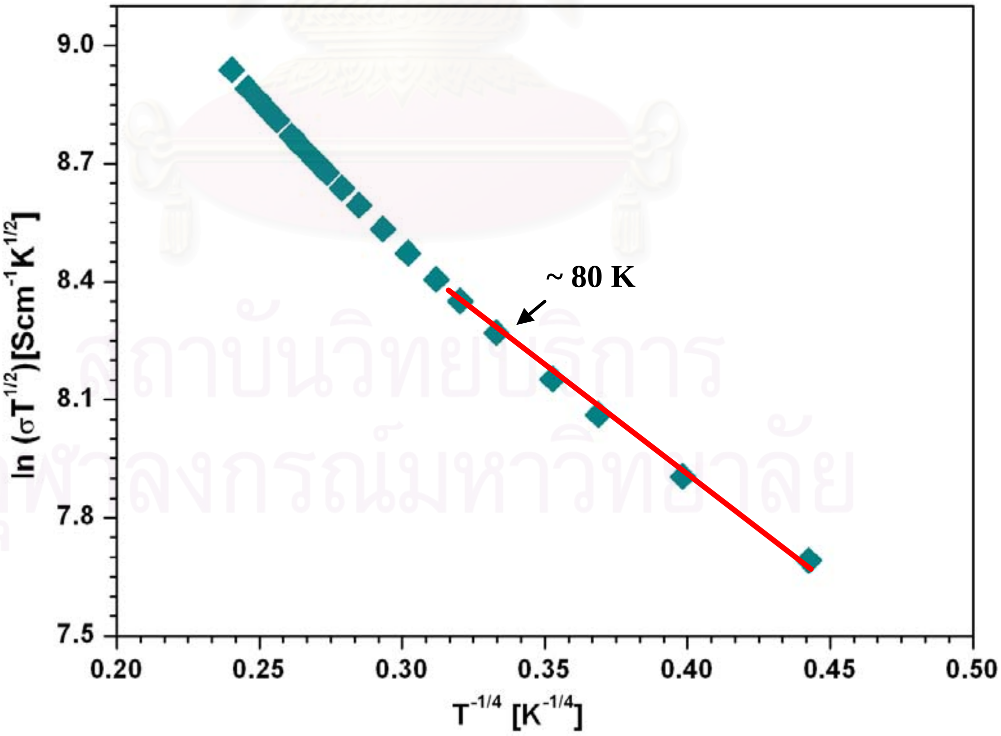

Figure 6.2: The plot of $\ln(\sigma T^{1/2})$ vs. $T^{-1/4}$.

By using the mechanism well suited for low temperature range for conduction known as variable range hopping described by Eqs. (6.2) to (6.4), Fig 6.2 shows the plot between $\ln(\sigma T^{1/2})$ and $T^{-1/4}$. There are about two different slopes for the data above 100 K and do not fit with Eq. (6.4). For the low temperature range, electrons are localized close to Fermi level and hop by their spatial distribution. The hopping length could vary for each hop. This is called variable range hopping mechanism (VRH)[14], where $\ln(\sigma T^{1/2})$ is proportional to $T^{-1/4}$ for the data below 80 K as shown in Fig. 6.2. The VRH mechanism in this case is in the temperature range 25 K - 80 K.

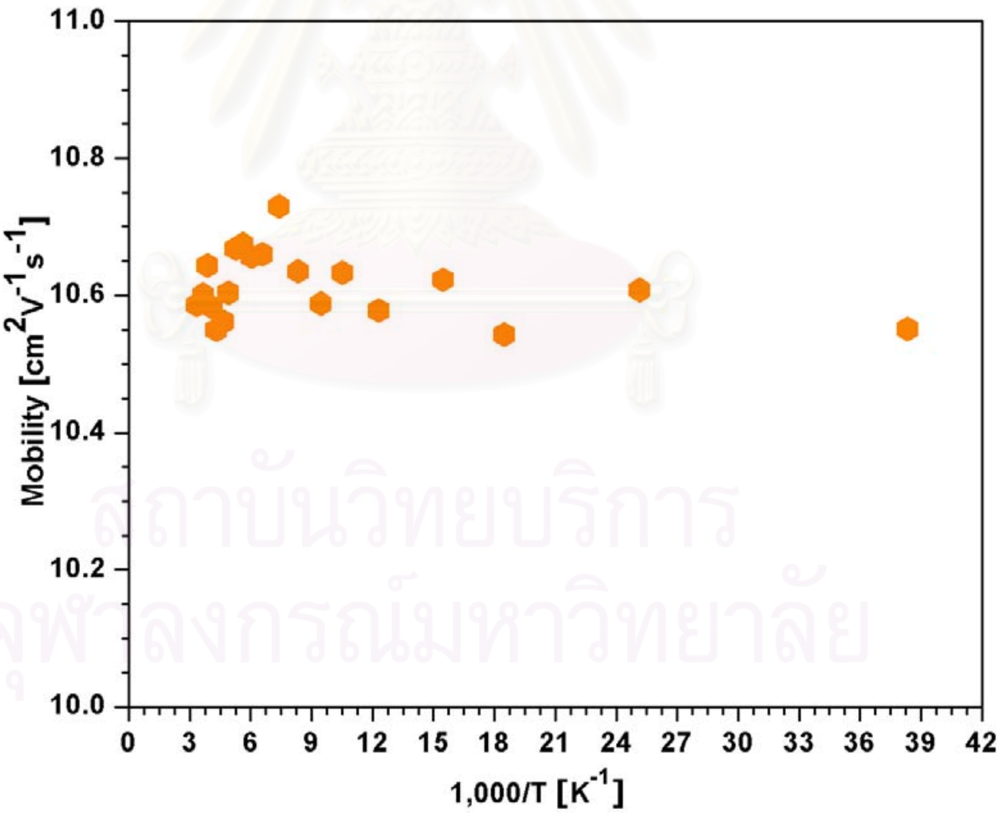

Figure 6.3: The plot of mobility vs. temperature of Al-doped ZnO thin film.

The conductivity data also agree with those from the plot of $\ln(n)$ vs. $1{,}000/T$ at the temperature above 100 K showing the increasing of intrinsic carriers for the temperature above 100 K. On the other hand, the carrier density is relatively constant below 80 K.

From the Hall measurement, the mobility was found to be relatively constant [15] with the average value of about 10.6 cm^2/Vs independent of temperature, with some fluctuation, throughout the range of the measurement from 25 - 300 K, as shown in Fig. 6.3.

The carrier concentrations of the Al-doped ZnO film (Fig. 6.4) shows the same temperature dependence as that of the conductivity and consistent with the relationship $\sigma = ne\mu$.

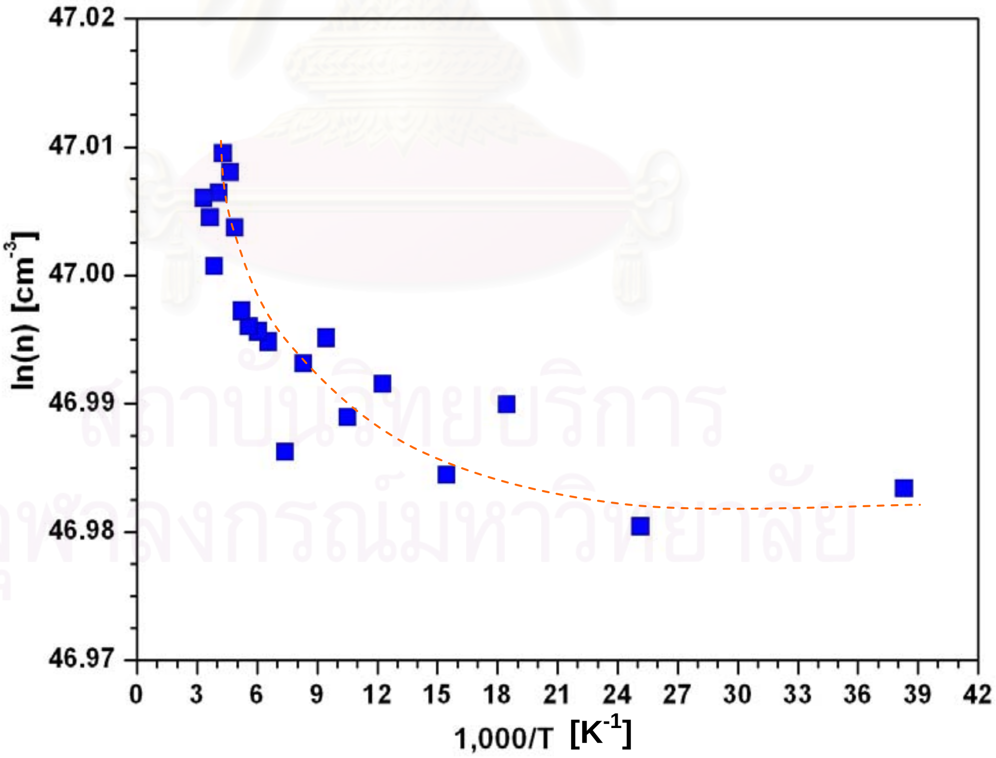

Figure 6.4: The temperature dependence of the carrier concentration of Al-doped ZnO thin film.

The carrier concentrations are ranging from 2.53×10^{20} cm^{-3} to 2.61×10^{20} cm^{-3}. The temperature dependence of carrier concentration crosses over from intrinsic range to saturation range at the temperature about 100 K (1000/T = 10 K^{-1}) as shown in Fig. 6.4.

6.4 Conclusions

For the AZO thin film, it was found that the mobility of the carriers was relatively independent of temperature throughout the range of measurement whereas the carrier concentration increases with the increasing temperature. In addition, the electrical conductivity showed temperature dependence and the thermally activated conduction was found to dominate in the temperature range above 100 K whereas the variable range hopping was dominant in the range 25 K to 80 K. The cross-over temperature was approximately in the range 80 K to 100 K. The thermal activation energy was found to be about 19 meV. The carrier concentrations confirmed that AZO was the degenerate semiconductor.

CHAPTER VII

CONCLUSIONS

In this thesis, the computer controlled van der Pauw and Hall effect measurement system have been designed and used for studying electrical properties of semiconductors such as InSb, ITO and AZO. InSb was used as the calibration sample by comparing the results obtained from the system designed in this thesis with the number released from the manufacturer. Finally, the thin films of ITO and AZO were used to study the temperature dependence of their electrical properties. The summary remarks of the work done are as followed.

In chapter 3, a list of equipment used in the system were mentioned including the wiring diagram. The software controlling equipment and analyzing data were described in details. In addition, the procedures for sample preparation were explained thoroughly.

The calibration results of the system are provided in chapter 4, using InSb wafers as the calibrating samples. The resistivity, mobility and carrier concentration of InSb were measured and compared with those obtained from the manufacturer certificate at 77 K. To achieve reliable results, the Ohmic contact using Ni/Au were thermally evaporated onto the surface of InSb. The results obtained from the designed system were in good agreement with the manufacturer certificate.

For the temperature dependent investigation of the ITO thin films in chapter 5, the lattice vibration becomes the main scattering mechanism at high temperature range. The competing behaviors of a conductor and a semiconductor are observed at intermediate temperature ranges. The results suggest that the electrical properties of ITO thin films are metal-like.

In chapter 6, the electrical conductivity of AZO showed temperature dependence and the thermally activated conduction was found to dominate in the high temperature range whereas the variable range hopping is dominant in the lower range. The thermal activation energy of the AZO is found to be about 19 meV. The temperature dependent of the carrier concentrations of AZO shows degenerate semiconductor behavior.

References

[1] W. R. Runyan. Semiconductor Measurements and Instrument. New York: 1975.

[2] van der Pauw L. J. A method of measuring the resistivity and Hall coefficient on lamellae of arbitrary shape. Phil. Tech. Rev. 20 (1958): 220-224.

[3] Donal A. Neaman. Semiconductor Physics & Device , USA: The Mc Graw-Hill Companies, Inc., 1997.

[4] Sze, S.M. Physics of Semiconductor Device , 2 nd ed. New York: John Wiley & Sons, 1981.

[5] John Singleton. Band Theory and Electronic Properties of Solids . Great Britain: Mc Graw-Hill, 2001.

[6] Smith, R. A. Semiconductor , 2nd ed. London: Cambridge University Press, 1978.

[7] M Levinshtein, S Rumyantsev and M Shur. Hand book series on Semiconductor Parameters , Singapore: world Scientific, 1996.

[8] Chanwit Chityuttakan, Panita Chinvetkivanich, Sojiphong Chatraphorn, Somphong Chatraphorn, Proceeding of the 4th Thailand Materials Science and Technology Conference (2006): 94-96.

[9] D. H. Zhang and H.L. Ma. Scattering mechanisms of charge carriers in transparent conducting oxide films. Appl. Phys. A 62 (1996): 487-492.

[10] P. S. Kireev. Semiconductor Physics Moscow: Mir ,1978.

[11] R. L. Petritz. Temperature dependent Hall measurements on PLD thin films. Phys. Rev. 104 (1956): 1508-1510.

[12] J. Bruneaux, H. Cachet, M. Froment, A. Messad. Correlation between structural and electrical properties of sprayed tin oxide films with and without fluorine doping. Thin Solid Films. 197 (1991): 129-142.

[13] Rajesh Kumar and Neeraj Khare. Temperature dependence of conduction mechanism of ZnO and Co-doped ZnO thin films. Thin Solid Films 516 (2008): 1302-1307.

[14] Jiaping Han, Mingrong Shen and Wenwu Cao. Hopping conduction in Mn-

doped ZnO. Appl. Phys. Letters 82 (2003): 67-68.

[15] J. Lee, W. Gao, Z. Li, M. Hodgson, J. Med Son, H Gong and U. Pal. Sputter Deposited Zinc Oxide Photoconductive Antenna on Silicon Substrate for Sub-Terahertz Time-Domain Spectroscopy. Appl. Phys. A 80 (2005): 1641-1643.

[16] Schroder D. K. Semiconductor Material and Device Characterization Singapore: John Wiley & Son: 1990.

APPENDIX A

NOTES ON SEMICONDUCTOR IN EQUILIBRIUM

Semiconductors are matters whose electrical properties are between these of metals and insulators. They can be single element materials found in group IV of the periodic table or combinations of group III and group V or group II and group VI or one more complicated ternary compounds. In this section, the semiconductors which can be categorized into two types by the free carrier in the thermal equilibrium i.e. the intrinsic semiconductor which is no impurity and the extrinsic semiconductor which impurities are added are described [16].

A.1 Intrinsic Semiconductors [6]

Some of the properties of intrinsic semiconductor is summarized here. Let $N_c(E)dE$ be the number of allowed levels in the conduction band with value of the energy level between E and $E+dE$. The number of electrons $n(E)dE$ in the conduction band including the spin degeneracy is given by

$$n(E)dE = 2N_c(E)P_e(E)dE. \qquad \text{(A.1)}$$

where $P(E) = \dfrac{1}{\exp[(E-E_F)/kT]+1}$;

E_F is the Fermi energy, k is the Boltzmann constant, T is the temperature in Kelvin

The total number of electron per unit volume n_i in the conduction band is

$$n_i = 2\int_0^{E_t} N_c(E)P_e(E)dE, \qquad \text{(A.2)}$$

where E_t is the energy corresponding to the top of the conduction band.

In k-space, the number of allowed states for a semiconductor which have a single minimum of conduction band with spherical symmetry and the electron effective mass m_e can be given by

$$N(k)dk = Vdk/8\pi^3, \qquad \text{(A.3)}$$

where *V* is the volume in the region of k- space. Then, the number of levels per unit volume between *E* and *(E+dE)* is

$$N_c(E)dE = 2\pi(2m_e)^{\frac{3}{2}}h^{-3}E^{\frac{1}{2}}dE. \qquad \text{(A.4)}$$

In the case of $E_t >> kT$, there is a very small probability of occupation of levels, Eq. (A.4) can be rewritten as

$$n_i = 4\pi(2m_e)^{\frac{3}{2}}h^{-3}\int_0^{\infty}\frac{E^{\frac{1}{2}}dE}{\exp[(E-E_F)/kT]+1}. \qquad \text{(A.5)}$$

Because $\exp[(E-E_F)/kT] >> 1$, Eq. (A.5) becomes

$$n_i = 2[\frac{2\pi m_e kT}{h^2}]^{\frac{3}{2}}\exp[\frac{E_F}{kT}],$$

$$= N_c \exp[\frac{E_F}{kT}], \qquad \text{(A.6)}$$

where $N_c = 2[\frac{2\pi m_e kT}{h^2}]^{\frac{3}{2}}$ and h is the Planck constant.

In the same case for the holes in the valence band, the number of holes per unit volume in the valence band occupied $p(E)dE$ between the energy level E and dE which is given by

$$p(E)dE = 2N_v(E)P_h(E)dE. \qquad \text{(A.7)}$$

The total number of electrons in the conduction band is equal to the total number of holes valence band. Thus, for the to the total number of holes per unit volume, p_i, is then given by

$$p_i = 2\int_{E_b}^{-\Delta E} N_v(E)P_h(E)dE, \qquad \text{(A.8)}$$

where E_b is the energy corresponding to the bottom of the valence band ΔE is the energy different between conduction band and valence band.

In k-space for the valence band, the number of levels for unit volume between E and *(E+dE)* is

$$N_v(E)dE = 2\pi(2m_h)^{\frac{3}{2}} h^{-3}(-\Delta E - E)^{\frac{1}{2}} dE\ . \qquad \text{(A.9)}$$

In the case of extending the upper limit to infinity where $(E - E_F) << kT$, we have

$$p_i = 4\pi(2m_h)^{\frac{3}{2}} h^{-3} \int_{-\infty}^{-\Delta E} \frac{(-\Delta E - E)^{\frac{1}{2}} dE}{\exp[(E_F - E)/kT] + 1}, \qquad (A.10)$$

and
$$p_i = 2[\frac{2\pi m_h kT}{h^2}]^{\frac{3}{2}} \exp[-\frac{E_F + E_g}{kT}],$$

$$= N_v \exp[-\frac{E_F + E_g}{kT}], \qquad (A.11)$$

where $N_v = 2[\frac{2\pi m_h kT}{h^2}]^{\frac{3}{2}}$, E_g is the energy gab between conduction band and valence band which is equal to $E_c - E_v$ and m_h is the effective mass of hole.

For the intrinsic semiconductor, the number of electrons and the number of holes are equal, that is

$$n_i = p_i\,. \qquad (A.12)$$

From the Eq. (A.6) and Eq. (A.11) the product of number of carriers can be written as

$$n_i p_i = n_i^2 = 2[\frac{2\pi m_e kT}{h^2}]^{\frac{3}{2}} 2[\frac{2\pi m_h kT}{h^2}]^{\frac{3}{2}} \exp[-\frac{E_g}{kT}], \qquad (A.13)$$

Inserting the numerical values of h and k, the Eq. (A.13) becomes

$$n_i = p_i = 4.82 \times 10^{15} T^{\frac{3}{2}} (\frac{m_e m_h}{m^2})^{\frac{3}{4}} \exp[-\frac{E_g}{kT}] \quad .$$

(A.14)

The equation for Fermi level in the term of N_c and N_v is given by

$$E_F = -\frac{1}{2} E_g + \frac{1}{2} kT \ln[\frac{N_v}{N_c}]\,. \qquad (A.15)$$

Equation (A.14) shows that the variation of the intrinsic carriers depends on the temperature in the exponential term.

A.2 Extrinsic Semiconductors [4][6]

The extrinsic semiconductor is the semiconductor with the impurity levels laying between the valence band and conduction band. Considering the non degenerate band, the concentration of free electrons in the conduction band is given in the same equation as in the intrinsic semiconductor.

$$n_i = N_c \exp[\frac{E_F}{kT}]. \qquad \text{(A.16)}$$

Also the holes concentration in the valence band can be expressed as

$$p_i = N_v \exp[-\frac{E_F + E_g}{kT}]. \qquad \text{(A.17)}$$

The impurity concentration affects the Fermi energy. The free carrier concentration relationship is

$$np = N_c N_v \exp[-\frac{E_g}{kT}] = n_i^2 . \qquad \text{(A.18)}$$

From the condition of electrical neutrality, the concentration of carriers is given by

$$n + n_d + N_a = p + n_a + N_d , \qquad \text{(A.19)}$$

where n is the electron concentration,

p is the hole concentration,

n_a is the non-ionized impurity acceptor concentration,

n_d is the non-ionized impurity donor concentration,

N_a is the ionized impurity acceptor concentration,

N_d is the ionized impurity donor concentration.

For the low impurity or high temperature, the intrinsic carriers and the impurity carriers are the main carriers. In this case, most impurities are ionized by the thermal energy. The equation of electrical neutrality is given by

$$n = p + (N_d + N_a), \qquad \text{(A.20)}$$

and

$$n = \frac{1}{2}[(N_d - N_a) + \sqrt{(N_d - N_a)^2 + 4n_i^2}, \qquad \text{(A.21)}$$

$$p = \frac{n_i^2}{n} \quad . \qquad \text{(A.22)}$$

In the high temperature range, the majority carriers are from the intrinsic one $|N_d - N_a| << n_i$, the carrier concentration is increases exponentially with temperature. This range is known as intrinsic region, then Eq. (A.21) and Eq. (A.22) are rewritten by

$$n = p = n_i. \qquad \text{(A.23)}$$

The saturation region is the case of the majority carriers are the ionized impurity and the intrinsic carriers are less than the impurity, $|N_d - N_a| >> n_i$, then constant impurity carriers are obtained in this range as following

$$n \cong N_d - N_a. \qquad \text{(A.24)}$$

For the high impurity concentration or low temperature, some of the impurities are unionized by the thermal energy. The equation of electrical neutrality can be given by

$$n = N_d - N_a - n_d\,, \qquad \text{(A.25)}$$

and
$$n_d = N_d[\frac{1}{1+\beta\exp\{-\frac{E_d + E_F}{kT}\}}]\,, \qquad \text{(A.26)}$$

where β is the degeneracy factor of the ground state of the donor carrier.

Equation (A.2.16), Eq. (A.24) and Eq. (A.26) can be rewritten by

$$n^2 + n(N_a + N_c^{/}) - (N_d - N_a)N_c^{/} = 0\,, \qquad \text{(A.27)}$$

where $N_c^{/} = \beta N_c \exp\{-\frac{E_d}{kT}\}$.

Using the binomial series expansion, the root of Eq. (A.27), where $E_d >> kT$, is

$$n \cong \frac{N_c^{/}(N_d - N_a)}{N_a + N_c}\,. \qquad \text{(A.28)}$$

If $N_a >> N_c^{/}$, Eq. (A.28) becomes

$$n \cong \frac{N_c^{/}(N_d - N_a)}{N_a} = \frac{(N_d - N_a)}{2N_a}\beta N_c \exp(-\frac{E_d}{kT}) \qquad \text{(A.29)}$$

If $N_d >> N_c^{/} >> N_a$, Eq. (A.28) becomes

$$\frac{n^2}{N_d} - N_c^{/} = 0 \qquad \text{(A.30)}$$

or
$$n \approx \sqrt{\beta N_d N_c}\,\exp(-\frac{E_d}{2kT})\,. \qquad \text{(A.31)}$$

Equation (A.29) and (A.31) show that when the temperature decreases, carrier concentration is decreasing exponentially with temperature. This region is known as the freeze-out region. The slope of this region are $\frac{E_d}{k}$ and $\frac{E_d}{2k}$ for the given Eq. (A.29) and (A.31), respectively. The general shape of curves giving the majority carrier concentration as a function of *1/T* is shown in Fig. A.1.

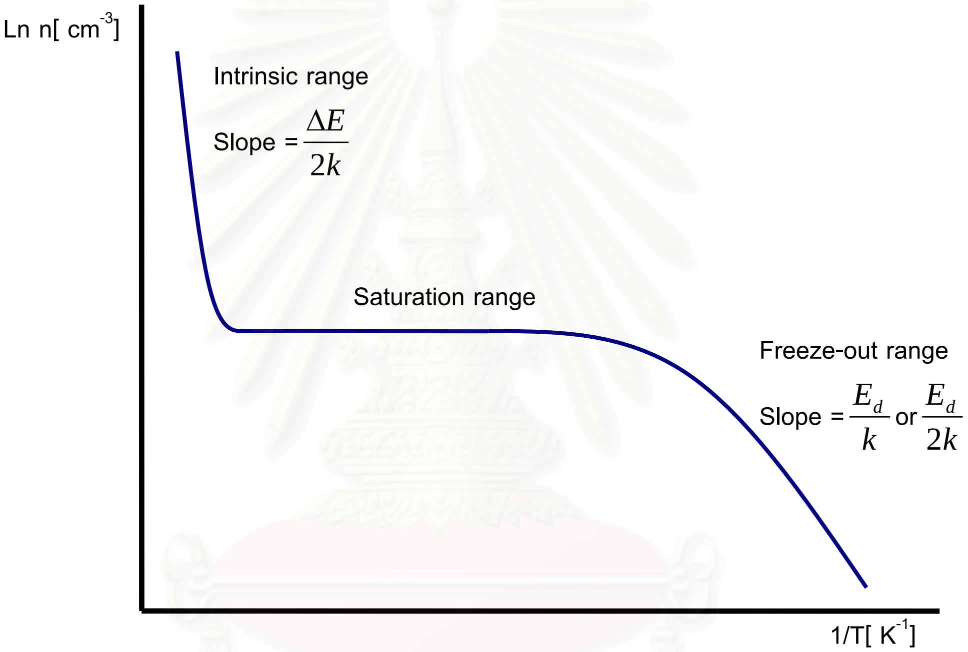

Figure A.1: The variation of carrier concentration and reciprocal temperature [16].

APPENDIX B

PRELIMINARY OPERATIONS

1. User should review and become familiar with entire procedures of the van der Pauw and the Hall effect measurements before beginning the measurement process.

2. Make sure that the cable are connected as shown in Fig. B.1 for the electrical properties measurement.

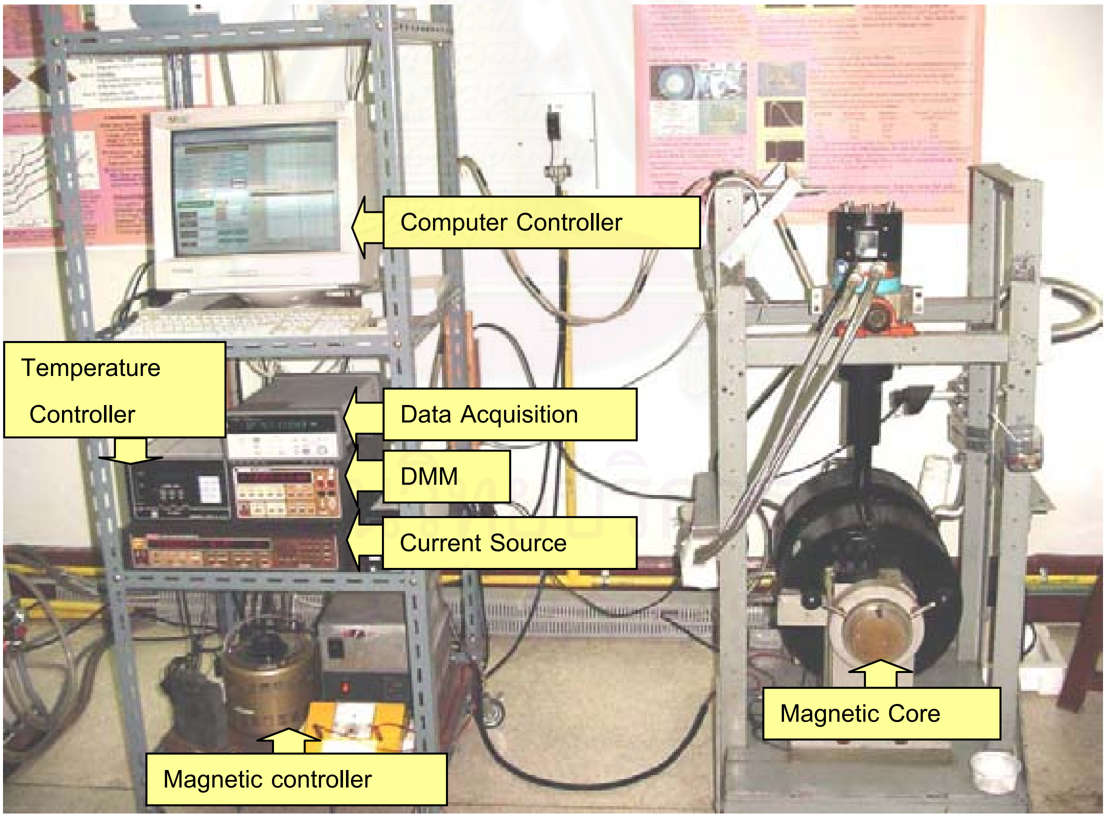

Figure B.1: The connection of the van der Pauw and the Hall effect measurement Program.

3. Check the address at the front panel for the equipment as listed in Table B.1.

4. Turn on the water cooling system of the magnetic field coils to avoid the heating of the coils inside the magnetic field generator.

5. Start the van der Pauw and the Hall measurement program using Agilent VEE, then the interface window will show up on the monitor.

   Note: the van der Pauw and the Hall effect measurement system is used in the case of room temperature measurement. For the temperature dependent measurement user can change to the Low temperature van der Pauw and the Hall effect measurement program.

6. Input the sample information, program information and the user information on the upper left of the display window and click ‘run’ button on the menu bar of the program according to Fig. B.2.

   The input details used in the process of the program are listed as the following;

   - Filename is used to be the name of the initialize Microsoft Excel program for the out put.

     Note: For the low temperature measurement program the initialized Microsoft excel program are named by filename together with the measured temperature.

   - Sample thickness, Positive B and Negative B are used to calculate the electrical properties in the following section.

   - R_Sample is used to calculate the current needed in the van der Pauw and the Hall effect measurement process.

Table B.1: The address of the used equipment in the van der Pauw and the Hall effect measurement system.

Equipment	Address
Data Acquisition	05
Current Source	06
Digital multimeter	07

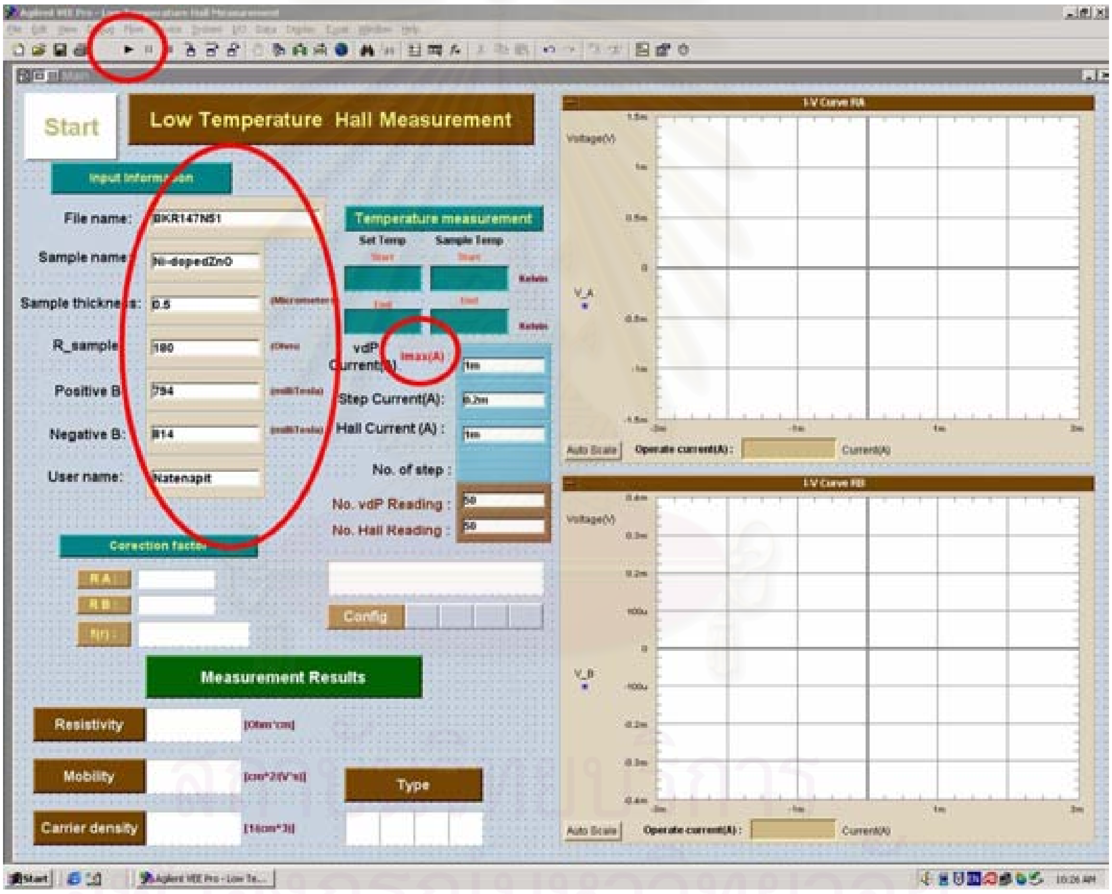

File name: BKR147NS1
Sample name: Ni-dopedZnO
Sample thickness: 0.5 (Micrometers)
R_sample: 180 (Ohms)
Positive B: 794 (milliTesla)
Negative B: 814 (milliTesla)
User name: Natenapit
vdP Current(A) Imax(A): 1m
Step Current(A): 0.2m
Hall Current (A) : 1m
No. of step :
No. vdP Reading : 50
No. Hall Reading : 50

Figure B.2: The interface window of measurement program. The input information on the upper left are used as parameters of the electrical properties calculation. The used current should be less than that shown on the middle of the interface program. The run button should be click after the user completed input the information.

The maximum voltage set for current source is 50 Volt, The value R_sample is used to obtain the allowed maximum current (Imax (A)) for the measurement program using Ohm’s law, shown on the interface program.

7. The Microsoft Excel will be initialized and will be displayed on the monitor of the computer. Then the user should complete the required current in the textbox not to exceed Imax recommended by the program.

- vdP Current stands for the current used in the van der Pauw measurement.
- Step Current stands for the current stepping used in the van der Pauw measurement loop.

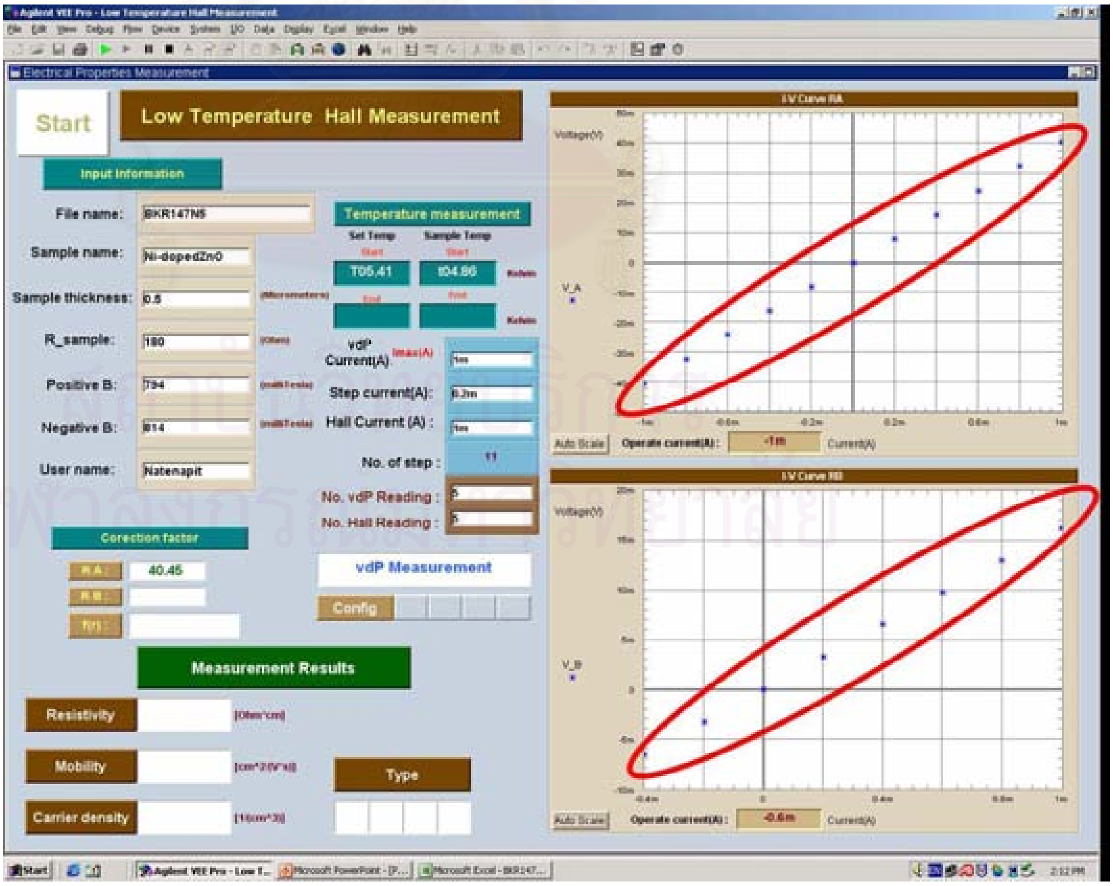

File name: BKR147N5

Sample name: Ni-dopedZnO

Sample thickness: 0.5 (Micrometers)

R_sample: 180 (Ohm)

Positive B: 794 (milliTesla)

Negative B: 814 (milliTesla)

User name: Natenapit

Set Temp Start: 105.41

Sample Temp Start: 104.86 Kelvin

vdP Current(A): 1m (Imax(A))

Step current(A): 0.2m

Hall Current (A): 1m

No. of step: 11

No. vdP Reading: 5

No. Hall Reading: 5

R A: 40.45

Operate current(A): -1m

Operate current(A): -0.6m

Figure B.3: The real time plot for the Ohmic contact check.

- Hall Current stands for the current used in the Hall effect measurement.

8. Click ‘Start’ button to run the program. The computer will process on the van der Pauw measurement first. The selected configuration was change by the switching unit. The currents are generates from the current source as a value of the input current data. Then the voltages across the sample are measured by the digital voltmeter. The both currents and voltages are collected and plotted real time as shown on the interface display on the right hand side.

9. The real time plot between the applied current and the measured voltage (Fig. B.3) is also used to verify the Ohmic contacts of the sample connectors. The resistances R_A and R_B are obtained by the calculations in chapter 2 and then shown on the interface program.

10. The two resistances R_A and R_B are used to calculate the correction factor $f\left(R_A/R_B\right)$ which is used to evaluate the resistivity described in chapter 2.

11. After the process of resistivity calculation is finished, then the message box in Fig. B.5, is shown on the screen.

12. To continue to the Hall effect measurement, the program are separated into three parts, i.e. the measurement of Hall configuration with no magnetic field, positive magnetic field and the negative magnetic field, respectively.

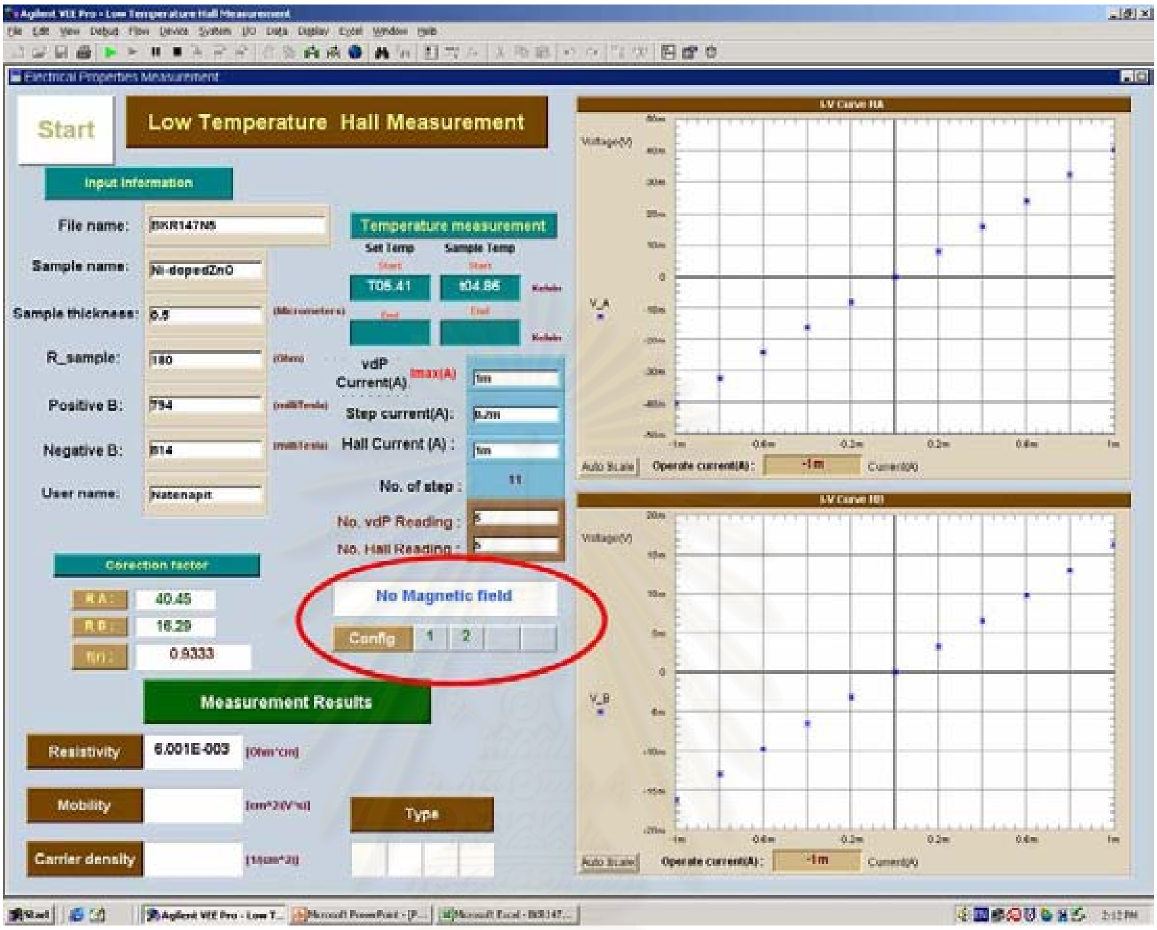

File name: BKR147N5

Sample name: Ni-dopedZnO

Sample thickness: 0.5 (Micrometers)

R_sample: 180 (Ohm)

Positive B: 794 (milliTesla)

Negative B: 814 (milliTesla)

User name: Natenapit

Set Temp Start: 105.41 Kelvin

Sample Temp Start: 104.86 Kelvin

vdP Current(A) Imax(A): 1m

Step current(A): 0.2m

Hall Current (A) : 1m

No. of step : 11

No. vdP Reading : 5

No. Hall Reading : 5

No Magnetic field

R A : 40.45

R B : 16.29

f(r) : 0.9333

Resistivity: 6.001E-003 [Ohm*cm]

Mobility: [cm^2/V*s]

Carrier density: [1/cm^2]

Operate current(A) : -1m

Figure B.4: The status of the Hall effect measurement are shown on the interface display. There are No Magnetic field, Positive Magnetic field and Negative Magnetic field.

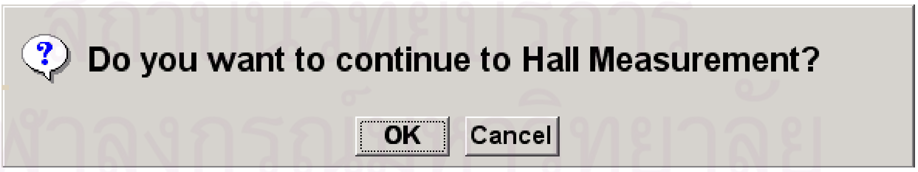
Do you want to continue to Hall Measurement?

Figure B.5: The message box of The van der Pauw measurement program will be end when "Cancel" is selected and will be continue to the Hall effect measurement in the case of "OK" was selected.

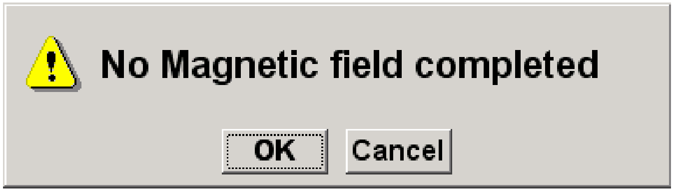
No Magnetic field completed

Figure B.6: The message box shows that the measurement of No magnetic field is complete.


Please turn on Magnetic field (Current +)

Figure B.7: The direction message box requires the magnetic field positive current.

The Hall measurement are summarized as followed:

i) No magnetic field: message box as follow Fig. B.6 show up and the Hall effect measurement program are running.

ii) Positive Magnetic field: When the message box in Fig. B.7 show up, the user should turn the positive magnetic field on and then the four configurations of the Hall measurement are measured with positive magnetic field. The message box is to turn off the magnetic field shows up when the measurement finishes(Fig B.8).

iii) Negative magnetic field: Similarly, the message box again shows up for the magnetic field in the negative direction (Fig. B.9). When the measurement finishes, the message box to turn off the magnetic field (Fig. B. 10) again shows up.

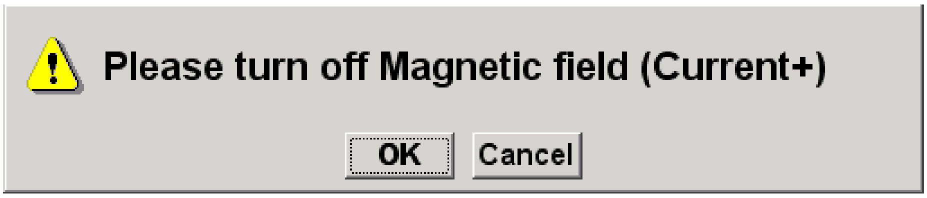

Please turn off Magnetic field (Current+)

Figure B.8: The message box shows that the user should turn the magnetic field off.

Please turn on Magnetic field (Current -)

Figure B.9: The turn on magnetic field negative current message box.

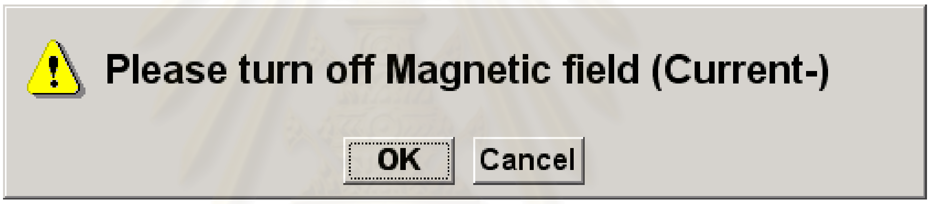

Please turn off Magnetic field (Current-)

Figure B.10: The turn off magnetic field negative current message box.

13 After all configurations of the three parts are finished. The four configurations of the Hall effect measurement are calculated. There are the evaluation of the carrier concentration together with the carrier type. Then the average of the electrical properties are obtained and are saved to the Microsoft Excel.

14 The data from the measurement results i.e. resistivity, mobility, carrier concentration and carrier type are reported in the Microsoft Excel worksheet as shown in Fig. B. 11.

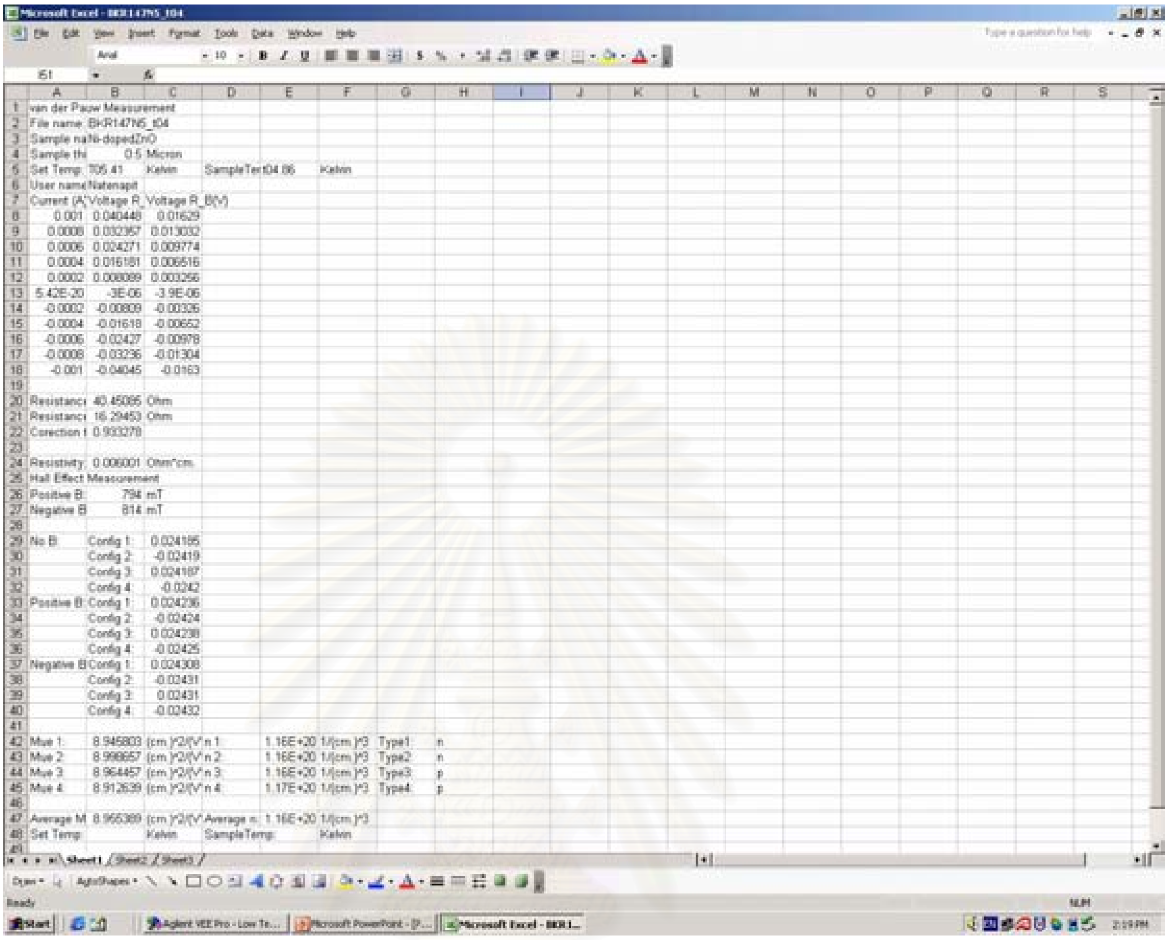

	A	B	C	D	E	F	G	H
1	van der Pauw Measurement							
2	File name:	BKR147N5_t04						
3	Sample na	Ni-dopedZnO						
4	Sample thi	0.5	Micron					
5	Set Temp:	305.41	Kelvin	SampleTem	304.86	Kelvin		
6	User name	Natenapit						
7	Current (A	Voltage R_	Voltage R_B(V)					
8	0.001	0.040448	0.01629					
9	0.0008	0.032357	0.013032					
10	0.0006	0.024271	0.009774					
11	0.0004	0.016181	0.006516					
12	0.0002	0.008089	0.003256					
13	5.42E-20	-3E-06	-3.9E-06					
14	-0.0002	-0.00809	-0.00326					
15	-0.0004	-0.01618	-0.00652					
16	-0.0006	-0.02427	-0.00978					
17	-0.0008	-0.03236	-0.01304					
18	-0.001	-0.04045	-0.0163					
19								
20	Resistanc	40.45085	Ohm					
21	Resistanc	16.29453	Ohm					
22	Corection f	0.933278						
23								
24	Resistivity:	0.006001	Ohm*cm.					
25	Hall Effect Measurement							
26	Positive B:	794	mT					
27	Negative B	814	mT					
28								
29	No B:	Config 1:	0.024185					
30		Config 2:	-0.02419					
31		Config 3:	0.024187					
32		Config 4:	-0.0242					
33	Positive B:	Config 1:	0.024236					
34		Config 2:	-0.02424					
35		Config 3:	0.024238					
36		Config 4:	-0.02425					
37	Negative B	Config 1:	0.024308					
38		Config 2:	-0.02431					
39		Config 3:	0.02431					
40		Config 4:	-0.02432					
41								
42	Mue 1:	8.945803	(cm)^2/(V	n 1:	1.16E+20	1/(cm)^3	Type1:	n
43	Mue 2:	8.998657	(cm)^2/(V	n 2:	1.16E+20	1/(cm)^3	Type2:	n
44	Mue 3:	8.964457	(cm)^2/(V	n 3:	1.16E+20	1/(cm)^3	Type3:	p
45	Mue 4:	8.912639	(cm)^2/(V	n 4:	1.17E+20	1/(cm)^3	Type4:	p
46								
47	Average M	8.955389	(cm)^2/(V	Average n:	1.16E+20	1/(cm)^3		
48	Set Temp:		Kelvin	SampleTemp:		Kelvin		

Figure B.11: The report worksheet in the Microsoft Excel.

Vitae

Miss Natenapit Chookunhom was born on December 27th, 1978 in Khonkean Thailand. She received her Bachelor degree of Science in Physics from Mahidol University in 2001 and joins National Institute of Metrology (Thailand) in the same year.

Conference Presentations:

2007 N. Chookunhom, C. Chityuttakan, et al., Thai J. Phys. 3, 15-17, (2007).

2008 N. Chookunhom, C. Chityuttakan, K. Wanthong, K. Yoodee and S. Chattraphorn, “Effect of Temperature on Electrical Properties of Al-Doped-Zinc-Oxide Thin Films”, The 3^{sd} Siam Physics Congress, Greenery Resort KhoaYai, Nakhorn Ratchasima , Thailand, March 21-22, (2008)

Permanent Address:

284 (78/214) Soi Chotiwat 3, Sapan 99,

Prachachuen Road, Bangsue,

Bangkok, Thailand.